Fakultät für Medizin

Investigation of species specificity of Na^+ taurocholate cotransporting polypeptide for HBV infection and the evaluation of novel HBV entry inhibitors

Fuwang Chen

Vollständiger Abdruck der von der Fakultät für Medizin der Technischen Universität München zur Erlangung des akademischen Grades eines

Doktors der Naturwissenschaften (Dr. rer. nat.)

genehmigten Dissertation.

Vorsitzender: Prof. Dr. Paul Thomas Pfluger

Prüfer*innen der Dissertation:

1. Prof. Dr. Ulrike Protzer
2. Prof. Dr. Matthias Feige

Die Dissertation wurde am 14.01.2022 bei der Fakultät für Medizin der Technischen Universität München eingereicht und durch die Fakultät für Medizin am 07.06.2022 angenommen.

Table of contents

Abbreviations 5
Abstract 9
Zusammenfassung 11
1. Introduction 13
1.1 Hepatitis B virus (HBV) 13
1.1.1 Classification 13
1.1.2 Morphology 14
1.1.3 Genome organization 15
1.1.4 Viral life cycle 15
1.1.5 The cccDNA – the persistent form of HBV 17
1.2 Sodium-taurocholate co-transporting polypeptide 18
1.3 *In vitro* and *in vivo* model systems to study HBV 20
1.3.1 *In vitro* model systems 20
1.3.2 *In vivo* model systems 22
1.4 Antiviral treatment for CHB 23
1.4.1 Current treatment for CHB 23
1.4.2 HBV entry inhibitors 24
1.5 Aims of the study 26
2. Results 27
2.1 Species specificity of NTCP for HBV infection 27
2.1.1 Establishment of NTCP expression and quantification systems 27
2.1.2 Analysis species specificity of NTCP for HBV infection 31
2.1.3 Modification of NTCPs for HBV infection 33
2.2 Characterization of horse-NTCP for enhancing HBV infection 39
2.2.1 Establishment of the huNTCP and hoNTCP comparison system 39
2.2.2 HoNTCP increases numbers of infected cells and single-cell infection level 45
2.2.3 HoNTCP enhances HBV infection by binding to more HBV particles 47
2.2.4 The localization levels of hoNTCP regulates HBV infection 51
2.3 HBV infection in murine hepatocyte cell line-AML12 57
2.3.1 HoNTCP enhances HBV infection on AML12 cells 57
2.3.2 Generation of NTCP expressing AML12 cell lines 60
2.4 Evaluation of HBV entry inhibitors 63

2.4.1 Two compounds were prescreened for inhibiting HBV infection. 63
2.4.2 Compounds inhibit HBV infection by targeting early steps 66
3. Discussion 73
3.1 Species specificity of NTCP for HBV infection 73
3.2 Overcoming the entry-barriers of hepatocytes for HBV infection 74
3.3 The impacts of other domains or amino acids for HBV infection 75
3.4 The comparison of huNTCP and hoNTCP for mediating HBV infection 76
3.4.1 The platforms for comparison of huNTCP and hoNTCP for HBV infection . . 76
3.4.2 HoNTCP enhances HBV infection via high surface localization efficiency . . 77
3.5 NTCP expression levels regulate HBV infection efficiency 78
3.6 Potential intracellular roles for NTCP in HBV entry 79
3.7 AML12 cells are susceptible for HBV infection upon NTCP expression 79
3.8 The impacts of new compounds on HBV establishment 81
3.9 Summary 82
4. Materials and Methods 84
4.1 Materials 84
4.1.1 Cell lines 84
4.1.2 Cell culture media. 84
4.1.3 Oligonucleotides for PCR 85
4.1.4 Kits 86
4.1.5 Antibodies 87
4.1.6 Plasmids 87
4.1.7 Chemicals and reagents 88
4.1.8 Laboratory equipment and consumables 89
4.1.9 Software 90
4.2 Methods 91
4.2.1 Cell culture. 91
4.2.2 Cloning 91
4.2.3 Production of in vitro transcribed (IVT) mRNA. 92
4.2.4 Transfection. 92
4.2.5 Fluorescence microscopy and Confocal Microscopy 92
4.2.6 Flow cytometry 93
4.2.7 HBV uptake and infection assay 93
4.2.8 Taurocholate Uptake assay 93

4.2.9 DNA isolation 94
4.2.10 DNA T5 digestion 94
4.2.11 Isolation of total RNA and cDNA synthesis. 94
4.2.12 Quantification of viral HBV markers using qPCR. 94
4.2.13 Statistical analysis. 95
5. References 96
Acknowledgement 108
Appendix 109

Abbreviations

aa	amino acid
AAV	Adeno-associated virus
AAV-HBV	Adeno-associated HBV
AdV	Adenovirus
Ad-HBV	Adeno-HBV
AML12	TGF alfa-mouse liver cells
ARCA	Anti-reverse cap analog
ASBT	apical bile salt transporter
CHB	chronic hepatitis B
Cluc	Cypridina luciferase
CsA	Cyclosporin A
CTB	Cell Titer Blue
DHBV	duck hepatitis B virus
DNA	deoxyribonucleic acid
DMSO	Dimethyl sulfoxide
dpt	days post transfection
dpi	days post infection
EC50	On centration for 50% of maximal effect
ELISA	Enzyme-Linked ImmunoSorbent Assay
Eq HBV	Equid HBV
ETV	entecavir
G	Glycine
GFP	Green fluorescent protein
HBV	hepatitis B virus
HBIG	Hepatitis B immunoglobulin
HBc	HBV core protein
HBs	HBV surface proteins
HBsAg	HBV surface antigen
L protein	Large HBV surface proteins
M protein	Medium HBV surface proteins
S protein	Small HBV surface proteins
HBeAg	hepatitis B e antigen
HBx	HBV X protein
P protein	polymerase protein
rcDNA	relaxed circular(rc) DNA

cccDNA	covalently closed circular DNA
HCC	Hepatocellular carcinoma
HCV	hepatitis C virus
HDV	Hepatitis Delta virus
HSPG	heparan sulfate proteoglycans
HuNTCP	HumanNTCP
HoNTCP	HorseNTCP
hpt	hours post transfection
hyPBase	hyperactive piggyBac transposase
IF	immunofluorescence
IFNα	interferon alpha
IL10	Interleukin 10
IP10	Interferon gamma-induced protein 10
IVT mRNA	In vitro transcribed message RNA
MFI	Mean fluorescent intensity
MOI	Multiplicity of infection
MyrB	Myrcludex B
MyrB-atto488	atto488 labelled MyrB
MyrB-atto594	atto594 labelled MyrB
N	Asparagine
NA	nucleos(t)ide analogues
NTCP	sodium-taurocholate cotransporting polypeptide
ORF	open reading frames
PEG-IFNα	pegylated-IFNα
pgRNA	pregenomic RNA
PHH	primary human hepatocytes
qPCR	Quantitative PCR
RNA	ribonucleic acid
sgRNA	subgenomic mRNAs
SNP	single nucleotide polymorphism
SVPs	subviral-particles
SOAT	Na+-dependent organic anion transporter
TDV	Tenofovir
TGFα	Transforming growth factor alpha
UTP	Uracil triphosphate
WHO	World Health Organization

G0	3-(2,3-dihydro-1H-inden-2-yl)-8-(3-furylmethyl)-1-(2methoxyethyl)-1,3,8-triazaspiro [4.5] decane-2,4-dione
A0	5-({3-[(2-ethyl-2,5-dihydro-1H-pyrrol-1-yl) carbonyl] isoxazol-5yl} methoxy) isoquinoline
A2	N, N-dipropyl-5-[(quinolin-6-yloxy) methyl] isoxazole-3carboxamide

Abstract

New therapies to cure the hepatitis B virus (HBV) infection have been limited by a lack of suitable animal models. The discovery of sodium-taurocholate co-transporting polypeptide (NTCP), bile acid transporter, has been identified to expand the selection of natural hosts for HBV. It has also allowed the generation of permissive cell lines supporting robust viral infection *in vitro*. The HBV-permissive cell lines provide a valuable tool to develop new drugs.

In this study, we first established a luciferase-NTCP co-expression-based assay to evaluate the animal species specificity of NTCP. The HBV binding and infection studies revealed that NTCPs from mammals including humans, woodchucks, ferrets, aardvark, horses, rabbits, whales, big brown bats, cats and rhinoceroses rendered HepG2 cells susceptible to HBV infection. A replacement of either HBV binding or functional domain of NTCPs from mice, macaques, pigs, or hamsters, with their counterpart in human NTCP enables or enhances viral infection in NTCP-expressing HepG2 cells. In addition, horse NTCP was the best candidate compared to all the other NTCP variants for supporting HBV infection including human NTCP.

In the second part, the capability of human NTCP and horse NTCP to mediate HBV infection was compared employing different approaches. HepG2 cell surface staining of NTCP demonstrated that horse NTCP was expressed on the plasma membrane at levels twice as high as human NTCP. Therefore, HBV particle binding was enhanced on the HepG2 cells expressing horse NTCP. Single amino acid mutation screening displayed that the residue G157 of horse NTCP increased efficiency for NTCP membrane localization. Moreover, horse NTCP rendered HepG2 cells more susceptible to HBV by increasing virus infection rates and covalently closed circular DNA (cccDNA) formation.

The third part of this thesis was to characterize the susceptibility of murine hepatocyte cell line AML12 to HBV infection upon human NTCP and horse NTCP expression. AML12 cells complemented with each of these NTCPs allowed for HBV uptake and infection, while horse NTCP also facilitated cccDNA formation. Southern blot analysis of cccDNA or relaxed circular DNA (rcDNA) proved the robust establishment of HBV infection in AML12 cells. Titration of HBV on AML12 cells expressing horse NTCP and human NTCP revealed a dose-dependent infection rate, and AML12 cells expressing horse NTCP even permitted lower titer HBV infection.

My thesis closed with an evaluation of the impacts of small molecules, naming as compounds A0, A2, and G0, on HBV infection. Compound A0 and A2 inhibited HBV infection

early events in HepG2-NTCP-K7 cells, HepaRG cells and primary hepatocytes, and G0 blocked HBV infection in HepaRG cells and primary hepatocytes. Furthermore, my results indicated that compounds A2 and G0 did not interfere with HBV binding to heparan sulfate proteoglycan (HSPG) and NTCP. Moreover, it seems that A2 interrupted HBV entry prior to the establishment of HBV infection but after HBV endocytosis on HepG2-NTCP cells and inhibited HBV endocytosis on HepaRG cells. In contrast, G0 interfered with HBV infection prior to cccDNA establishment but during later steps of uptake.

Overall, my study provides new sights into the species specificity of NTCP and identifies an advanced HBV receptor that mediates highly efficient HBV infection on human and murine hepatocyte cell lines, and identifies two chemical compounds limiting HBV infection.

Zusammenfassung

Bis heute sind neue Therapien zur Heilung einer Hepatitis-B-Virus (HBV)-Infektion durch den Mangel an geeigneten Tiermodellen eingeschränkt. Die Entdeckung des Gallensäuretransporters Natrium-Taurocholat-Cotransport Polypeptid (NTCP) hat die Auswahl an natürlichen Wirten für HBV erweitert. Dies ermöglichte auch die Erzeugung permissiver Zelllinien, die eine robuste Virusinfektion *in vitro* unterstützen. Die HBV-permissiven Zelllinien sind ein wertvolles Instrument für die Entwicklung neuer Medikamente.

In dieser Studie wurde zuerst ein Assay für die Koexpression von Luciferase und NTCP etabliert, um die Speziesspezifität von NTCP zu bewerten. Die HBV-Bindungs- und Infektionsstudien zeigten, dass NTCPs von Säugetieren wie Menschen, Murmeltieren, Frettchen, Erdferkeln, Pferden, Kaninchen, Walen, großen braunen Fledermäusen, Katzen und Nashörnern HepG2-Zellen anfällig für eine HBV-Infektion machten. Der Austausch von entweder HBV-bindenden oder funktionellen Domänen des NTCP-Rezeptors aus Mäusen, Makaken, Schweinen und Hamstern gegen ihr menschliches NTCP-Gegenstück ermöglicht oder verstärkt die virale Infektion von NTCP-exprimierenden HepG2-Zellen. Darüber hinaus war das Pferde-NTCP im Vergleich zu anderen NTCP-Varianten, einschließlich des menschlichem NTCPs, der beste Kandidat.

Im zweiten Teil dieser Studie wurde die Fähigkeit von humanem NTCP und Pferde-NTCP eine HBV-Infektion zu vermitteln in verschiedenen Ansätzen verglichen. Die HepG2-Zelloberflächenfärbung von NTCP zeigte, dass Pferde-NTCP auf der Plasmamembran doppelt so stark exprimiert wurde wie menschliches NTCP. Daher war die Bindung von HBV-Partikeln an HepG2-Zellen, die das Pferde-NTCP exprimieren, verstärkt. Das Screening einzelner Aminosäuremutationen zeigte, dass der Rest G157 des Pferde-NTCPs die Effizienz für die NTCP-Membranlokalisierung erhöhte. Darüber hinaus machte Pferde-NTCP HepG2-Zellen anfälliger gegenüber HBV, indem es die Virusinfektionsrate und die Bildung der cccDNA (covalently closed circular DNA) erhöhte.

Im dritten Teil dieser Arbeit wurde die Anfälligkeit der murinen Hepatozyten-Zelllinie AML12 für HBV-Infektionen bei Expression des menschlichem NTCPs und des Pferde-NTCPs charakterisiert. AML12-Zellen, die mit jedem dieser NTCPs komplementiert wurden, ermöglichten eine HBV-Aufnahme und -Infektion, während das Pferde-NTCP auch die Bildung der cccDNA erleichterte. Southern Blot Analysen der cccDNA oder der rcDNA (relaxed circular DNA) bewiesen die robuste Etablierung einer HBV-Infektion in AML12-Zellen. Die Titration von HBV zeigte eine dosisabhängige Infektionsrate in AML12-Zellen,

die Pferde- und menschliches NTCP exprimierten. AML12-Zellen, die Pferde-NTCP-exprimierten, ermöglichten sogar eine HBV-Infektion mit niedrigerem Virustiter.

Am Ende dieser Arbeit wurden die Auswirkungen von kleinen Molekülen, die als Komponenten A0, A2 und G0 bezeichnet wurden, auf eine HBV-Infektion untersucht. Die Komponenten A0 und A2 hemmten frühe Ereignisse der HBV-Infektion in HepG2-NTCP-K7-Zellen, HepaRG-Zellen und primären Hepatozyten. G0 blockierte eine HBV-Infektion von HepaRG-Zellen und primären Hepatozyten. Darüber hinaus zeigten die Ergebnisse, dass die Komponenten A2 und G0 eine HBV-Bindung an Heparansulfatproteoglykan (HSPG) und NTCP nicht beeinträchtigten. Des Weiteren scheint A2 den HBV-Eintritt vor der Etablierung einer HBV-Infektion, aber nach der HBV-Endozytose in HepG2-NTCP-Zellen zu unterbrechen und die HBV-Endozytose in HepaRG-Zellen zu hemmen. G0 dagegen beeinträchtigte die HBV-Infektion vor der Etablierung der cccDNA, jedoch während späteren Schritten der Aufnahme.

Zusammenfassend liefert meine Studie neue Einblicke in die Speziesspezifität von NTCP und identifiziert einen fortgeschrittenen HBV-Rezeptor, der eine hocheffiziente HBV-Infektion auf menschliche und murine Hepatozyten-Zelllinien vermittelt. Darüber hinaus wurden zwei chemische Komponenten identifiziert, die die HBV-Infektion begrenzen.

1. Introduction

Two-hundred fifty-seven million individuals suffer from chronic hepatitis B (CHB) infection worldwide with increased risk of liver cirrhosis or hepatocellular carcinoma (HCC), that lead to an estimated 820,000 deaths in 2019 (WHO 2021). A major issue with current treatments is the ineffective targeting of the viral transcriptional template in infected hepatocytes. This thesis therefore addresses the establishment of new infection models and the evaluation of novel hepatitis B virus (HBV) entry inhibitors.

1.1 Hepatitis B virus (HBV)

The following chapter introduces molecular biology, the viral entry receptor, various animal infection models, and different CHB treatment options of HBV.

1.1.1 Classification

Human HBV is the prototype of the *Hepadnaviridae* family and a small enveloped DNA virus, sharing liver tropism and a narrow species specificity (Meyer et al. 1997; Schaefer 2007; Watashi and Wakita 2015). *Hepadnaviridae* family are divided into two genera; 1. *Orthohepadnaviridae* and *2. Avihepadnaviridae* (Schaefer 2007). The *Orthohepadnaviridae* members like human HBV, woodchuck hepatitis virus (WHV) or ground squirrel hepatitis virus (GSHV) mainly infect mammals, while members of the *Avihepadnaviridae* genus like duck hepatitis B virus (DHBV) and heron hepatitis B virus (HHBV) preferentially infect birds (Summers et al. 1978; Mason et al. 1980; Schaefer 2007) .

HBV subdivides phylogenetically into nine genotypes, A–I, based on a nucleotide divergence of more than 7.5% across the whole genome sequence (Kramvis 2014; Velkov et al. 2018). HBV genotypes are distributed geographically (**Figure 1**). Genotype A exists predominantly in Europe, South Africa, and Central America. Genotypes B and C are most frequently found in Asia, Oceania, and Australia. Genotypes F and H are distributed in Southern and Central America. Genotype D can be found worldwide, whereas genotype E is most common in Western and Central Africa; genotype G, in parts of Europe and America; and genotype I, in Asia (Kramvis 2014). The proposed new genotype J was discovered in a Japanese patient in 2009 (Tatematsu et al. 2009). Additionally, HBV can be classified into nine different serological subtypes, based on the antigen variability of the surface protein (HBs), which can be categorized in four major serotypes *ayw, ayr, adw,* and *adr* (Kramvis 2014).

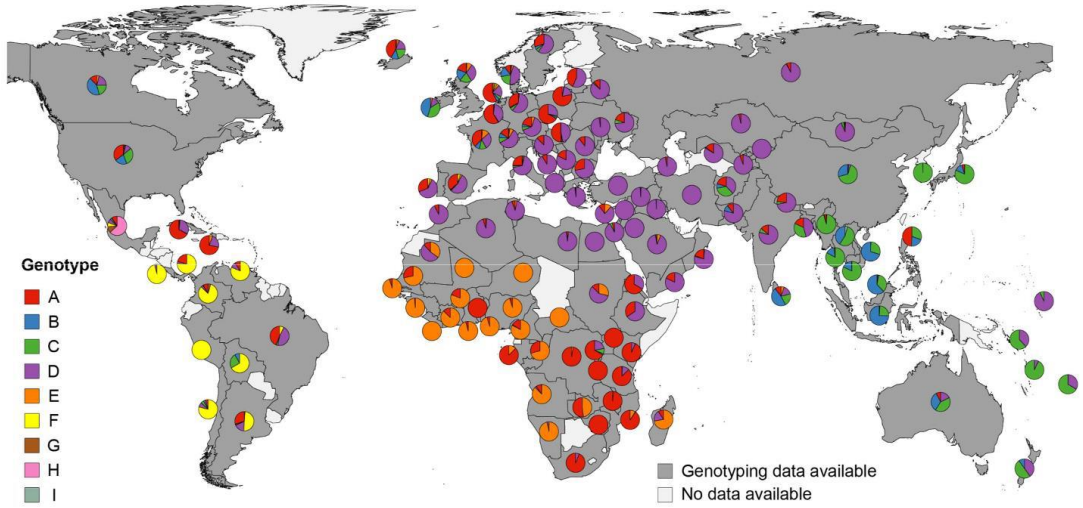

Figure 1: **Graphical representation of global HBV genotype distribution**. Pie charts reflects statistical representation of each HBV genotype in each respective region (Velkov et al. 2018).

1.1.2 Morphology

HBV infectious virions, also designated as “Dane particles,” are 42 nm in diameter (Dane et al. 1970). As depicted in **Figure 2**, HBV particles are enveloped by an outer layer containing small (S), middle (M), and large (L) HBs that are embedded in a lipid bilayer and share a C-terminal region (Nassal 2015). The icosahedral capsid is formed of 120 dimers of T3- or T4-core protein subunits (HBc) (Crowther et al. 1994). Within the capsid resides the partially double-stranded relaxed circular(rc) DNA as viral genome, bonded covalently to the viral polymerase protein (P protein) by its 5’ end of the minus strand (Gerlich and Robinson 1980; Nassal 2015). Aside from the infectious HBV particles, DNA-free subviral-particles (SVPs) are produced, termed spheres, with a size of 22 nm and filaments. Spheres are formed of S and M proteins, whereas filaments contain all three forms of HBs. Subviral-particles are produced in 1000-fold to 10,000-fold excess during viral replication, probably explaining the immune evasion mechanism (Bruns et al. 1998; Urban et al. 2014a).

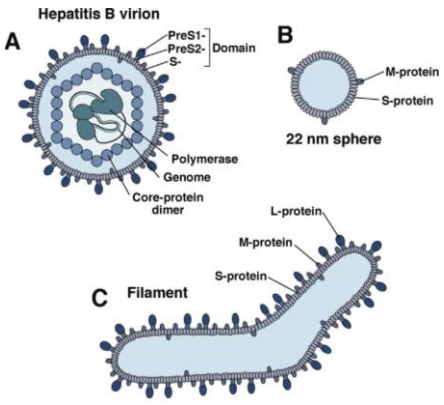

Figure 2: A schematic representation of the virion and subviral particles’ structure of HBV. (A) HBV virion, Dane particle with a DNA-containing nucleocapsid, which is enclosed in the compactly packed protein envelope comprising the L, M, and S surface protein. (B) Spherical 22 nm SVP consisting of mostly S and M proteins. (C) Filamentous SVP comprising of L, M, and S proteins (Urban et al. 2014a).

1.1.3 Genome organization

The HBV rcDNA genome has a total length of only 3.2 kb and is therefore tightly organized with four partially or fully overlapping open reading frames (ORF), termed S, C, P, and X (**Figure 3**); these frames encode for the seven viral proteins. The HBV surface protein variants (S, M, L) share the same C-terminal domain(s) but differ in the additional N-terminal extension named preS2 (for M) and preS1 (for L), respectively. ORF C encodes for the precore (preC) protein containing the entire sequence of the core protein (HBc) resembling the subunits for viral capsid plus an amino-terminal extension. PreC is proteolytically processed and secreted as hepatitis B e antigen (HBeAg) (Seeger and Mason 2015). HBeAg thereby seems important for the induction of certain immune responses, such as the down-regulation of host T-cell response to core antigen (Chen et al. 2005). The P protein encodes enzymes by ORF P for synthesis of the viral genome (reverse transcriptase, RNaseH and primer) (Seeger and Mason 2015). The non-structural HBV X protein (HBx; X) is responsible for the initiation and maintenance of viral transcription (Lucifora et al. 2011).

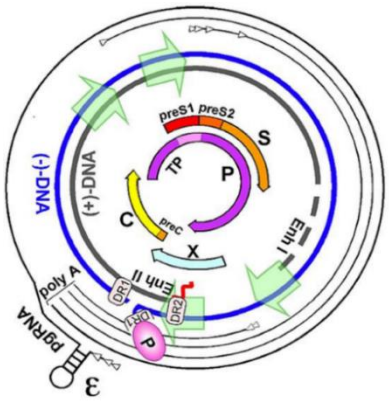

Figure 3: HBV Genome organization. Outer lines denote viral transcripts with arrow heads indicating transcription starts, where ε stands for the RNA encapsidation signal on pregenomic (pg) RNA. Green arrows depict promoters, Enh I/Enh II, transcriptional enhancers, (DR)1/DR2 direct repeats, wiggly red line RNA primer on (+)-DNA) (Nassal 2015).

1.1.4 Viral life cycle

HBV replication cycle is depicted schematically in **Figure 4**. HBV life cycle is initiated by the interaction of Dane particles with glycosaminoglycan side chains of cellular heparan sulphate proteoglycans (HPSG) (Schulze et al. 2007). Next, the myristolylated preS1 motif of the L-protein specifically binds to sodium-taurocholate co-transporting polypeptide (NTCP), which has been identified as an entry receptor for HBV and hepatitis delta virus (HDV) (Yan et al. 2012; Ni et al. 2014). The interaction of the virus with its entry receptor results in internalization via the endocytic route by clathrin- and caveolin-dependent pathways (Huang et al. 2012a; Herrscher et al. 2020; Chakraborty et al. 2020). During endocytosis, viral particles are proposed to fuse with the endosomal membrane, initiating uncoating, which is followed by the release of the genome-containing capsids into the host cytoplasm. From there they are transported to the nuclear membrane and disassembled at

the nuclear basket leading to the release of rcDNA into the nucleus (Schmitz et al. 2010). There, rcDNA is converted or repaired to fully double-stranded, covalently closed circular DNA (cccDNA), persistently located as an episome in the nucleus of the infected cells. As a transcriptional template, cccDNA serves uses the host the RNA polymerase II to produce all viral transcripts, including subgenomic mRNAs (sgRNA), the pregenomic RNA (pgRNA), and precore RNA. pgRNA offers as a template for P and for core proteins but is also reverse-transcribed by viral P protein into rcDNA in novel capsids (Datta et al. 2012; Nassal 2015; Seeger and Mason 2015). Mature rcDNA-containing capsids are either reimported into the nucleus to maintain cccDNA pool (Lucifora and Protzer 2016; Ko et al. 2018) or transported to the endoplasmic reticulum for enveloping and subsequent secretion via multivesicular bodies into the extracellular space (Ko et al. 2017).

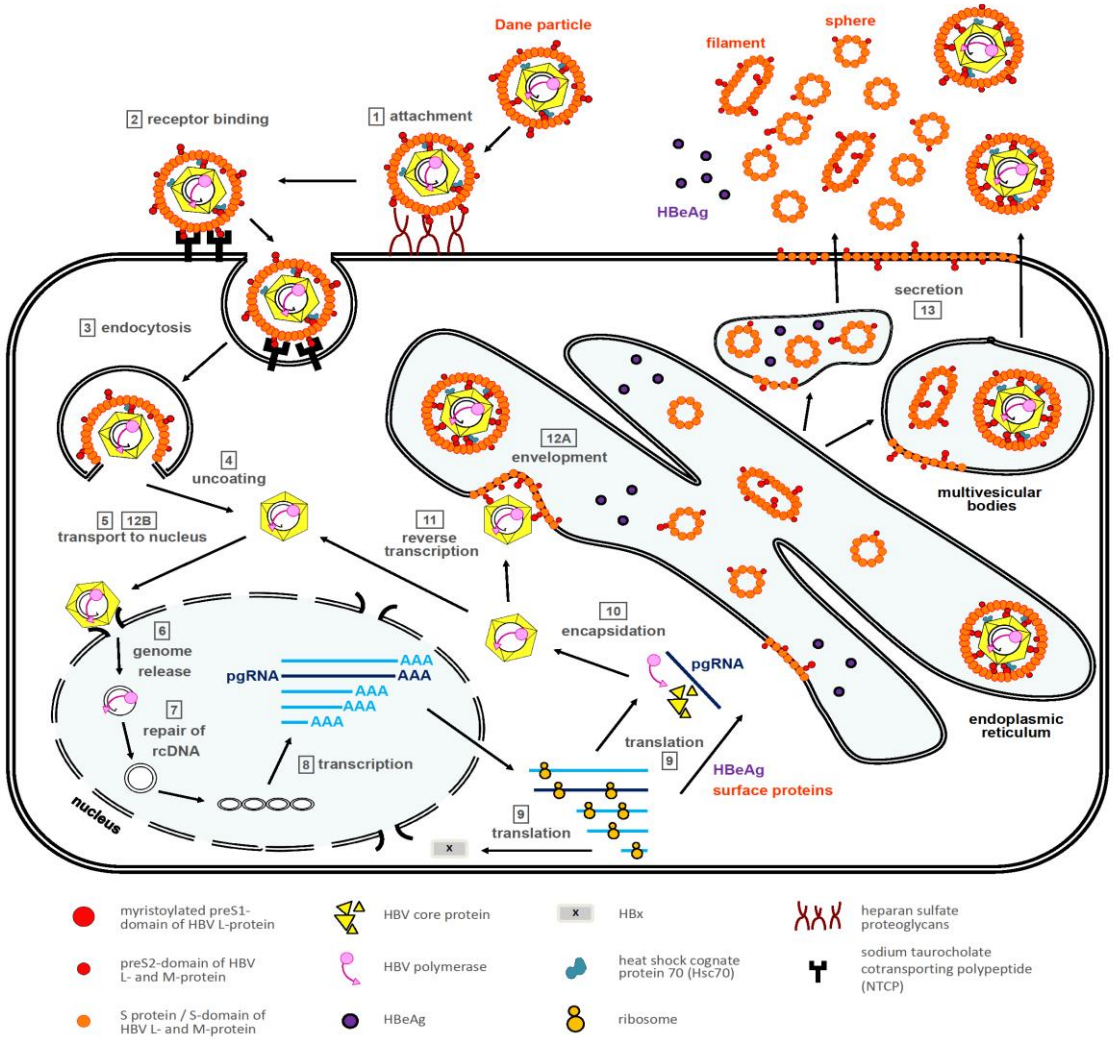

Figure 4: HBV life cycle in hepatocytes. Initial attachment of HBV to HSPG, followed by subsequent specific interaction with NTCP. Viral particles are internalized by endocytosis and uncoated, leading to the release of capsids into the cytoplasm. Next, capsids are transported to the nuclear membrane, where the genome is released into the nucleus. There, rcDNA is converted to cccDNA, which serves as a template for all viral transcripts. The pgRNA is

encapsidated together with polymerase (P protein) in newly formed capsids, where it is reverse transcribed to rcDNA. Newly formed rcDNA-containing capsids are either re-transported into the nucleus or enveloped at the endoplasmic reticulum and released via multivesicular bodies (Ko et al. 2017).

1.1.5 The cccDNA – the persistent form of HBV

HBV cccDNA is associated with cellular proteins forming an episomal minichromosome. It represents the type of viral persistence in infected hepatoma cells and lacks efficient targeting by current anti-viral treatments, for example IFN-alpha or nucleos(t)ide analogues (NA). Treatment of chronic HBV infection with such components can rarely result in a functional cure, but complete eradication of cccDNA pool is required to achieve clearance of the virus (Nassal 2015; Schreiner and Nassal 2017). The cccDNA is converted from rcDNA by removal of the viral polymerase linked to the 5′ end of the (-) strand DNA and one of the redundant sequences (either in the 3′ and 5′ end), followed by the removal of the RNA primer linked to the 5′ end of the (+) strand and completion of the viral (+) strand DNA. Finally, the DNA extremities for both (+) and (-) strands are ligated. As shown in **Figure 5**, the HBV mini-chromosome is associated with the histone proteins H3 and H2B, but only with minor levels of H4, H2A, and H1M alongside non-histone proteins (Bock et al. 2001; Nassal 2015). HBc protein binds to the CpG island of HBV cccDNA (Guo et al. 2011), potentially rearranging the chromatin architecture through the reduction of the nucleosome spacing of the nucleoprotein complexes by 10% (Bock et al. 2001). Transcription from the cccDNA template depends on histone posttranslational modification (PTM) levels demonstrating defined correlation of transcription status with certain PTM (Tropberger et al. 2015). Notably, in the absence of HBx, cccDNA appears to be rapidly silenced, whereas HBx promotes a transcriptionally active state by preventing deacetylation of cccDNA-attached histones (Lucifora et al. 2011; Rivière et al. 2015) and avoiding deposition repressive marks of cccDNA histones (Rivière et al. 2015). The cccDNA-bound H3/H4 histones acetylation status is essential for HBV replication (Pollicino et al. 2006), whereas repression is induced by methylation of cccDNA (Rivière et al. 2015). HBV cccDNA persists in infected cells in low copy numbers but is demonstrated a long half-life time. For chronically infected ducks, a mean of 10 cccDNA copies per cell (Zhang et al. 2003) and 35 days half-life time (Addison et al. 2002) were described, whereas in mean of 2.4 cccDNA copies per cell (Tropberger et al. 2015) and approx. 40 days half-life time (Ko et al. 2018) were observed for HBV. Meanwhile, it was demonstrated that maintenance of the cccDNA pool is achieved by secondary HBV infection and intracellular recycling pathways of rcDNA-containing nucleocapids (Ko et al. 2018).

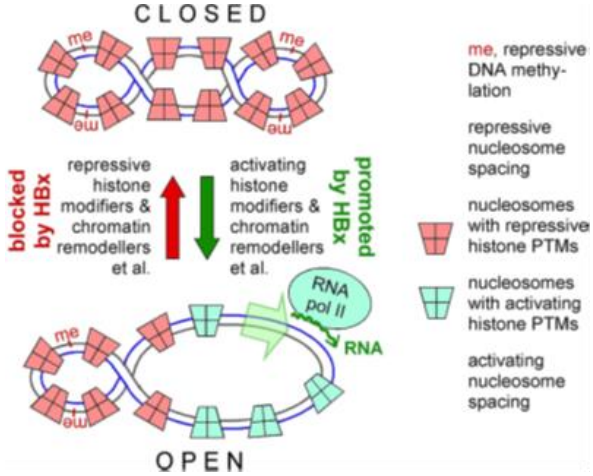

Figure 5: Epigenetics of covalently closed circular DNA. Nuclear cccDNA is associated with nucleosomes consisting of the histones H2A, H2B, H3, H4, and H1. HBx regulates translation activity by either stimulating activating modifications or blocking repressive modifications (or both) (Nassal 2015).

1.2 Sodium-taurocholate co-transporting polypeptide

NTCP, a bile acid transporter, was first identified as an important viral receptor through a combined biochemical and proteomic approach using primary cultures of treeshrew hepatocytes (Yan et al. 2012), This finding was further validated by subsequent bioinformatic analysis of comparative expression arrays (Ni et al. 2014). The long-standing questions of whether (*a*) HBV/HDV specifically infects the liver and whether (*b*) cross-species, the entry-level barrier prevents the infection of other animals with human HBV were immediately answered by the discovery of HBV receptor (Li 2015). The discovery of NTCP as viral receptor led to the establishment of new cell culture models such as HepG2-NTCP or HuH7-NTCP stably overexpressing human NTCP. These new tools enabled the investigation of HBV entry mechanisms, including visualization of the entry processes of the virus, and allowed high-throughput screenings for antiviral substances.

NTCP is encoded by human *SLC10A1* gene and is mainly associated with sodium-dependent bile acid uptake from the portal blood and important for the homeostasis of enterohepatic levels of bile acids. The expression of NTCP is highly liver-specific and regulated by microenvironment (e.g., bile acids, cytokines, and hormones) (Jung et al. 2004; Zhang et al. 2016). NTCP was shown to be rapidly downregulated in isolated primary hepatocytes, indicating for a half-life time of less than 24 h (Rippin et al. 2001; Li 2015). The NTCP gene *SCL10A1* belongs to the SCL10A transporter gene family, including six other members, but only NTCP, ASBT (apical bile salt transporter; SLC10A2), and SOAT (Na+-dependent organic anion transporter; SLC10A6) can transport the substrate, including bile salt (NTCP, ASBT) and sulphated taurolithocholate as well as sulphated steroid metabolites (SOAT) (Anwer and Stieger 2014). NTCP is embedded in the plasma membrane on basolateral/sinusoidal side of hepatocytes, while ASBT is localized at the apical membrane

of cholangiocytes, ileum, and renal proximal tubules (Anwer and Stieger 2014). Despite the sequence and structure being similar to those of NTCP, neither ASBT nor SOAT show binding of MyrB-preS1 or support HBV infection (König et al. 2014).

NTCP is a multi-span transmembrane protein with the N-terminus being exo- and C-terminus endo-cytoplasmic. The complete protein structure remains unknown; however, X-ray crystallographic studies of ASBT might indicate that NTCP has nine transmembrane domains and harbors several extracellular loops (Hu et al. 2011; Zhou et al. 2014; Yan and Li 2015). As shown in **Figure 6**, two N-linked glycosylation sites are presented, located within the exoplasmic N-terminus of NTCP, as five sites were predicted (Hallén et al. 2002). N-linked glycosylation of NTCP influences efficient NTCP localization at the plasma membrane. In addition, low cellular abundance and insufficient HBV infection were observed in HepG2 cells expressing glycosylation-deficient NTCP (Appelman et al. 2017). Interestingly, non-glycosylated NTCP expressing on differentiated HepaRG cells, can mediate culture-derived HBV infection after being introduced into the HepG2 cell line, but demonstrating differential susceptibility (Lee et al. 2018). These findings indicate that other host factors are involved in mediating HBV entry, outside of the N-linked glycosylation of NTCP. Residues 157–165 of NTCP were indicated as key determinant for preS1-NTCP interaction during NTCP discovery (Yan et al. 2012; Ni et al. 2014). The phylogenetical analysis in new world monkey NTCPs also revealed aa158 to play a significant role in HBV infection (Müller et al. 2018; Takeuchi et al. 2019). The substitution of amino acid (aa) at position 158 of the human NTCP to the monkey sequence abrogated the capacity for HBV infection, demonstrating aa158 to be a crucial position for HBV L protein binding (Takeuchi et al. 2019). Moreover, modification of mouse NTCP with the use of human NTCP to mediate HBV infection indicated residues 84–87 to be another restriction site, in addition to the 157–165 motif (Yan et al. 2013). Furthermore, the mutations of residues in NTCP associated with sodium-binding (Q68, S105N106, E257) and bile-acid binding (Q261 N262, Q293 and L294) were found to interfere with viral infection, suggesting common essential residues for substrate transport and viral entry (Yan et al. 2014; Yan and Li 2015). The single nucleotide polymorphism (SNP) S267F in Asian groups, at a frequency ranging from 3.1% to 9.2%, abolishes bile acid uptake and HBV infection, decreasing the risk of cirrhosis and HCC (Yan et al. 2014; Hu et al. 2016).

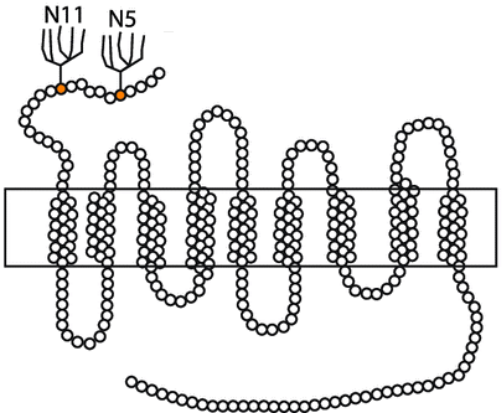

Figure 6: Structure of human NTCP. NTCP was present at the cell surface exposed N-terminus. It is a muti-span transmembrane protein located on the basolateral/ sinusoidal side of hepatocytes. N-linked glycosylation sites at N-terminus are indicated (Appelman et al. 2017).

Although the function for substrate transportation by NTCP is conserved in mammalians, the protein sequences of NTCP are specific to certain species (Yan et al. 2012). A comparison of HBV receptors, NTCP and GPC5, over millions of years of primates, rodents, and bats, revealed positive selection of HBV-binding motif in those species and different selection patterns also suggested NTCP to be a naturally-occurring genetic barrier for cross-species transmissions (Jacquet et al. 2019). The cells were rendered susceptible to HBV infection by overexpression of macaque and pig NTCP modified with the human aa157–165 or 157-167 binding motif as well as mouse NTCP harboring aa84–87 of human NTCP in HepG2 cell lines (Yan et al. 2013; Wettengel 2019; Protzer et al. 2019). The only species known to be susceptible to HBV and HDV infection are humans, chimpanzees, and a small mammal, the treeshrew. Other species either prevent infection through entry-level barriers or narrow species liver tropism. Cynomolgus macaque, rhesus macaque, and pig hepatocytes, complemented with human NTCP, allowed for the establishment of HBV infection (Lempp et al. 2017) and the *in vivo* expression of human NTCP overcame the entry barriers of macaque to HBV infection (Burwitz et al. 2017). In contrast, mice are susceptible only to HDV rather than HBV, upon expression of humanized mouse NTCP (He et al. 2015). Interestingly, the species difference was also indicated on the post-translational regulation of the plasma membrane localization of human and rodent NTCP (Anwer and Stieger 2014).

1.3 *In vitro* and *in vivo* model systems to study HBV

1.3.1 *In vitro* model systems

The shortage of reliable appropriate cell culture models and laboratory animals limited the study of HBV infection and the development of new therapies for the CHB virus infection.

The commonly used cell culture models include primary human hepatocytes (PHH), HepaRG cells, NTCP-complement hepatoma cells (HepG2-NTCP), and human hepatoma cell lines stably transfected with HBV DNA constructs (e.g., HepG2.2.15 and HepAd38). The

evaluation of PHH susceptibility to HBV infection demonstrates a physiological system allowing infection with serum and cell-culture-produced HBV particles supporting whole life cycle, especially under the condition of optimized cell culture (Gripon et al. 1988; Schulze-Bergkamen et al. 2003). However, HBV infection efficiency depends on the host's genetic background and the loss of cell polarization after culturing (Gripon et al. 1988; Glebe and Urban 2007). Primary hepatocytes isolated from the treeshrew *Tupaia belangeri* acts as an alternative for HBV infection experiments (Glebe et al. 2003) and were used as a valuable tool for the identification of NTCP as viral receptor (Yan et al. 2012). HepaRG cells display more physiological features than hepatoma cell lines. These cells are bipotent progenitor cell lines isolated from the liver tumor of a female patient suffering from HCC and hepatitis C infection (Gripon et al. 2002). The cell line exhibits specific hepatocyte functions and hepatocyte-like morphology but supports HBV infection only in the presence of corticoids and dimethyl sulfoxide (DMSO) (Gripon et al. 2002). However, the time-consuming differentiation steps of HepaRG to achieve hepatocyte-like cells and the low level of viral infection make this cell culture model impractical for high-throughput screening approaches (Hu et al. 2019).

Overexpression of NTCP on the hepatoma cell line HepG2 made the full life cycle of HBV possible in vitro, enabling HepG2-NTCP cells as an in vitro model for the study of the early stages of HBV infection, cccDNA establishment, and maintenance (Qi et al. 2016; Luo et al. 2017; Long et al. 2017; Ko et al. 2018), as well as for testing antiviral agents (Seeger and Sohn 2014; Shimura et al. 2017). HBV infection efficiency was increased with the addition of polyethylene glycol (PEG) into inoculum, and the cells were maintained in present of DMSO (Ko et al. 2018). The transformed HepG2-NTCP cells are absent of many features of human hepatocytes, influencing the susceptibility to HBV infection (Hu et al. 2019).

HepG2.2.15 cells (Sells et al. 1987) and HepAd38 cells (Ladner et al. 1997) supporting full viral gene expression and viral replication were generated by stably transfected recombinant HBV DNA constructs. HepG2.2.15 cells contain HBV DNA as chromosomally integrated sequences and episomally as relaxed circular, covalently closed, and incomplete copies of the HBV genome (Sells et al. 1987), while HepAd 38 directly constitutes cDNA of pgRNA under tetracycline-responsive CMV-IE promoter (CMVtet) control (Landmann et al. 1998; Ladner et al. 1997). Moreover, these cells have been widely used to produce cell culture-derived HBV, antiviral-drug screenings and as convenient systems for studying HBV replication including capsid assembly, as well as the cccDNA formation and secretion of virion particles. The significant shortcomings of these cells include their usage limitations and failure to reflect many aspects of response in the infected hepatocytes *in vivo*, including potential innate immune response (Hu et al. 2019).

In addition, the murine hepatocyte cell line AML12 (TGFα-mouse liver) overexpression of human NTCP was found susceptible to HBV infection. This cell line were isolated and immortalized from human-TGFα transgenic CD1 mice liver (Wu et al. 1994; Lempp et al. 2016b; Qiao et al. 2018). However, in contrast to HepG2-NTCP, AML12-NTCP cells demonstrated lower infection rates, indicating inefficient HBV entry or cccDNA establishment. Nevertheless, the discovery of murine hepatocyte cells AML12 as a HBV-permissive cell line enables the development of new mouse models for HBV infection, but also may help to identify the host factors limiting HBV infection in murine hepatocytes.

1.3.2 *In vivo* model systems

Mice are the most convenient and best-characterized small laboratory animals, but not infectable with HBV. Therefore, HBV transgenic mice expressing either single viral proteins – for example, HBsAg (Chisari et al. 1985; Chisari et al. 1986), HBeAg (Milich et al. 1990), HBcAg (Milich et al. 1994) and HBx (Kim et al. 1991), or entire viral genomes (Guidotti et al. 1995) – were generated. The HBV virions produced by these mice are infectious and morphologically indistinguishable from human-derived virions (Guidotti et al. 1999). These mice were used to investigate oncogenic potential of each viral protein, allowing the evaluation of the efficacy of antiviral agents and innate immune responses (Allweiss and Dandri 2016; Hwang and Park 2018). However, since the HBV genome is integrated, full clearance of the virus cannot be achieved in these models. To overcome the limitations of HBV transgenic mice, vectors are used to introduce HBV DNA into mouse livers.

Two types of vectors contain HBV genomes, based on plasmids delivering adenovirus (AdV)- or adeno-associated viruses (AAV). HBV protein production can be observed up to three months after intravenous injection of high doses of adenoviral vectors containing HBV (Ad-HBV). High doses of Ad-HBV injection mimicking an acute infection result in strong B-cell and T-cell mediated responses against HBV proteins and the AdV itself (Sprinzl et al. 2001; Hartman et al. 2007; Freyend et al. 2011), followed by HBV clearance. In contrast, low doses of Ad-HBV lead to persistent infections in immune-competent mice, resembling chronic infection of HBV. The adeno-associated virus–HBV (AAV-HBV), in general, mimics chronic HBV infection and does not induce certain immune responses, resulting in HBV persistence in injected immune-competent mice (Huang et al. 2012b). Since these mice establish an immune tolerance to HBV, they can be used to develop therapeutic HBV vaccine. In addition, injection of mice with AAV-HBV results in establishment of cccDNA that is distinguishable with injected AAV-HBV genome (Lucifora et al. 2017; Ko et al. 2021; Xu et al. 2021). Therefore, mice injected with AAV-HBV could provide a unique platform for studying HBV cccDNA and developing novel antivirals against HBV infection. Aside from

viral vectors, previous approaches used plasmids containing overlength HBV DNA, delivered using hydrodynamic injection to allow transient gene expression in the hepatocytes. Such a delivery approach is very stressful for the animals and could lead to significant liver damage (Kobayashi et al. 2004). However, as with Ad-HBV, hydrodynamic injection of the plasmids containing HBV DNA results in high levels of HBV replication, high serum DNA, and strong immune response, leading to a rapid clearance of HBV (Yang et al. 2002).

In contrast to transgenic or transduced mouse models, human liver-chimeric mice are generated by engraftment of human hepatocytes. To achieve the engraftment and reconstitution of mouse liver with PHH, requirements must be met: the destruction of endogenous murine hepatocytes to create the space and regenerative stimulus, as well as the reduction of immunity to enable the survival of transplanted xenogeneic hepatocytes (Allweiss and Dandri 2016). The most widely used human liver chimeric mouse models are the albumin-urokinase-type plasminogen activator (alb-uPA)/severe combined immunodeficiency (SCID) mouse and triple knockout $FAH^{-/-}RAG2^{-/-}IL2RG^{-/-}$ (FRG) mouse (Mercer et al. 2001). These mice support HBV infection and cccDNA formation in transplanted hepatocytes; they are therefore useful for the study of *in vivo* viral infection and related diseases. However, due to the deficiency of their immune system, they are unsuitable for the study of immune responses induced by HBV or vaccine development.

1.4 Antiviral treatment for CHB

1.4.1 Current treatment for CHB

No specific treatment exists for acute HBV infection, since it is a self-limiting disease. Therefore, maintaining adequate comfort and nutritional balance and avoiding unnecessary medications are more carefully considered than the treatment itself in the clinic (WHO 2021). For CHB, the current treatments contain mainly two classes: interferon alpha (IFNα) or pegylated-IFNα (PEG-IFNα) and nucleos(t)ide analogues (NA), such as entecavir (ETV), lamivudine (LAM), adefovir, telbivudine, tenofovir (TDV), and tenofoviralafenamid (TFA) (Rajbhandari and Chung 2016).

Treatment with IFNα or PEG-IFNα can eliminate cccDNA in different ways. Firstly, IFNα as a cytokine, triggers innate and adaptive immune responses, eliminating the cccDNA (Bloom et al. 2018). Secondly, treatment with IFNα can induce transmembrane proteins (IFITMs), a triparticle motif-containing protein 5 alpha (TRIM5α), and especially APOBEC3 family proteins such as APOBEC3A or APOBEC3B. Deamination by these proteins gives rise to

apurinic/apyrimidinic (AP) sites in the cccDNA, leading to cccDNA degradation, initiated by the activation of the TNT receptor superfamily member lymphotoxin (LT)-β receptor (Lucifora et al. 2014; Wang et al. 2021). In addition, IFNα indirectly represses cccDNA transcription by targeting enhancer 1/promoter region of the HBx gene, and effects on epigenetic modification of cccDNA also lead to repression of HBV (Wang et al. 2021). However, long-term IFNα administration is inefficient for entire seroconversion, with only 38.8% of patients who can experience HBeAg seroconversion (Wang et al. 2021). Additionally, IFNα has severe side effects such as fatigue, bone marrow suppression, depression, or the unmasking of autoimmune diseases, as can be observed in treated, chronic HBV infection patients (Zoulim et al. 2016).

TDV and ETV, as oral drugs, are recommended as first-line monotherapies for treatment of CHB by the WHO (WHO 2021). TDV and ETV are effective antiviral drugs for CHB, as they target reverse transcriptase and HBV polymerase, respectively (Rivkin 2005; Marcellin et al. 2008; Langley et al. 2007). Treatment with ETV or TDV in HBeAg-positive yielded a loss of HBV DNA in 67% and 76% of patients, respectively, while HBeAg seroconversion was observable in 21% of patients for both treatments after one year (Rijckborst et al. 2011). In an HBeAg-negative patient, the HBV DNA was undetectable in 90% and 93% of patients post-treatment (Rijckborst et al. 2011). In addition, it has been confirmed that TDV is effective in CHB patients whose treatments with previous NAs had failed (Marcellin et al. 2008; Rijckborst et al. 2011).

1.4.2 HBV entry inhibitors

Aside from these approaches described above, novel therapies aiming to interfere with HBV life cycle (e.g., HBV entry, translation, capsid assembly and HBsAg secretion) and to activate innate and adaptive immunity have been investigated in humans (Fanning et al. 2019). As this thesis focuses mainly on the HBV entry, the following chapter concentrates on HBV entry inhibitors.

Either blockage of the HBV envelop protein or host cellular HBV receptor are suited to reduce HBV infection at the entry level. During HBV infection, specific neutralizing antibodies targeting either the antigenic loop/preS1-region of L-, M- or S-HBsAg can interfere with the attachment to HSPG on hepatocytes or the preS1-region that block the binding to NTCP (Corti et al. 2018; Hehle et al. 2020). Hepatitis B immunoglobulin (HBIG) was first used in liver transplantations for HBV positive patients (Samuel et al. 1993). The long-term treatment with HBIG after transplantation decreased the reinfection of graft tissue and significantly improved patient survival rates. In addition, combined treatment with HBIG and HBV vaccines benefits new-borns, preventing vertical transmission from mother to child (Lempp

and Urban 2014; Urban et al. 2014b). IgGs from HBsAg specific memory B cells encode various neutralizing HBV antibodies that recognize different HBsAg epitopes suppressing viremia in vivo HBV mouse models and allowing post-therapy control of the infection (Hehle et al. 2020). However, monoclonal antibodies remain under investigation; for example, S protein specific antibodies entered clinical trials reporting viral suppression and HBsAg clearance post-treatment.

The novel HBV entry inhibitor, Myrcludex B (MyrB), contains aa2–48 of preS1-domain of HBV L-protein that specifically binds to NTCP, therefore interfering with HBV/HDV binding to their specific receptor NTCP and blocking HBV/HDV entry into hepatocytes (Petersen et al. 2008; Meier et al. 2013; Yan et al. 2012; Ni et al. 2014). Since this blockage is highly specific, MyrB can be used as a potential drug in treatment of HBV, but especially HDV (Cheng et al. 2021). This potential was confirmed in clinical trials, in which MyrB demonstrated a 2.84-fold decrease of HDV RNA levels after 48 weeks of treatment. This effect was enhanced through a combination approach with IFNα over the same dosing period and increased amounts of MyrB (a 4.81 log decrease for 2 mg MyrB and a 5.59 log decrease for 5 mg MyrB) (Fanning et al. 2019). In 2020, the European Union (EU) approved MyrB, whose commercial name is Hepcludex, as a first-in-class entry inhibitor for chronic HDV infection applied for HDV-RNA-positive adult patients as well as compensated liver diseases (Gilead 2020; Kang and Syed 2020). Another HBV entry inhibitor is Cyclosporin A (CsA), which has been identified to suppress the replication of various viruses, including HBV (Watashi et al. 2014). CsA was demonstrated to target the binding between NTCP and HBV L proteins, significantly reducing HBV internalization, but it also has slight effects on the attached HBV DNA (Nkongolo et al. 2014; Watashi et al. 2014). In addition, CsA-derivate SCYX1454139 was identified as harboring higher anti-HBV potency, with a median inhibitory concentration of <0.2 µM (Watashi et al. 2014).

1.5 Aims of the study

The natural hosts of HBV are only humans and chimpanzees. An explanation of this strict host-tropism can be offered through either a species-specific NTCP protein sequence or certain host factors limiting HBV infection and cccDNA establishment. Since current available antiviral treatments are unsuitable to eradicate established cccDNA, targeting HBV replication, especially HBV entry, represents a promising approach by which to interfere with HBV infection. Therefore, the overall aim of this thesis is to analyze the NTCP's species specificity for animals of interest and to enable the development of new HBV animal models and entry inhibitors.

The first aim of this thesis was to define which animal NTCP permits HBV infection and which domains of NTCP contributing to species-specific entry-barriers. Therefore, MyrB-atto488 staining and HBV infection should be performed on HepG2 cells transfected with selected animal NTCP, to define whether the respective NTCP supports HBV binding and infection.

The second aim was to further characterize the physiology of the horse NTCP, which demonstrated enhancement towards HBV infection, as compared to the human variant. For that purpose, hepatoma cells should be transfected with horse NTCP variants. In addition, HepG2-humanNTCP and HepG2-horseNTCP cell lines should be generated and used to depict the effect of HBV infection mediated by horse NTCP, to investigate which domains of horse NTCP promote HBV infection and which entry steps are supported.

The third aim of this work was to analyze whether the expression of horse NTCP enhances HBV infection in murine hepatocyte cell lines. Transfection of IVT mRNA should be used to express similar amounts of human and horse NTCP proteins. Subsequent infection with HBV should be quantified by HBV infection parameters, and cccDNA formation should be detected by southern blot.

The final aim of this thesis was to evaluate prescreened, novel HBV entry inhibitors. Therefore, HepG2-NTCP cells, HepaRG cells, and PHH cells were to be used to evaluate the inhibition effects of different compounds. To this end, it should be analyzed which step of viral entry is blocked and whether this effect applies for all cell lines. Furthermore, a potential synergic effect to inhibit HBV entry and stimulate adaptive immune response should be investigated.

2. Results

2.1 Species specificity of NTCP for HBV infection

2.1.1 Establishment of NTCP expression and quantification systems

Sections 2.1.1 and 2.1.2 were completed in collaboration with Dr Wettengel, and some of the results in section 2.1.1 have also been reported in Dr Wettengel's Ph.D. thesis (Wettengel 2019).

As mentioned in that thesis, the lack of specific NTCP detection antibodies for Western blots or immunofluorescence (IF) staining for different species variants stimulated the generation of the vector pcDNA_CMV_Cluc_Linker_dNTCP (P-Cluc-dNTCP). This construct allows for the co-expression of NTCP and Cypridina luciferase (Cluc), connected via a linker sequence consisting of a furin sequence, a V5 epitope, a GSGS linker, and a T2A sequence (**Figure 7A**). Since Cluc is secreted in the supernatant of transfected cells, expression of Cluc and linked NTCP can be easily measured.

To check whether the Cluc and the NTCP are co-expressed, HepG2 cells were transfected with P-Cluc-humanNTCP (P-Cluc-hNTCP). Cluc expression in the supernatant was measured three days post transfection (dpt). Control vector (P-Cluc), which expressed only Cluc, served as positive control (**Figure 7B**). In addition, hNTCP protein expression was detected by a Western blot. HepG2-NTCP cells used as positive control (**Figure 7C**). The results demonstrated that Cluc and NTCP were both expressed. To confirm membrane localization of NTCP as well as specific HBV-NTCP interactions, atto488-labelled MyrB was used. MyrB containing aa2–48 of preS1-domain of HBV L-protein interacts specifically with aa157–165 of NTCP (Gripon et al. 2005; Yan et al. 2012; Yan et al. 2013; Zhong et al. 2013; Ni et al. 2014) (**Figure 7D**). Human NTCP linked to Tdtomato served as a positive control. The results indicated expressed NTCP localizing in the plasma membrane. To analyze the function of NTCP as HBV receptor, P-Cluc-hNTCP transfected HepG2 cells were differentiated for two days. Differentiated NTCP expressing HepG2 cells were inoculated with either radioactive labelled bile acids (taurocholate [^{3}H]) for 15 min, or HBV particles at an multiplicity of infection (MOI) of 1000 vp/cell for 24 h. Internalized radioactive bile acids (**Figure 7E**) and HBeAg secreted at four and seven days post infection (dpi) (**Figure 7F**) were detected, demonstrating that the expressed NTCP constructs were functional for bile acid uptake and HBV infection.

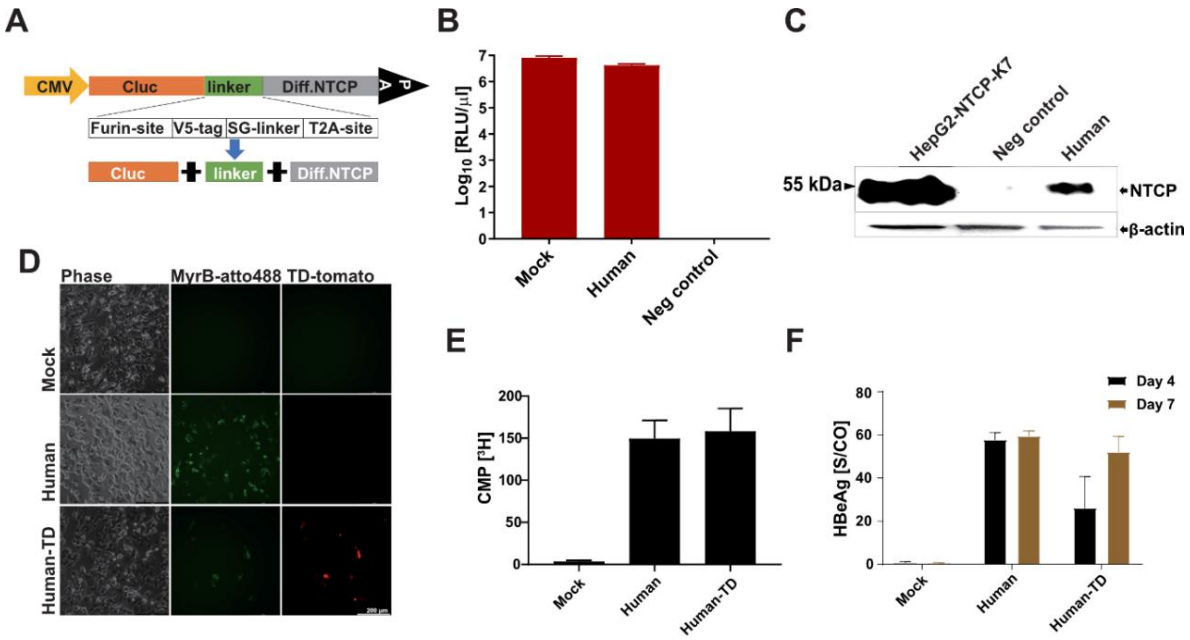

Figure 7: Evaluation of the NTCP co-expression construct. (**A**) Construction of Cluc and NTCP co-expression plasmid connected via a linker sequence containing a furin sequence, a V5 epitope, a GSGS linker and a T2A sequence. HepG2 cells were transfected with P-Cluc-hNTCP and analyzed at 3 dpt. Cluc expression by luciferase assay (**B**) and NTCP protein expression by western blot (**C**) were measured at 3 dpt. (**D**) Fluorescence images of P-Cluc-hNTCP transfected HepG2 cells were stained with MyrB-atto488 at 3 dpt. (**E**) Uptake of ^{3}H taurocholate was determined at 3 dpt in P-Cluc-hNTCP transfected HepG2 cells. Measurement was performed using a scintillation analyzer. (**F**) P-Cluc-hNTCP transfected HepG2 cells were differentiated for two days and inoculated with HBV particles at an MOI of 1000 vp/cell in the presence of PEG for 24 h before removal of the inoculum. Secreted HBeAg was detected at 4 and 7 dpi. Data represent one experiment as technical triplicates.

To further validate the co-expression approach, we generated constructs encoding NTCPs from diverse species. Therefore, we obtained the sequences from public databases for the mouse (Yan et al. 2013), woodchuck (Fu et al. 2017), guinea pig (Caroline Gähler 2011), capuchin (Carvalho Dominguez Souza et al. 2018), gibbon (Bancroft et al. 1977), ferret (Wettengel 2019), macaque (Müller et al. 2018; Wettengel 2019), and tupaia (Yan et al. 2012) as well as pig (Protzer et al. 2019). We compared their functional motif (aa80 to 90) and binding region sequences (aa150 to 180) with corresponding human residues (**Figure 8A**). To address the HBV binding capabilities and subsequent susceptibilities for viral infection, the NTCP sequences of each species were inserted into the P-Cluc and transfected into HepG2 cells. Protein expression, binding capability, and HBV infection were analyzed using either MyrB-atto488 staining or inoculation with HBV particles at an MOI of 1000 vp/cell for 24 h. The results indicated that the NTCPs from mouse, woodchuck, capuchin, ferret and tupaia could bind with MyrB-atto488 (**Figure 8B**), but only woodchuck, ferret, and tupaia NTCPs rendered HepG2 susceptible to HBV infection. In contrast, the guinea pig, gibbon, macaque, and pig NTCP neither bound with MyrB-atto488 nor mediated HBV infection, though Cluc levels showed comparable expression levels (**Figure 8C**).

Woodchuck and ferret NTCPs permitted only low HBV infection (**Figure 8C**). The NTCPs of guinea pig, gibbon, macaque, and pig lacked an interaction with MyrB-atto488, thereby preventing HBV entry and infection. In parallel, radioactive labelled bile acids uptake was determined in NTCP expressing HepG2 cells. Bile acid uptake was detected in mouse, woodchuck, capuchin, ferret, macaque, tupaia, and pig NTCP expressing HepG2 cells (**Figure 8D**), but with low levels of mouse NTCP expressing HepG2 cells and even undetectable levels for guinea pig and gibbon NTCP expressing HepG2 cells (**Figure 8D**).

In summary, expression of NTCP from different species using our panel of Cluc-NTCP co-expression plasmids was established, and the function of NTCP for bile acid uptake and to enable HBV infection was evaluated. These results demonstrated that the constructs expressing Cluc-NTCP coupled proteins are sufficient for the evaluation of species-dependent HBV/NTCP interactions and HBV infection mediated by diverse NTCPs.

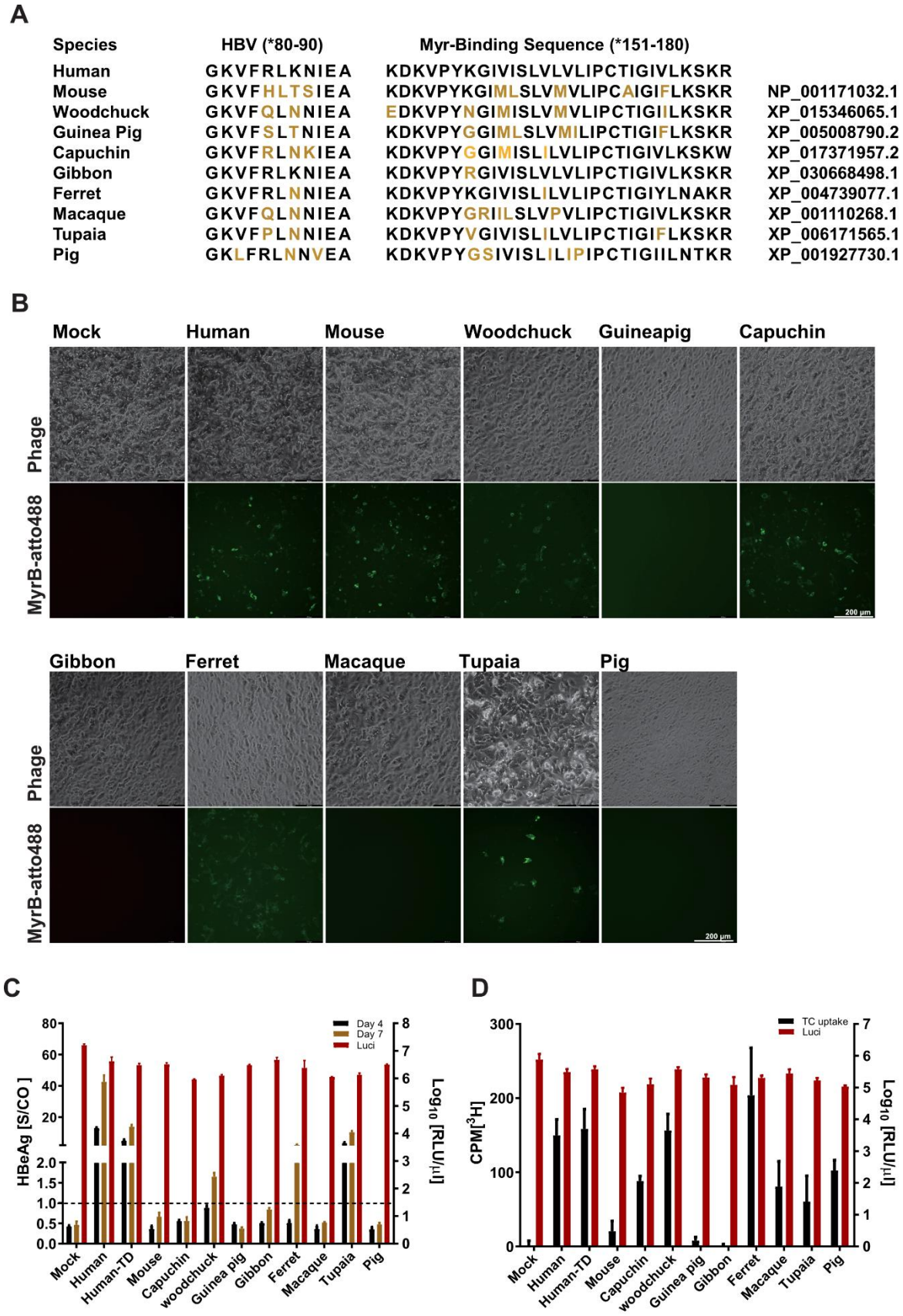

Figure 8: Analysis of various NTCPs based on NCBI database. (**A**) Sequence comparison of the functional motif (aa 80 to 90) and binding region sequences (aa150 to 180) with corresponding human residues of selected NTCP based on GenBank database are described. (**B**) Representative fluorescence images of P-Cluc-dNTCP transfected HepG2 cells stained with

MyrB-atto488 at 3dpt are shown. (**C**) Cluc-expression (3 dpt) and HBeAg (4 and 7 dpi) of P-Cluc-dNTCP-transfected HepG2 cells were measured. (**D**) Cluc-expression and uptake of ^{3}H taurocholate were determined 3 dpt using P-Cluc-dhNTCP-transfected HepG2 cells. Measurement of ^{3}H taurocholate was performed using the scintillation analyzer. Data represent one experiment as technical triplicate.

2.1.2 Analysis species specificity of NTCP for HBV infection

Since the preliminary experiments demonstrated robust results, additional NTCP sequences of interesting species were compared with corresponding human residues concerning the functional motif and the binding region (**Figure 9A**). The functional motif and the binding region of NTCP for listed animals are conserved, except for the NTCPs from the duck, clawed frog, and zebrafish (**Figure 9A**). To analyze NTCP capability to bind HBV and subsequent render HepG2 cells susceptible to HBV infection, as well as bile acid uptake, P-Cluc-NTCPs of all species were generated and transfected into HepG2 cells. Again, HBV binding and infection were detected either by MyrB-atto488 staining or inoculation with HBV particles at an MOI of 1000 vp/cell. HBeAg expression was measured at 4 and 7 dpi. Bile acids uptake was determined through a measurement of ^{3}H taurocholate after 15 min incubation. The results showed that NTCPs from horse, rabbit, whale, big brown bat, cat, rhinoceros, aardvark, and hedgehog were expressed at comparable levels (**Figure 9C**), demonstrating binding with MyrB-atto488 (**Figure 9B**). They rendered HepG2 cells susceptible to HBV infection (**Figure 9C**) and mediated bile acid uptake (**Figure 9D**). In contrast, NTCPs from goat, hamster, cow, dog, seal, and little brown bat were able to bind with MyrB-atto488 (**Figure 9B**), but HBV infection were not observed, even though NTCP expressions were comparable (**Figure 9C**). NTCPs from dolphin, duck, clawed frog, and zebrafish did not demonstrate an interaction with MyrB-atto488 (**Figure 9B**), thereby preventing HBV infection (**Figure 9C**). In the meantime, bile acid uptake of the NTCPs from goat, hamster, cow, dog, seal, dolphin, and clawed frog but not from little brown bat, duck and zebrafish were observed (**Figure 9D**). This absence might be due to the high diversity of the NTCP sequence. Altogether, these data further demonstrate that NTCP harbors two crucial domains that responsible to binding (aa157-167) and internalization (aa84-87) of HBV. The binding and internalizing function of the two domains for HBV seems to be species-specific. The data reveals that the NTCPs from horse, rabbit, whale, big brown bat, cat, rhinoceros, and aardvark support the internalization of HBV, rendering hepatocytes susceptible to HBV upon the expression of these NTCP variants. Therefore, it would also be interesting to check the susceptibility of hepatocytes from those animals, to improve knowledge of HBV hosts, identify host factors, or develop new infection models for HBV.

A

Species	HBV (*80-90)	Myr-Binding Sequence (*151-180)	NCBI Number
Human	GKVFRLKNIEA	KDKVPYKGIVISLVLVLIPCTIGIVLKSKR	NP_003040.1
Horse	GKVFQLNNVEA	KDKVPYGGIVISLILVLIPCTIGIFLNAKR	XP_001500613.1
Rabbit	GKVFRMNNIEA	KDKVPYGGIMISLVMILIPCTIGIILKSKR	NP_001076237.1
Whale	GKVFQLNNVEA	KDKVPYGGIIISLILILIPCTIGIILKSKR	XP_007184433.1
Big brwon bat	GKLFRLNNIEA	KDKVPYGGIVLSLILTLVPCTIGIFLNAKR	XP_008137122.1
Cat	GKVFQLNNIEA	KDKVPYGGIVISLILVLIPCATGIFLNAKR	XP_003987831.1
Rhinoceros	GKVFRLNNVEA	KDKVPYGGIVISLILVLIPCTIGIFLNAKR	XP_004426350.1
Tuhnik	GKLFRLNNIEL	KDKVPYGGIVISLVLVLIPCSIGIFLNAKR	XP_007940520.1
Hedgehog	GKVFRLNHIEA	KDKVPYKGIVVSLVLVLIPCTMGILLNAKR	XP_007535314.1
Goat	GKFFQLNNVEA	KDKVPYGGIVISLFLILIPCTIGIILKSKR	XP_005686078.2
Hamster	GKVFHLKPIEA	KDKVPYGGIMISLVMVLIPCSLGIFLKTKR	XP_005072871.1
Cow	GKFFQLNNVEA	KDKVPYGGIMISLILILIPCTIGIILKSKR	NP_001039804.1
Dog	GKVFRLNNIEA	KDKVPYKGIVSSLVLVLIPCTIGIFLKAKR	XP_038529936.1
Seal	GKVFQLNNIEA	KSKIPYKGIVISLVLVLIPCTIGIFLNAKR	XP_021535576.1
Little brown bat*	GKLFRLNNIEA	KDKVPYGGIVLSLIMILIPCTIGIFLNAKR	XP_023611648.1
Dolphin	GKVFQLNNVEA	KDKVPYGGNIMISLILILIPCTIGIILKSKR	XP_026967429.1
Duck*	GKLFQLGPTES	KGKVPYKGIITSLTLMLIPCAIGIILNEKK	XP_012956913.3
Clawed Frog*	VHIFQLTTTES	HNAVPFEKIIEILVLTIFPCCTGILIKTKR	XP_018086602.1
Zebrafish*	ANLFRLSPMES	VDFVPFTGIIFSLILILVPCGIGILLNYRV	XP_690745.4

B

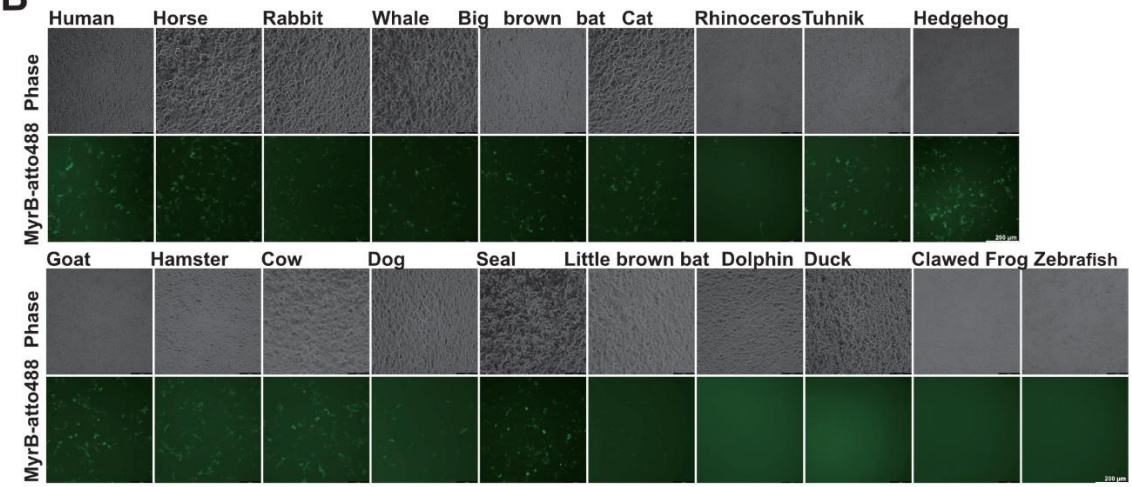

C

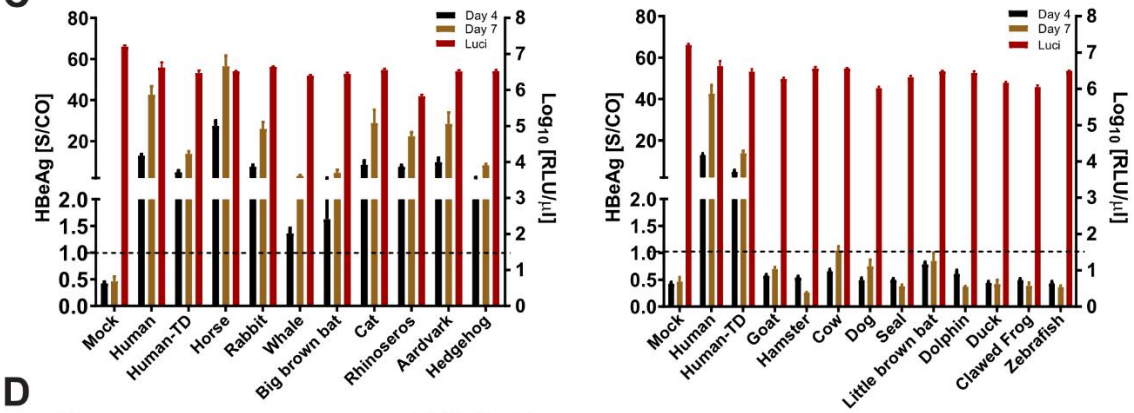

D

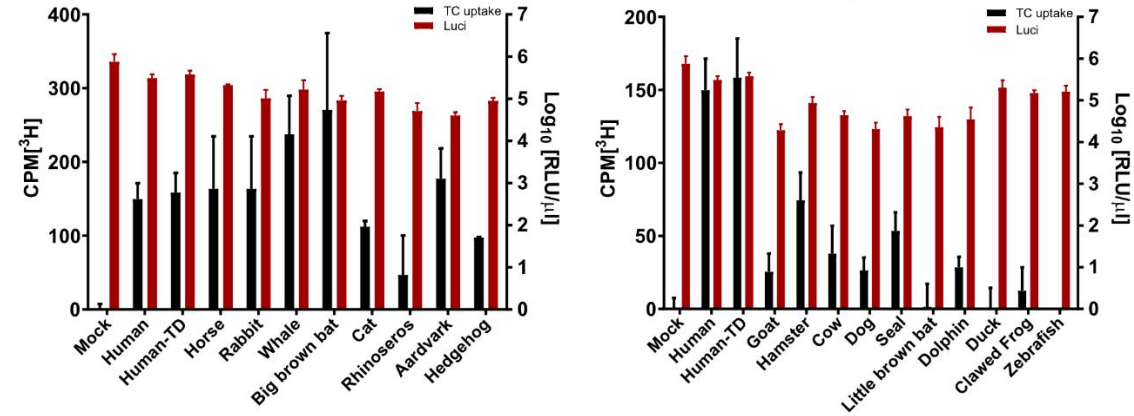

Figure 9: Comparison of diverse NTCPs from various species. (**A**) Sequence comparison of the functional motif (aa80 to 90) and binding region sequences (aa150 to 180) corresponding to human residues of selected NTCPs by the GenBank database. (**B**) Fluorescence images of P-Cluc-dNTCP transfected-HepG2 cells stained with MyrB-atto488 at 3 dpt. (**C**) Cluc-expression on P-Cluc-dNTCP transfected HepG2 cells at 3 dpt and secretion of HBeAg at 4 and 7 dpi were measured. (**D**) Cluc-expression and uptake of ^{3}H taurocholate were determined at 3 dpt in P-Cluc-dNTCP transfected HepG2 cells. Measurement of ^{3}H taurocholate was performed using a scintillation analyzer. Data represent one experiment as technical triplicates. Both domains of little brown bat, duck, clawed frog, and zebrafish are not located in the aa80–90 and aa150–180, due to sequence species specificity.

2.1.3 Modification of NTCPs for HBV infection

The NTCPs permitting HBV infection can be characterized by harboring the conserved functional domains aa84–87, 84 R/Q, and 87K/N, as well as HBV binding domains aa157–165 and 158G (Yan et al. 2013; Müller et al. 2018; Takeuchi et al. 2019). NTCP variants lacking the essential domains for infection with HBV were replaced with homologous counterparts leading to infection to generate chimeric NTCP. The ability of the chimeric NTCPs to mediate HBV infection and bile acid uptake were measured by transfection of the Cluc-chimeric-NTCPs co-expression constructs into HepG2 cells, following with either inoculation with HBV particles at an MOI of 1000 vp/cell or ^{3}H taurocholate for 15 min. Measurement of HBeAg was performed at 4 and 7 dpi, and bile acids uptake was determined after 15 min incubation. Pig and macaque NTCPs share high sequence similarity with human NTCP orthologs (**Figure 10A**), but reduced capability to bind HBV particles, which impeded HBV infection (**Figure 9B and C**). In contrast, with the substitution of the HBV binding parts of pig and macaque NTCP by the human NTCP HBV binding part (macaque-human and pig-human chimeric NTCP), these chimeric NTCPs became capable of binding HBV particles and supporting subsequent HBV infection (**Figure 10A and B**) (Wettengel 2019; Protzer et al. 2019). In addition, substituting the HBV binding parts of pig and macaque NTCP to the human NTCP HBV binding part did not change bile acid uptake capability (**Figure 10D**).

A

Species	HBV (*80-90)	Myr-Binding Sequence (*151-180)
Human	GKVFRLKNIEA	KDKVPYKGIVISLVLVLIPCTIGIVLKSKR
Macaque	GKVFQLNNIEA	KDKVPYGRIILSLVPVLIPCTIGIVLKSKR
Pig	GKLFRLNNVEA	KDKVPYGSIVISLILIPIPCTIGIILNTKR
Macaque-Human	GKVFQLNNIEA	KDKVPYKGIVISLVLVLIPCTIGIVLKSKR
Pig-Human	GKLFRLNNVEA	KDKVPYKGIVISLVLVLIPCTIGIVLKSKR

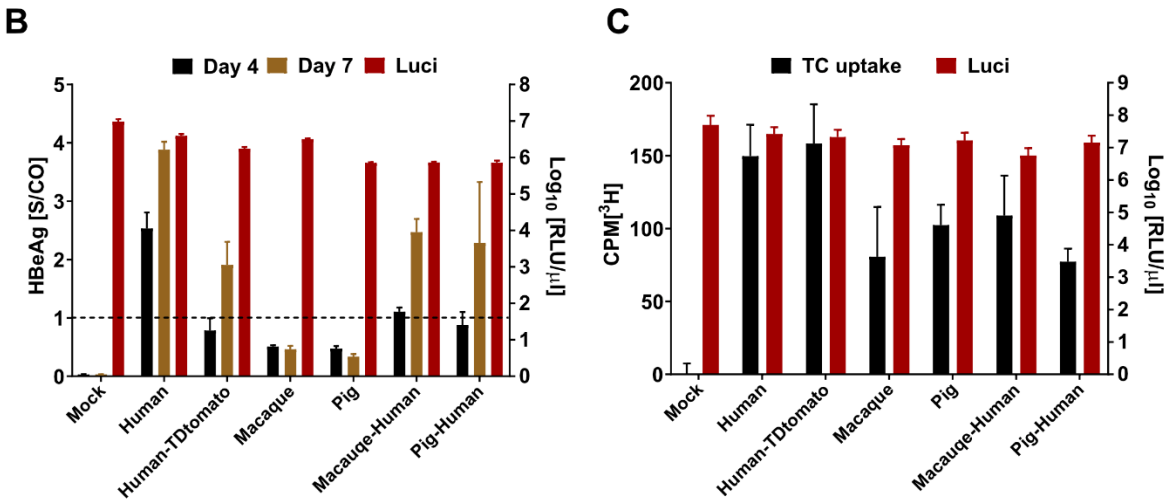

Figure 10: Modification and determination of functional domains of NTCPs supporting HBV infection. (A) Schematic representation of macaque-human and pig-human chimeric NTCPs. **(B)** Cluc-expression on P-Cluc-dNTCP transfected HepG2 cells at 3 dpt and secreted HBeAg at 4 and 7 dpi were measured. (**C**) Cluc-expression and uptake of ^{3}H taurocholate were determined at 3 dpt in P-Cluc-dNTCP transfected HepG2 cells. Measurement of ^{3}H taurocholate was performed using a scintillation analyzer. Data represent one experiment as technical triplicates.

In contrast, for the NTCPs supporting the binding of MyrB-atto488 but lacking a support of HBV infection, HBV functional motifs were modified to test whether they could obtain the capability to mediate HBV infection (**Figure 11A**). Mouse and hamster NTCP interacted only with MyrB-atto488, but impaired HBV entry (**Figure 9B and C**). Therefore, point mutations were inserted into the functional motif residues at 84–87 of mouse to 85R-86K-87N (Yan et al. 2013) and 84–87 of hamster to 84R–87N. Repetition of the infection experiment demonstrated, such that modifications supporting subsequent infection of HBV were indicated by HBeAg expression at 4 and 7 dpi (**Figure 11B**). Meanwhile, bile acid uptake was not abolished with those point mutations in mouse and hamster NTCPs (**Figure 11C**).

A

Species	HBV (*80-90)	Myr-Binding Sequence (*151-180)
Human	GKVFRLKNIEA	KDKVPYKGIVISLVLVLIPCTIGIVLKSKR
Mouse	GKVFHLTSIEA	KDKVPYKGIMLSLVMVLIPCAIGIFLKSKR
Hamster	GKVFHLKPIEA	KDKVPYGGIMISLVMVLIPCSLGIFLKTKR
MouseH84R-T86K-S87N	GKVFRLKNIEA	KDKVPYKGIMLSLVMVLIPCAIGIFLKSKR
HamsterH84R-P87N	GKVFRLKNIEA	KDKVPYGGIMISLVMVLIPCSLGIFLKTKR

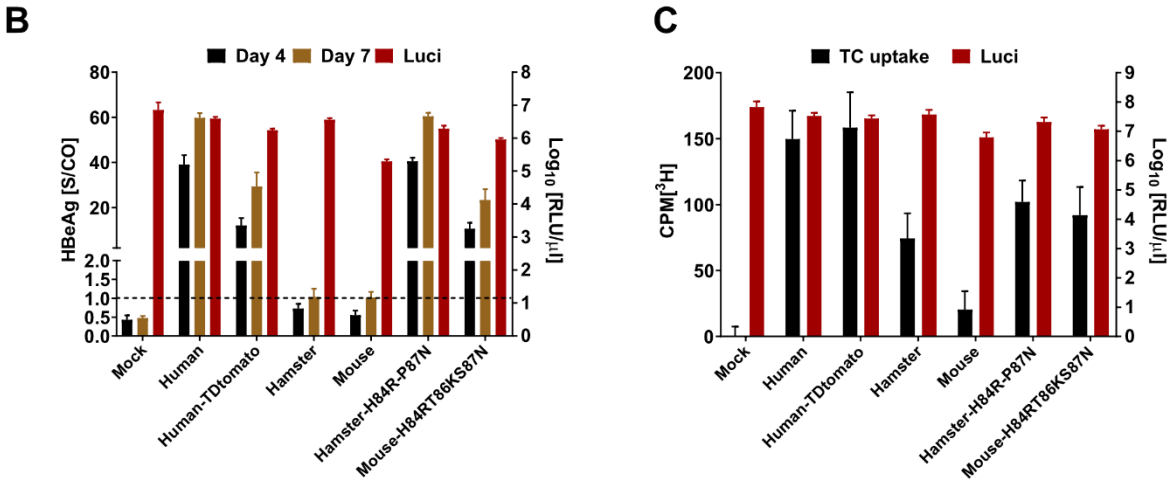

Figure 11: Modification and determination of functional domains of NTCPs for HBV infection. (A) Schematic view of mouse NTCP_H84R-T86K-S87N and hamster NTCP_H84R-P87N. **(B)** Cluc-expression on P-Cluc-dNTCP transfected HepG2 cells at 3 dpt and secreted HBeAg at 4 and 7 dpi were measured. (**C**) Cluc-expression and uptake of ^{3}H taurocholate were determined at 3 dpt in P-Cluc-dNTCP transfected HepG2 cells. Measurement of ^{3}H taurocholate was performed using a scintillation analyzer. Data represent one experiment as technical triplicates.

In summary, the results of the NTCP-modification of mouse, hamster, pig, and macaque indicated that the functional motif enabling HBV infection and HBV binding domain are pivotal for HBV internalization, as well as infection in HepG2 cells. However, cow, goat, seal, dog, and little brown bat NTCPs harbor the functional motifs and binding domain, but none of them mediate HBV infection or allowed only quite low HBV infection rates (**Figure 9A-C**). This result reveals that there might be other critical regions for HBV infection. To validate this hypothesis, we compared the residues between positions 80 and 90 of cat, goat, and cow NTCP and we found that aa at position 82 of goat and cow NTCP is phenylalanine(F) instead of Valine(V) in cat NTCP (**Figure 12A**). That region is potentially to be functional residues rendering L-mediated HBV infection. The exchange of F to V in goat and cow NTCP led to HBV infection but with lower efficiency than observed in the cat NTCP (**Figure 12B**) and maintaining their capability for bile acid uptake (**Figure 12B**).

A

Species	HBV (*80-90)	Myr-Binding Sequence (*151-180)
Cat	GKVFQLNNIEA	KDKVPYGGIVISLILVLIPCATGIFLNAKR
Goat	GKFFQLNNVEA	KDKVPYGGIVISLFLILIPCTIGIILKSKR
Cow	GKFFQLNNVEA	KDKVPYGGIMISLILILIPCTIGIILKSKR
GoatF82V	GKVFQLNNVEA	KDKVPYGGIVISLFLILIPCTIGIILKSKR
CowF82V	GKVFQLNNVEA	KDKVPYGGIMISLILILIPCTIGIILKSKR

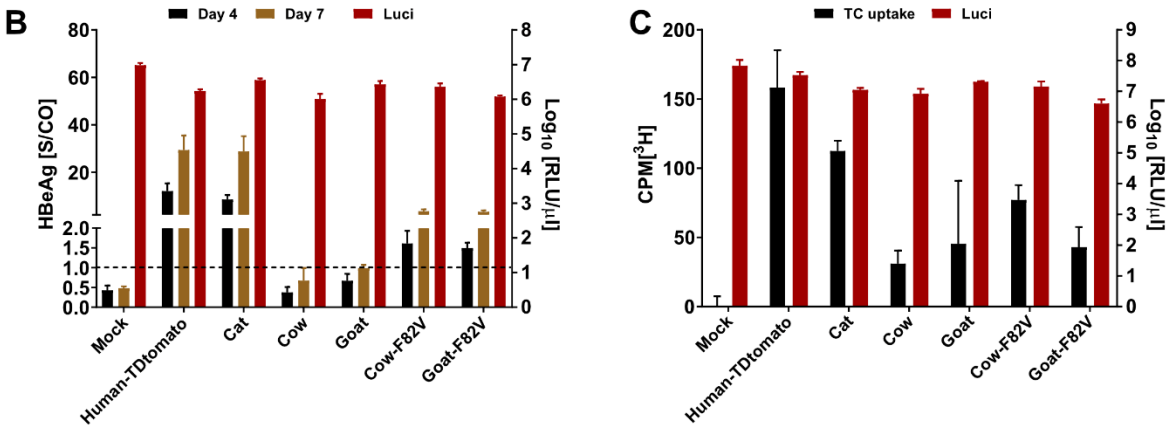

Figure 12: Modification and determination of functional domains and amino acids of NTCPs for HBV infection. (A) Schematic of goatNTCP-F82V and cow-F82V. **(B)** Cluc-expression on P-Cluc-dNTCP transfected HepG2 cells at 3 dpt and secreted HBeAg was measured at 4 and 7 dpi were measured. (**C**) Cluc-expression and uptake of ^{3}H taurocholate were determined at 3 dpt in P-Cluc-hNTCP transfected HepG2 cells. Measurement of ^{3}H taurocholate was performed using a scintillation analyzer. Data represent one experiment as technical triplicates.

The NTCPs of dog and seal harbor the complete functional HBV domain but still do not support HBV infection (**Figure 9A-C**). Therefore, we aligned the aa residues of horse, dog and seal NTCP and generated chimeric NTCPs by swapping counterparts of each species with horse variants (**Figure 13A**). We tested the functionality by transfecting those variants into HepG2 cells, following by incubation with HBV or ^{3}H taurocholate. The results indicated that HBV infection was established upon transfection with P-Cluc-horse-170-dog-NTCP and P-Cluc-seal-170-horse-NTCP into HepG2 cells, respectively (**Figure 13B**), and with all those NTCPs being functional for bile acid uptake (**Figure 13B**). The data revealed that aside from the domains already described, others are involved in viral attachment and rendering cells permissive for virus infection. According to our results these domains are located in the N-terminus of dog (aa0–170) and the C-terminus of seal NTCP (aa170–349). Still, further studies are required to characterize the global function of NTCP.

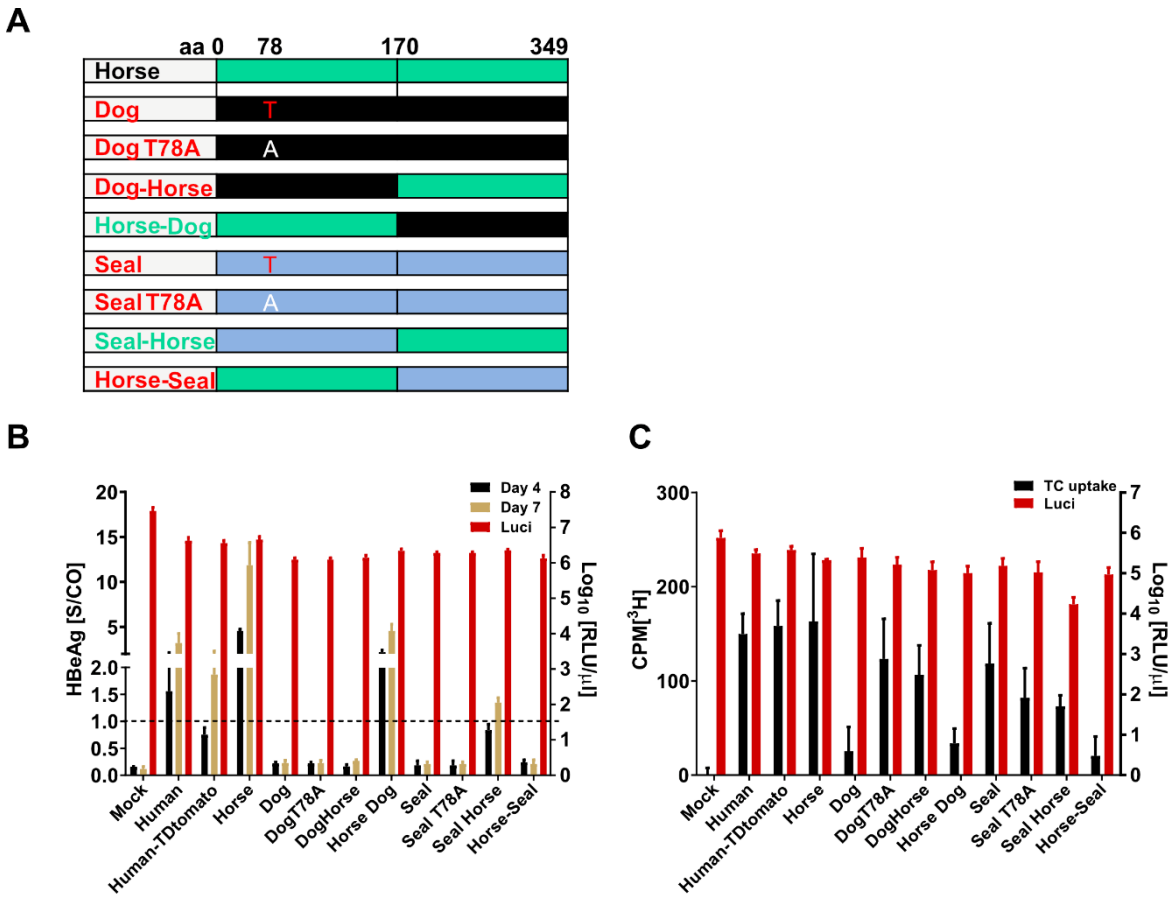

Figure 13: Modification and determination of functional domains of NTCPs to support HBV infection. (**A**) Schematic of dogT78A, dog-170-horse, horse-170-dog, sealT78A, seal-170-horse, horse-170-seal NTCPs. (**B**) Cluc-expression on P-Cluc-dNTCP transfected HepG2 cells at 3 dpt and secreted HBeAg at 4 and 7 dpi were measured. (**C**) Cluc-expression and uptake of ^{3}H taurocholate were determined at 3 dpt in P-Cluc-dNTCP transfected HepG2 cells. Measurements were performed using a scintillation analyzer. Data represent one experiment as technical triplicates.

In summary, for pig, macaque, mouse, and hamster NTCPs, the HBV functional motif aa 84-87 and binding domain aa 157-165 are crucial for HBV infection. In contrast, goat, cow, dog, and seal NTCPs are insufficient to unveil NTCP fully functionally for HBV infection. Our results indicated that there have to be additional, as-yet unknown functional regions within the NTCP sequence, which must be further described to fully explain the HBV infection mechanism.

Since we were interested in the phylogenetic development of the various NTCPs, we generated a phylogenetic tree (kindly provided by Stoyan Velkov) based on the fully published NTCP sequence (NCBI number in **Figure 8A** and **Figure 9A**) (**Figure 14**). Interestingly our data revealed that NTCPs rendering cells permissive for HBV infection are exclusively associated with mammals. In contrast, NTCPs classified to *Amphibia, Actinopteri,* and *Aves* are shown to be non-functional for HBV infection. Among mammals, NTCPs from

the orders *Artiodactyla, Primates,* and *Rodentia* are mostly restrictive to HBV infection, except those from whales, humans, and woodchucks. NTCPs from the other orders (*Carnivora, Boreoeutheria, Scandentia, Perissodatyla, Eulipotyphla and Lagomorpha*) are mostly supportive of HBV infection except for dog, seal, and little brown bat NTCP. Interestingly, although the macaque, gibbon, and capuchin primary hepatocytes can permit HBV infection upon the expression of human NTCP, their own NTCPs lack the ability to mediate HBV infection.

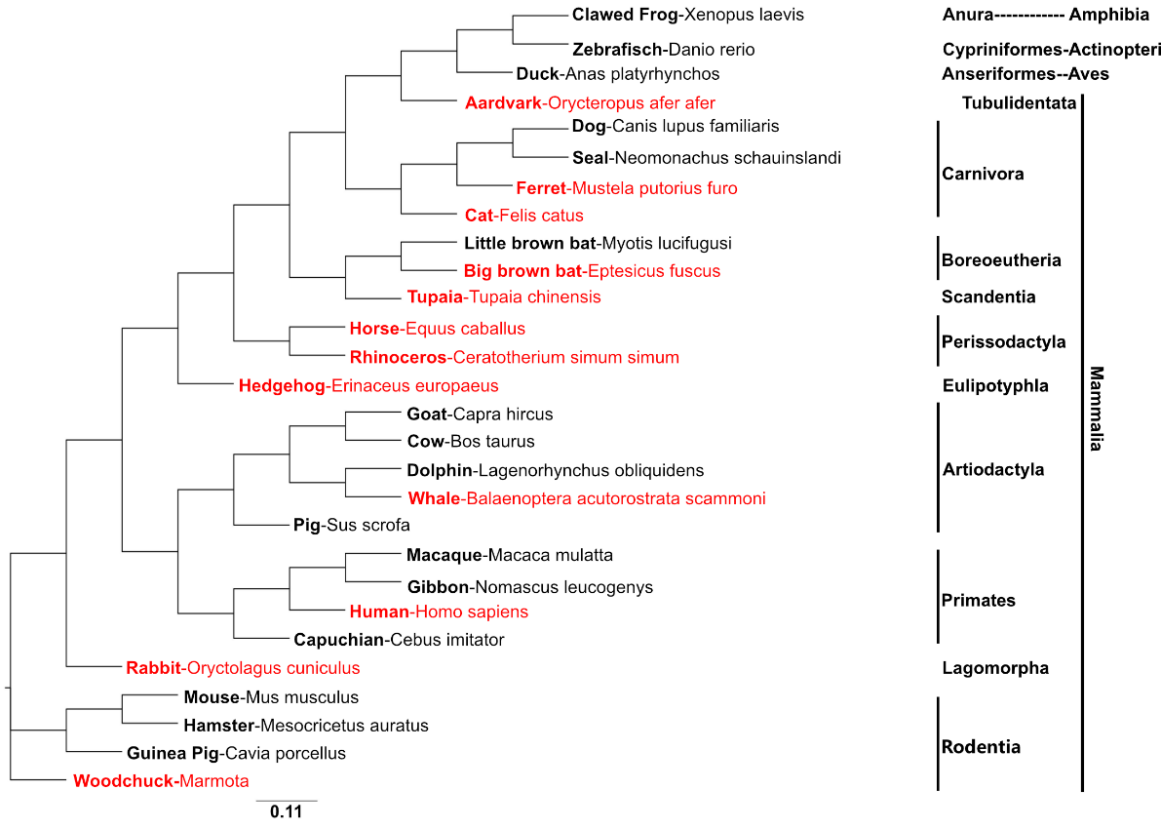

Figure 14: The phylogenetic classification of cloned NTCPs from different animals. The figure was created by RAxML-NG and displays the phylogenetic relationship of NTCPs from different animals. Common names, given in front of the species names, are used instead of the full species names throughout the manuscript. Red with HBV infection and black without HBV infection (in collaboration with Stoyan Velkov).

2.2 Characterization of horse-NTCP for enhancing HBV infection

Since horse NTCP (hoNTCP) significantly increased HBV infection in HepG2 cells when compared to human NTCP (huNTCP) (**Figure 15**), the underlying mechanism is studied in this part.

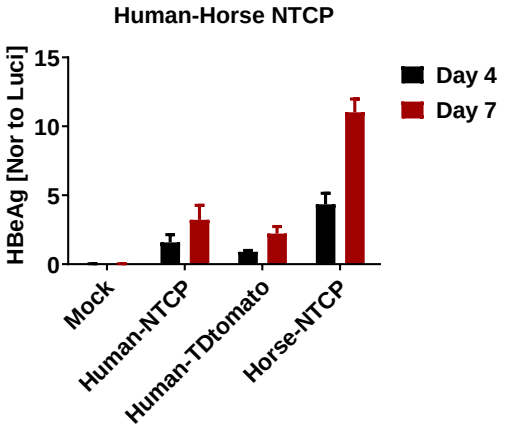

Figure 15: Comparison of huNTCP and hoNTCP for supporting HBV infection. Measurement of secreted HBeAg on P-Cluc-dNTCP transfected HepG2 cells at 4 and 7 dpi, and normalization HBeAg value to Cluc levels of measured on P-Cluc-dNTCP transfected HepG2 cells at 3 dpt. Data represent one experiment as technical triplicates.

2.2.1 Establishment of the huNTCP and hoNTCP comparison system

2.2.1.1 Optimization of IVT mRNA NTCP and HBV dose for HBV infection

To investigate hoNTCP and huNTCP, we took advantage of an established and optimized IVT mRNA-based system (Oswald et al. 2021) to compare both variants. For this purpose, we produced IVT mRNA encoding for huNTCP and hoNTCP harboring a 5' ARCA cap and ψ-UTP/m5CTP modifications. To detect huNTCP and hoNTCP, we implemented an HA-tag at the C-terminal of the NTCP sequence (**Figure 16A**). We transfected differentiated HepG2 cells with both NTCP IVT mRNAs using a three-fold titration from 1000 ng to 1 ng and an additional 2000 ng per well. According to Oswald et al. 2021, expression of NTCP reaches a peak expression at 24 hpt (hpt) of IVT mRNA, and transfection of extracellular RNAs may trigger immune responses and lead to cytotoxicity. Therefore, we first determined cell viability by using the Cell Titer Blue (CTB) assay 24 hpt of IVT mRNAs. The results of the CTB (**Figure 16B**) showed no adverse effect for any of the tested concentrations, as compared to untreated control. NTCP protein expression was analysed by Western blot using an anti-HA tag antibody (**Figure 16C**), and their function for bile acid uptake was determined by measurement of ^{3}H taurocholate (**Figure 16D**). Since NTCP is usually glycosylated, we performed an additional deglycosylation step by using PNGaseF treatment

to allow detection of both, glycosylated (~50 kDa) and deglycosylated (~37 kDa), forms (Hagenbuch and Meier 1994; Ho et al. 2004; Döring et al. 2012). Western blot analysis showed that 1000 ng–100 ng of IVT mRNA transfection resulted in dose-dependent expression of huNTCP and hoNTCP in cells in glycosylated form and deglycosylated form after PNGaseF treatment (**Figure 16C**). The bile uptake assay revealed dose-dependent uptake in cells transfected with 1000 ng–100 ng of IVT mRNA of human and horse NTCP. To verify the HBV-NTCP interaction, MyrB-atto488 staining was performed with 24 hpt of titrated mRNA. Fluorescence microscopy (**Figure 16E**) demonstrated that IVT mRNA-derived huNTCP and hoNTCP were located on the cell membrane and interacted with MyrB. In addition, fluorescence microscopy (**Figure 16E**) and flow cytometry (**Figure 16F**) revealed a dose-dependent expression for both NTCPs, while hoNTCPs showed a higher percentage of MyrB positive cells than did huNTCP. Additionally, calculation of the mean fluorescence intensity (MFI) showed twice as much hoNTCP as huNTCP on positive population (**Figure 16F**). In contrast to our IVT mRNA-transfected cells, HepG2-NTCP-K7 cells, which stably express human NTCP, displayed even higher expression than did the cells transfected with 2000 ng.

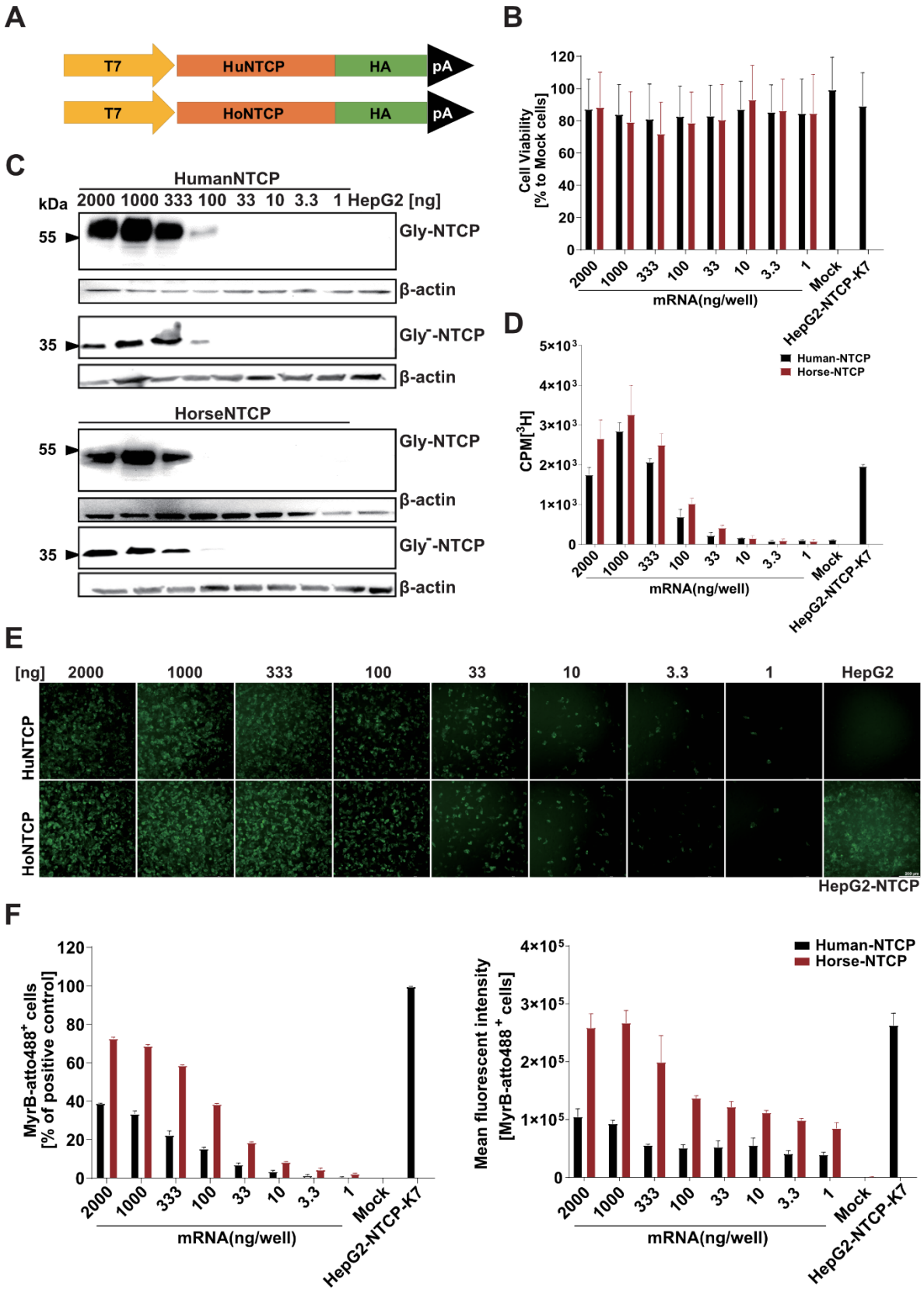

Figure 16: Optimization and characterization of IVT mRNA-derived huNTCP and hoNTCP. (**A**) Schematic view of the construct including NTCP with an HA tag. Determination of cell viability via CTB assay (**B**) and the huNTCP and hoNTCP expression (**C**) by western blot. (**D**) Bile acid uptake was determined with ^{3}H taurocholate incubation for 15 min in NTCP mRNA-transfected HepG2 cells. Measurement was performed using a scintillation analyser. (**E**) Surface located

NTCP staining with MyrB-atto488 24 hpt were performed on three-fold titrated NTCP IVT mRNA from 1000 ng to 1 ng plus with an additional 2000 ng well transfected on differentiated HepG2 cells. (**F**) Determination of MyrB-Atto488+ cells (left) and calculation of MFI (right) were performed with flow cytometry.

Since protein expression and MyrB binding of the introduced NTCP protein were confirmed, we were interested in whether HBV infection would show dose dependency. Therefore, differentiated HepG2 cells were transfected with three-fold titrated IVT mRNA from 1000 ng to 1 ng, with an additional 2000 ng/well. At 24 hpt, cells were inoculated with HBV particles at an MOI of 200 vp/cell. HBV infection efficacy was determined by the measurement of secreted HBeAg (**Figure 17A**) and established cccDNA formation (**Figure 17B**) at 7 dpi. Dose-dependent HBeAg secretion was observed in cells transfected with 333–3.3 ng of hoNTCP IVT mRNA and 333–10 ng of huNTCP IVT mRNA. Relative quantification of cccDNA revealed corresponding results, showing a significant formation of cccDNA molecules in cells transfected with 2000–3.3 ng IVT mRNA, along with dose-dependent cccDNA formation in the transfection of both NTCPs with 333–3.3 ng IVT mRNA.

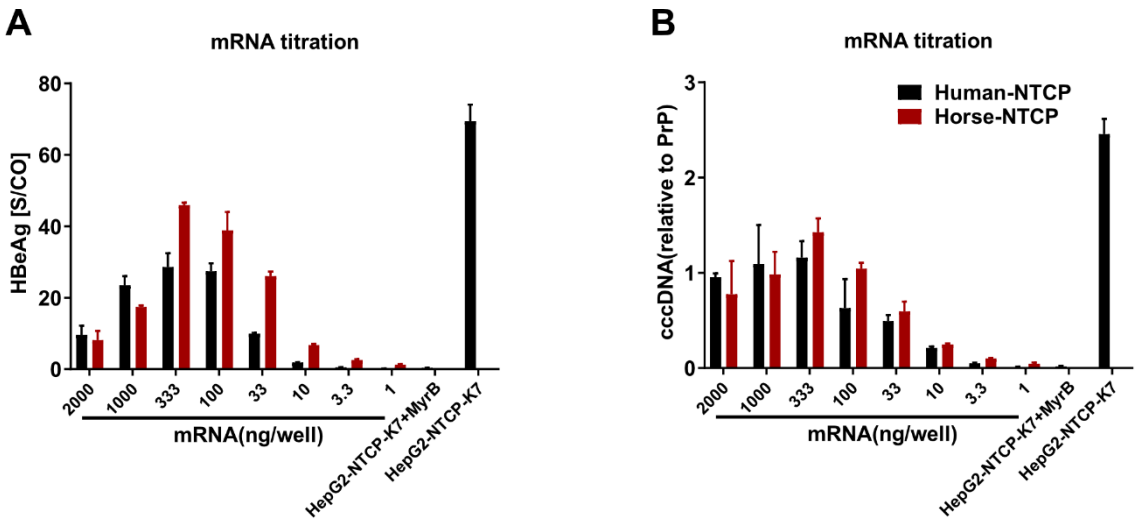

Figure 17: Evaluation of NTCP dose-dependent infection with HBV. Differentiated HepG2 cells were transfected with three-fold titrated NTCP IVT mRNA from 1000 ng to 1 ng plus with an additional 2000 ng/well, and 24 hpt wtHBV at an MOI of 200 vp/cell was inoculated in the presence of 4% PEG for 24 h. Measurements of secreted HBeAg (**A**) and quantification of cccDNA molecules (**B**) were performed at 7 dpi. HepG2-NTCP-K7 cells with and without 200 nM MyB served as controls.

Notably, HBeAg and cccDNA results both demonstrated a maximum level of viral markers with 333 ng IVT mRNA. In addition, for both parameters, transfection with hoNTCP showed a higher infection rate than did huNTCP. To ensure comparable protein expression for both NTCP variants, we performed Western blot analysis at 24 hpt (**Figure 18**). The results

demonstrated comparable protein expressions of glycosylated huNTCP and hoNTCP in cells transfected with 333 ng of IVT mRNA.

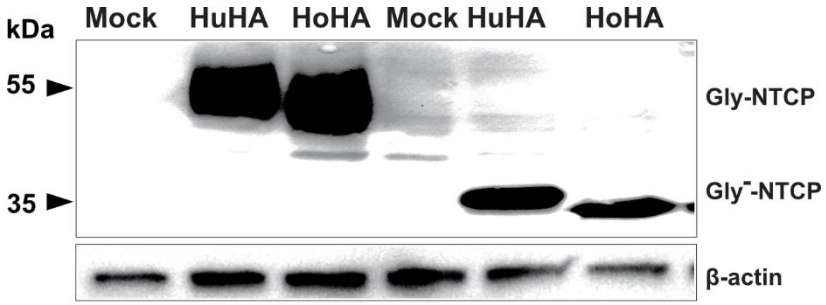

Figure 18: Western blot analysis of NTCP expression in differentiated HepG2 cells. Western blot analysis of NTCP IVT mRNA expression in differentiated HepG2 cells using 333 ng/well for 24 hpt. Detection of glycosylated (top) and de-glycosylated (PNGaseF treatment) (bottom) NTCP. β-actin was used as a loading control.

After confirming that the expression levels of both NTCP variants were comparable, we were interested in the uptake behavior of HBV in a synchronized HBV infection upon huNTCP and hoNTCP expression. Therefore, differentiated HepG2 cells were transfected with 333 ng/well IVT mRNA and inoculated HBV with MOI titration of 500–5 vp/cell 24 hpt. HBV infection efficacy was determined by measurement of secreted HBeAg (**Figure 19A**) and established cccDNA (**Figure 19B**) at 7 dpi. HBeAg and cccDNA results showed a significant dose-dependent secretion of HBeAg and formation of cccDNA molecules in cells infected with MOI 500 to 100 vp/cell. Notability, HBeAg and cccDNA results both showed a decreasing infection rate at a maximum level with an MOI 500 vp/cell. Thereby, as observed previously, hoNTCP showed increased infection rates that were indicated by higher HBeAg as well as cccDNA levels when using MOI 200 and 500 vp/cell, respectively.

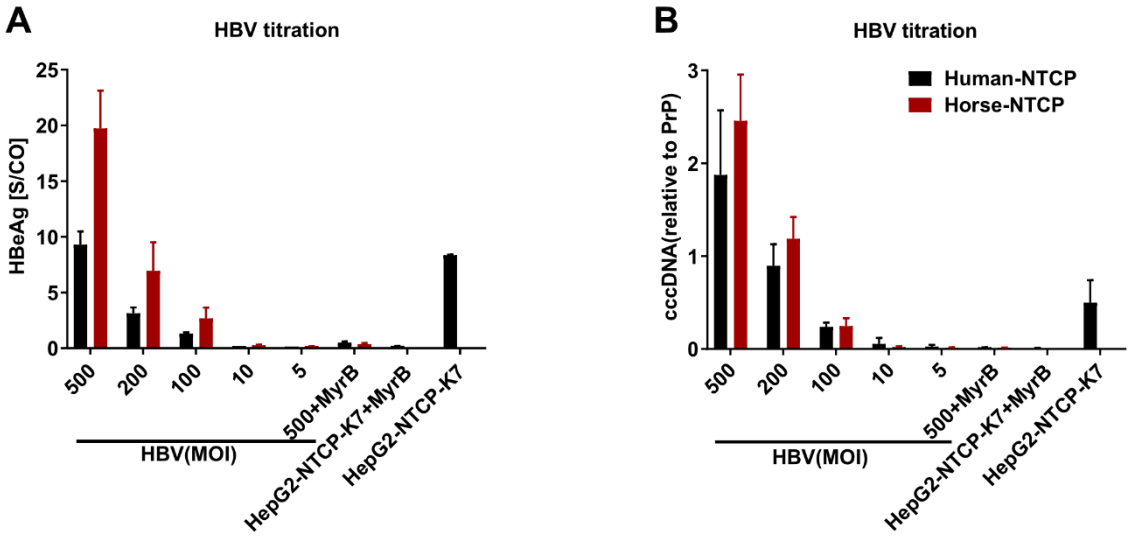

Figure 19: Analysis of HBV dose-dependent infection with IVT mRNA-derived NTCP. Differentiated HepG2 cells were transfected with 333 ng/well NTCP IVT mRNA and infected with

titrated wtHBV of MOI 500–5 vp/cell 24 hpt. Measurements of secreted HBeAg (**A**) and quantification of cccDNA molecules (**B**) were performed at 7 dpi. HepG2-NTCP-K7 cells with and without 200 nM MyrB treatment served as controls.

In summary, our data suggested that titration of IVT mRNA allowed dose-dependent expression of encoded protein, and that huNTCP and hoNTCP IVT mRNA expressed comparable protein levels at 333 ng IVT mRNA/well. Thereby, highest infection rates were reached when using a maximum of 333 ng IVT mRNA/well. Titration of wtHBV showed a decreasing infection rate correlating to inoculated MOI in cells transfected with 333 ng IVT mRNA/well. Importantly, we could observe an overall increased infection efficiency using hoNTCP when compared to huNTCP which we further investigate in the following chapters.

2.2.1.2 Generation of HepG2-HuNTCP and HepG2-HoNTCP cell lines

As observed in the previous chapter, NTCP IVT mRNA was used to analyze specific characteristics of the synchronized HBV infection on HepG2 cells mediated by huNTCP and hoNTCP. To further analyze both NTCP variants we decided to generate HepG2-huNTCP and HepG2-hoNTCP cell lines to reveal the mechanism of how hoNTCP improve HBV infection. For the generation of HepG2-huNTCP and HepG2-hoNTCP, huNTCP-HAtag and hoNTCP-HAtagged sequences were cloned into vectors harboring a TTR promotor and hyperactive piggyBac transposase (hyPBase) cutting sites. The final constructs (TTR promoter-hu/hoNTCP-HAtag-hyPBase-cutting site castle) were co-transfected with a hyPBase expression plasmids into HepG2 cells using a 2.5:1 ratio. Two days after transfection, cells were selected for 9 days treatment with kanamycin. Finally, all cell clones were screened for huNTCP and hoNTCP proteins expression by Western blot. The results showed 7 of 12 HepG2-huNTCP cell clones and 11 of 12 HepG2-hoNTCP cell clones were expressing huNTCP and hoNTCP (**Figure 20A**), respectively. For the visualization of correct NTCP localization, 2 of 7 HepG2-huNTCP and 4 of 11 HepG2-hoNTCP cells clones were stained with MyrB-atto488 (**Figure 20B**), additionally NTCP levels were quantified by flow cytometry (**Figure 20C**). The results confirmed NTCP surface expression of all 6 cell clones demonstrating by efficient binding of MyrB-atto488. The analysis showed that HepG2-huNTCP-C12 and HepG2-hoNTCP-C5 displayed comparable MyrB-atto488 positive cell percentages with 68.2% and 68%, but different MFI levels (124240±7071.07 for huNTCP and 346097±42426.41 for hoNTCP) (**Figure 20C**). In contrast, overall NTCP expression levels were almost the same regarding expression of glycosylated proteins (**Figure 20D**). In addition, HepG2-hoNTCP-C5 showed a higher uptake efficiency of bile acid than HepG2-huNTCP-C12 cells (**Figure 20E**). Thus, HepG2-huNTCP-C12 cells and HepG2-hoNTCP-C5 cells were used for further study.

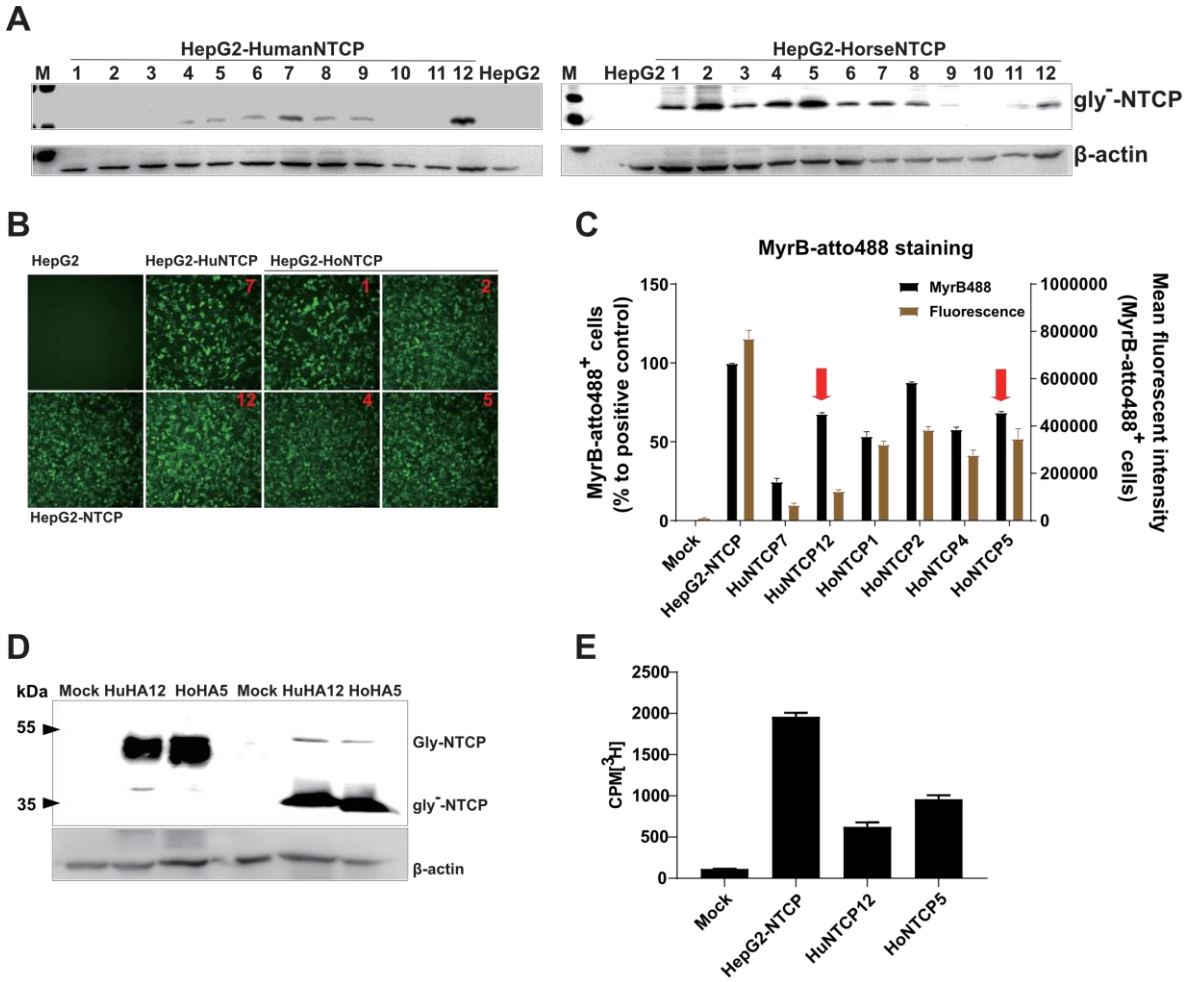

Figure 20: Generation of HepG2-HuNTCP and HepG2-HoNTCP cell line. (**A**) Western blot analysis HepG2-huNTCP and HepG2-hoNTCP cell clones after 9 days of kanamycin selection. NTCP was de-glycosylated by treatment with PNGaseF. β-actin was used as loading control. (**B**) Images of stained surface located NTCP with MyrB-atto488 of 2 out of 7 HepG2-huNTCP and 4 out of 11 HepG2-hoNTCP cell clones. (**C**) Determination of MyrB-Atto488+ cells were performed with flow cytometry. (**D**) Western blot analysis of HepG2-huNTCP-C12 and HepG2-hoNTCP-C5 cells. Glycosylated (top) and de-glycosylated (PNGaseF treatment) (bottom) NTCP were analyzed. β-actin was used as loading control. (**E**) Bile acid uptake was determined with ^{3}H taurocholate incubation for 15 min in NTCP mRNA-transfected HepG2 cells. Measurement was performed using a scintillation analyzer.

2.2.2 HoNTCP increases numbers of infected cells and single-cell infection level

To further characterize the higher infection rates of hoNTCP over huNTCP, we infected both cell lines with increasing MOI of wtHBV, from 100 to 1000 vp/cell, MyrB pretreated and uninfected cells were used as controls. Analysis of HBV infection was performed by intracellular core (HBc) protein staining at 7 dpi to determine the total number of HBV-infected cells (**Figure 21A**). HBV cccDNA was quantified at 7 dpi by qPCR relative to house keeper PRNP (**Figure 21B**) or subsequently normalized to HBc positive cells to calculate single-cell level of infection (**Figure 21B**). The results indicated a dose-dependent HBV infection and more HBV-infected HepG2-hoNTCP-C5 cells than HepG2-huNTCP-C12 cells

at various MOI, reaching 52.8% in HepG2-hoNTCP cells compared to 16.8% in HepG2-huNTCP cells at the MOI 2000 vp/cell, while with 68% MyrB-atto 488 positive rate for both cell lines. The cccDNA quantification and normalization indicated higher single-cell infection efficiency to be mediated by hoNTCP rather than huNTCP. The data here demonstrated that hoNTCP expressed on HepG2 cells enhances viral infection frequency and single-cell infection efficiency.

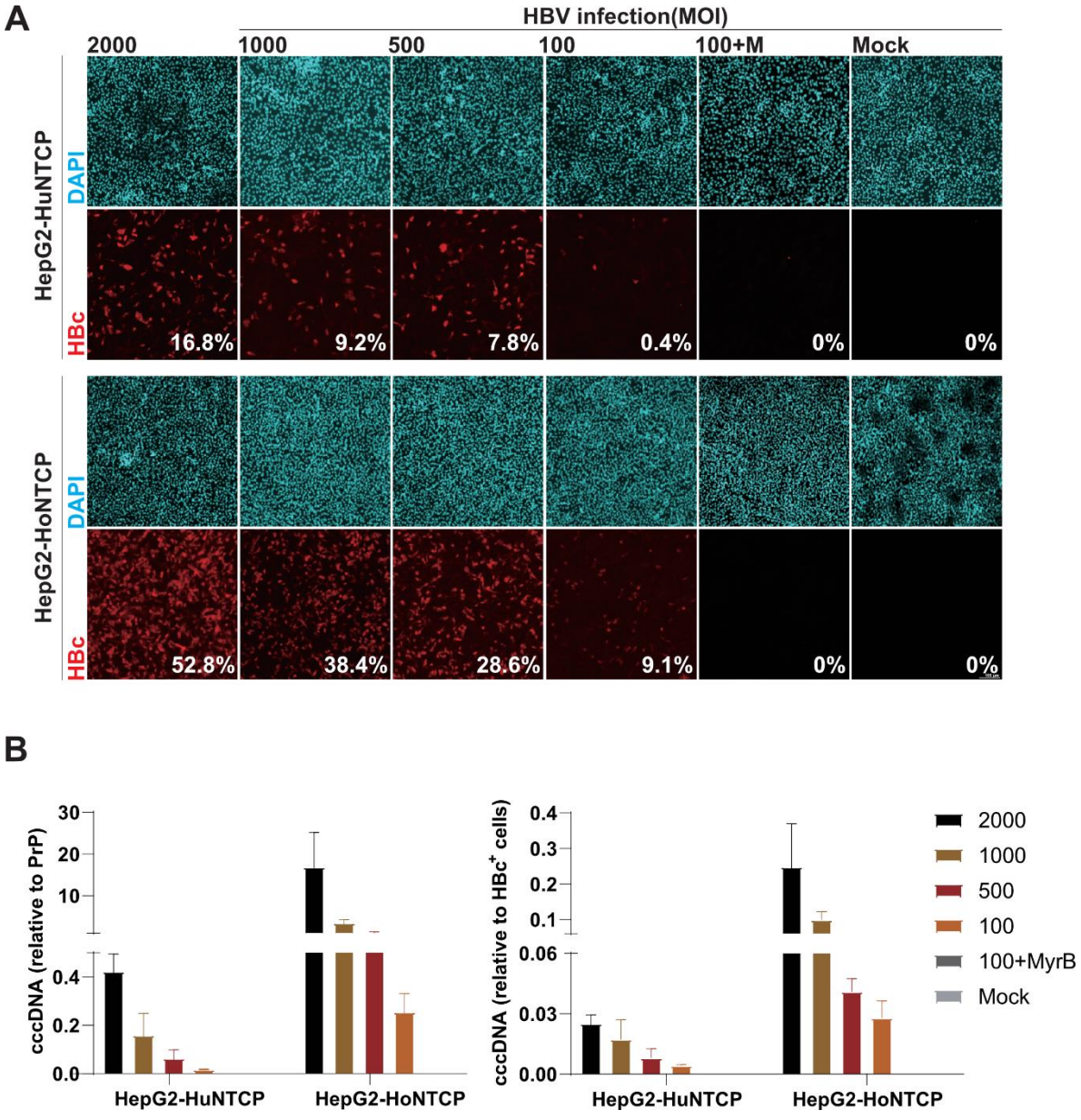

Figure 21: Comparison of HBc and cccDNA levels of HBV infection mediation by HuNTCP and HoNTCP. (A) HepG2-huNTCP-C12 cells and HepG2-hoNTCP-C5 cells were infected with decreasing MOI (2000, 1000, 500, and 100 vp/cell) of wt HBV. Cells were fixed and stained for HBc protein at 7 dpi. The percentage of positive cells is denoted at the bottom-right corner of each image. (**B**) HBV cccDNA inside the cells were quantified by qPCR at 7 pdi (right) and normalised to HBc positive cells (left).

2.2.3 HoNTCP enhances HBV infection by binding to more HBV particles

To answer the questions which part(s) and which steps of hoNTCP are crucial to enhance HBV infection, we analyzed HBV infection kinetics early in the viral life cycle. For this purpose, HepG2 cells expressing comparable huNTCP and hoNTCP were used, which included huNTCP/hoNTCP IVT mRNA transfection cells (333 ng/ well) and the stable cell lines (HepG2-huNTCP-C12 and HepG2-hoNTCP-C5). NTCP expression levels were similar for each group. Virus inoculations were performed with an MOI of 500 vp/cell for 1 h at 4 °C and then cells were either used to quantify HBV binding or shifted to 37 °C for indicated time points (3, 6, 24 h, and 7 days) to monitor internalization, uptake, and infection. At each time point, the cells were either washed twice with PBS (HBV binding) or trypsinized (HBV internalization and uptake) prior to harvesting, for total HBV DNA analysis. HepG2-NTCP-K7 cells were selected as a positive control, since HBV infection of these cells is very efficient (Ko et al. 2018). As shown in **Tab.1,** with an hour inoculation at 4 °C, hoNTCP bound 1.5 times of HBV particles better compared to huNTCP on NTCP IVT mRNA-transfected HepG2 cells and HepG2-hoNTCP cells bound twice as well as HepG2-huNTCP cells. This superior performance might suggest a strong binding affinity for hoNTCP. HBV internalization and uptake assay showed two to three times the amount of intracellular HBV DNA on HepG2 cells expressing hoNTCP than cells expressing huNTCP. Interestingly, HepG2-hoNTCP bound a similar amount of HBV particles as HepG2-NTCP-K7 cells, but established only half the cccDNA levels, with differences becoming obvious 4h post infection. This result suggests an intracellular function of NTCP 6-24 h post infection. Moreover, the HBV cccDNA established in hoNTCP expressing HepG2 cells was two to four times higher than that in cells expressing huNTCP.

Tab.1 Absolute quantification of HBV DNA in early events in the life cycle.

		mRNA transfection		Stable cell lines		HepG2-NTCP-K7
	Time	Human	Horse	HepG2-huNTCP-C12	HepG2-hoNTCP-C5	
		% of input	% of input	% of input	% of input	% of input
HBV inoculum		—	—	—	—	—
Total HBV DNA	1 hpi	12.6±0.5	18.7±1.8	17.2±0.6	33.5±0.8	36.1±5.9
Total intracellular HBV DNA	3 hpi	4.3±0.6	8.6±0.7	8.1±0.2	17.7±2.9	18.8±1.7
	6 hpi	4.0±0.5	8.2±0.2	6.7±1.4	14.0±0.6	16.9±1.3
	24 hpi	2.9±0.4	6.5±0.4	3.1±0.4	5.6±1.2	12.1±1.8
cccDNA	7 dpi	0.06±0.01	0.24±0.08	0.07±0.03	0.17±0.06	0.40±0.16

Absolute HBV DNA copy numbers relative to cm^2 of cell-associated HBV for 1 hour at 4 °C (attachment), total intracellular HBV DNA after 3, 6, 24 hours uptake and cccDNA were determined. Relative percentages from the input virus (MOI 500 vp/cell) which was set to 100% were displayed in huNTCP, hoNTCP expressing HepG2 cells and HepG2-NTCP K7 cells. The experiment was repeated three times. Data represent one experiment as technical triplicates.

As the previous results showed that HepG2 cells expressing hoNTCP can bind more HBV particles than huNTCP expressing HepG2 cells – therefore enhancing HBV infection – we next address how hoNTCP increases HBV particles' attachment over that of huNTCP. In parallel, various chimeras of huNTCP and hoNTCP were constructed basing on the sequence alignment on functional motifs and binding domains by overlap PCR to evaluate the contributions of various domains. Each domain of huNTCP was replaced by its hoNTCP counterparts or vice versa (**Figure 22A**). Transfection of P-Cluc-chNTCPs into HepG2 cells was conducted as previously described, followed by 2 days DMSO differentiation. Differentiated and transfected cells were inoculated with HBV particles at an MOI of 1000 vp/cell. Supernatants were collected at 3 dpt before HBV inoculation to quantify NTCP expression. Secreted HBeAg in the supernatant of wild-type and chimeric forms of NTCPs expressing HepG2 cells were measured at 4 and 7 dpi and subsequently normalized to expression levels of Cluc (**Figure 22B**). The results illustrated that chimeric forms of NTCPs containing the replacement HBV binding part of huNTCP with their corresponding hoNTCP fragment (human-QN-GIF, human-GIF) enhanced viral infection, while the chimeric forms horse-RK-KVV and horse-KVV reduced viral infection. The replacement of the functional motif between huNTCP and hoNTCP did not change viral infection efficiency. The data revealed that the hoNTCP HBV binding region is important in facilitating HBV infection. In parallel, bile acid uptake was determined in NTCP variants expressing HepG2 cells. Bile acids uptake was detected in all NTCP variant-expressing HepG2 cells, indicating that the modified NTCP variants did not lose their function for bile acid uptake (**Figure 22C**).

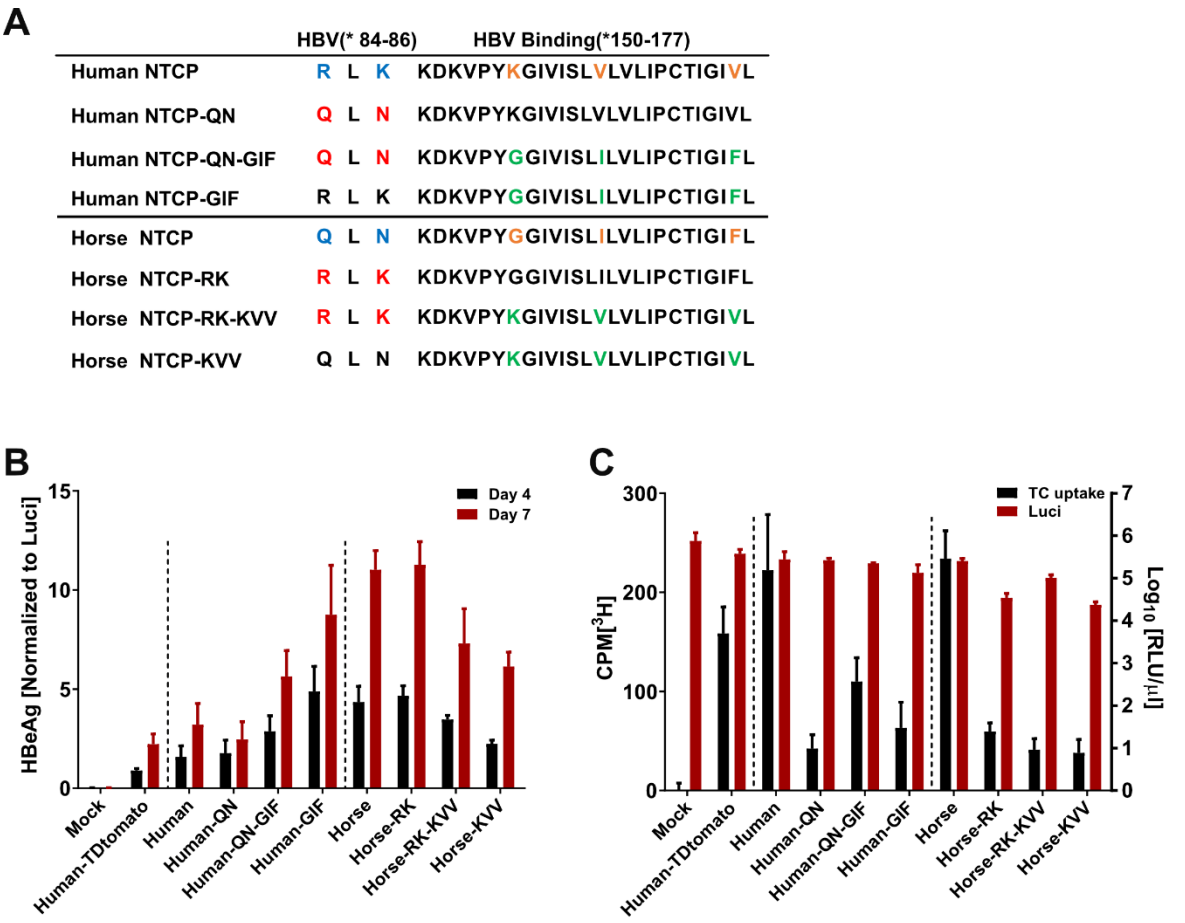

Figure 22: Modification and determination the amino acid(s) of hoNTCP that enhance HBV infection. (**A**) Schematic diagram of chimeric NTCP. (**B**) HepG2 cells were transfected with Cluc-chimera NTCP constructions or a vector control. Secreted HBeAg in the supernatant was measured at 4 and 7 dpi and normalized to Cluc. (**C**) Bile acid uptake was determined with ^{3}H taurocholate incubation for 15 min in NTCP variants expressing HepG2 cells. Measurement was performed using a scintillation analyzer. Corresponding Cluc-expressions were measured at 3dpt.

Next, we focused on the contributions of various sites of the hoNTCP HBV binding region in viral infection. The hoNTCP HBV binding region here consists of 18 amino acids from residues 150–177, thus three residues differ between the huNTCP and hoNTCP sequences. Single point mutations (K157G, V164I, and V175F) were introduced into huNTCP, with corresponding mutations in hoNTCP (G157K, I164V, and F175V) (**Figure 23A**). Replacing residue 157 of huNTCP with the hoNTCP counterpart enhanced HBV infection, while replacing residue 157 of hoNTCP with huNTCP counterpart reduced HBV infection (**Figure 23B**), demonstrating that residue 157 of NTCP correlates with HBV infection levels. In addition, bile acid uptake for NTCP variants expressing HepG2 cells were detected, indicating that the modified NTCP variants did not lose their function in bile acid uptake (**Figure 23C**).

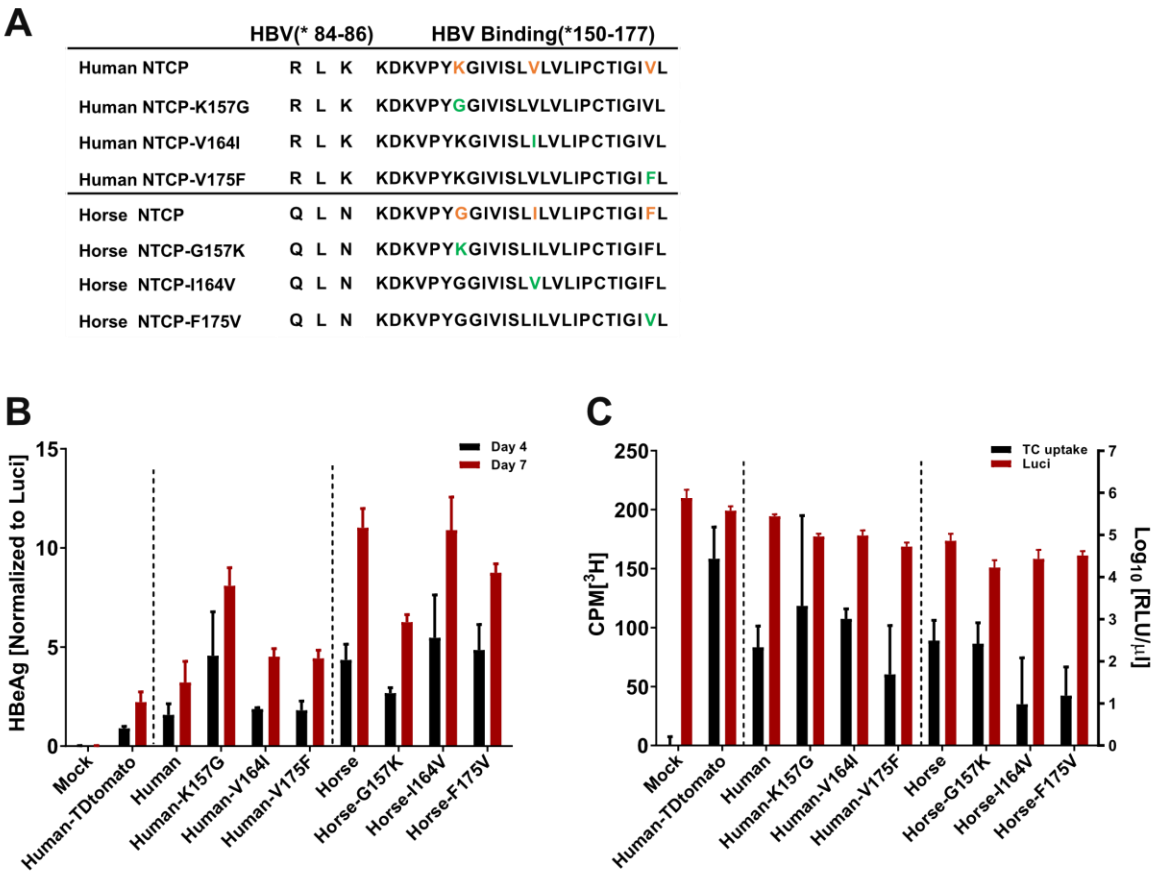

Figure 23: Modification and determination of the amino acid(s) of hoNTCP that enhance HBV infection. (**A**) Schematic diagram of chimeric NTCP. (**B**) HepG2 cells were transfected with Cluc-chimera NTCP constructions or a vector control. Secreted HBeAg in the supernatant was measured at 4 and 7 dpi and normalized to Cluc. (**C**) Bile acid uptake was determined with ^{3}H taurocholate incubation for 15 min in NTCP variants expressing HepG2 cells. Measurement was performed with a scintillation analyzer. Corresponding Cluc-expressions were measured at 3dpt.

As residue 157 is located within the HBV binding region, we were interested in whether G157 of hoNTCP contributes to HBV binding. The experimental results were similar, showing improved HBV binding for huNTCP-K157G, whereas lowered by hoNTCP-G157K (**Figure 24A**), therefore regulating HBV infection levels (**Figure 24B**). Evidently, residue 157 in the HBV binding region of hoNTCP contributes to the promotion of binding with HBV particles, increasing the efficiency of HBV infection.

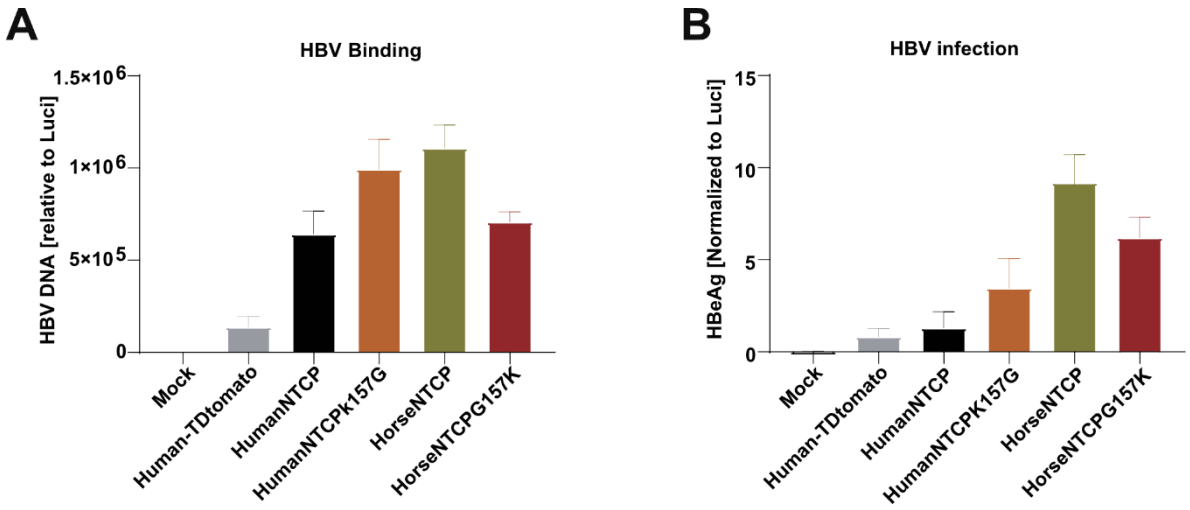

Figure 24: Evaluation of HBV binding on NTCP-157 expression HepG2 cells. HepG2 cells were transfected of NTCP-157 chimeras or a vector control. HBV binding and infection were performed at 3 dpt. **(A**) HBV attachment (MOI 1000 vp/cell) in NTCP expressing HepG2 cells was assessed and normalized to Cluc. **(B**) Secreted HBeAg for HBV infection at 7 dpi in the supernatant was measured and normalized to Cluc.

2.2.4 The localization levels of hoNTCP regulates HBV infection

Next, we addressed the issue of why hoNTCP demonstrates higher infection rates. This result could be associated with more efficient trafficking and localization at the plasma membrane, the greater affinity of hoNTCP for HBV particles, or a combination of the two. NTCP is a multi-pass transmembrane protein comprising an extracellular N-terminus and cytoplasmic C-terminal domain. To investigate whether the hoNTCP has higher plasma membrane localization levels or greater affinity with HBV, flag-tag and HA-tag were introduced at the N-and C-terminus, respectively, of NTCP to determine relative surface and total expression of NTCP, respectively. Single mutations of residue 157 were introduced as well, to analyze whether residue 157 contributes to the regulation of hoNTCP trafficking and localization or rather has an impact on binding affinity (**Figure 25A**). Hu/hoNTCP-HA (hu/hoHA), flag-hu/hoNTCP-HA (Fhu/hoHA), and flag-hu/hoNTCP157-HA (Fhu/ho157HA) IVT mRNA were produced and transfected into differentiated HepG2 cells, with 333 ng per well. To visualize surface expression, MyrB atto488 staining was performed. The results demonstrated NTCP expression and localization at the cell membrane of all variants tested (**Figure 25B**).

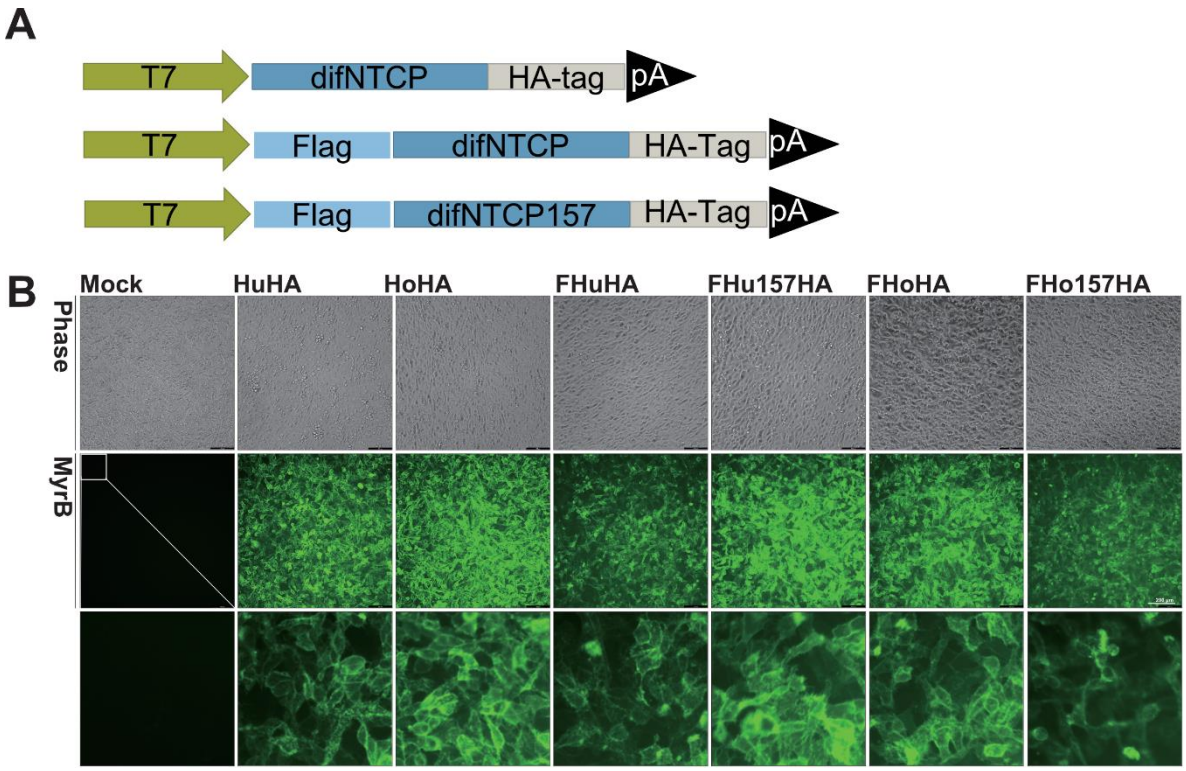

Figure 25: Comparison and characterization flag-tag-NTCP expression. (**A**) Schematic of construction of NTCP with flag-tag and HA-tag. (**B**) Fluorescence images of surface located NTCP staining with MyrB-atto488.

To exclude adverse effects of our tagged constructs, bile acid uptake, HBV binding and infection were carried out on NTCP IVT mRNA-transfected HepG2 cells, as described. Here, hu/hoHA IVT mRNA served as positive controls. The results indicated that all reconstituted Fhu/hoHA and Fhu/ho157HA maintained their function of supporting bile acid uptake (**Figure 26A**), HBV binding (**Figure 26B**), and infection (**Figure 26C**) with a promotion by hoNTCP expression. Furthermore, replacement residue 157 of NTCP for huNTCP with its counterpart of hoNTCP, improved HBV binding and infection, while replacing residue 157 of hoNTCP with its counterpart of huNTCP reduced HBV binding and infection. In addition, HBc staining of infected cells demonstrated a similar tendency regarding HBV binding and infection, indicated that flag-tagged NTCP did not alter NTCP function and could be used to investigate localization efficiency alongside binding affinity with HBV (**Figure 26D**).

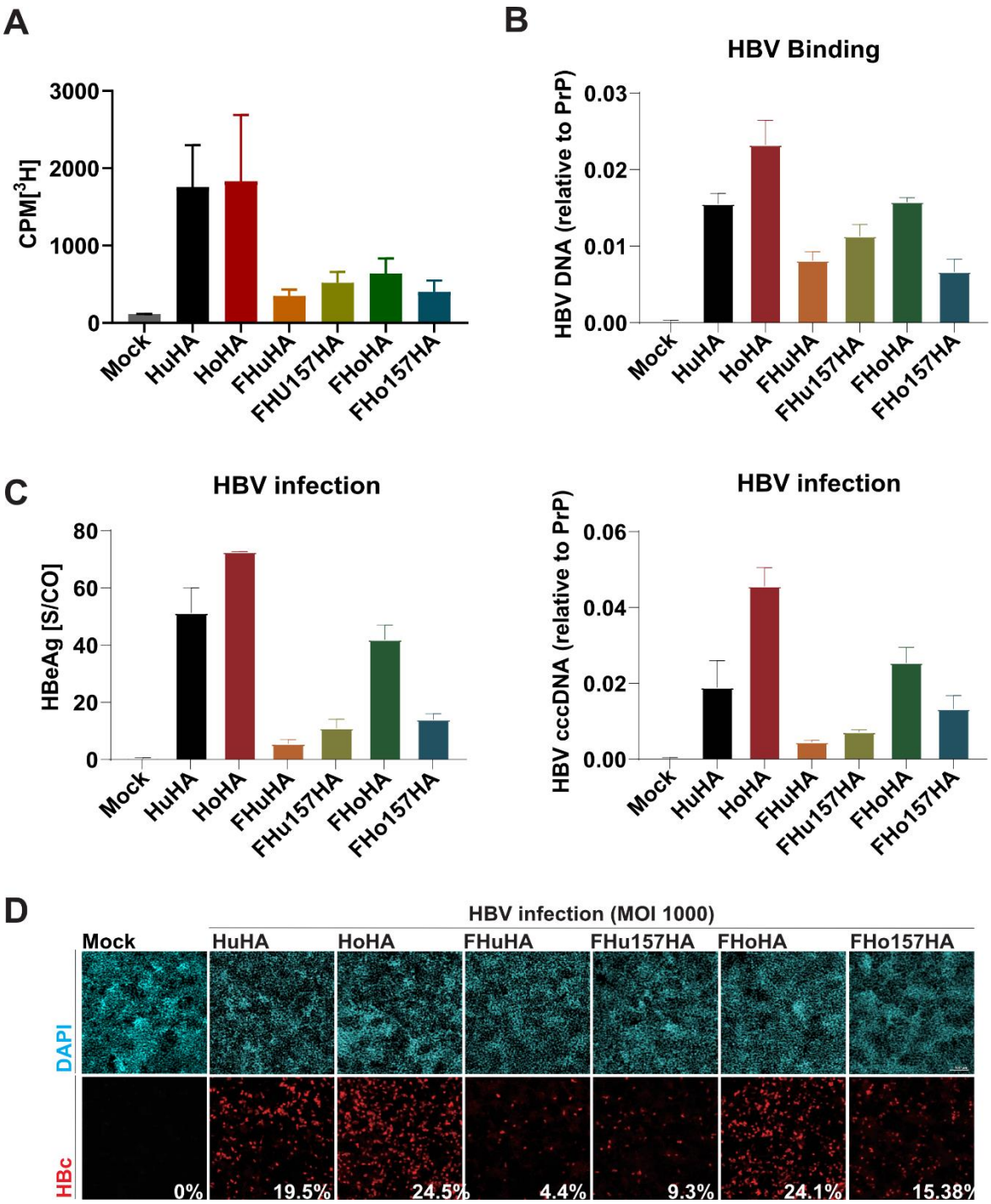

Figure 26: Comparison and characterization of flag-tag-NTCP function for supporting bile acid uptake and HBV infection. (**A**) Bile acid uptake was determined with ^{3}H taurocholate incubation for 15 min in NTCP mRNA-transfected HepG2 cells. (**B**) Attached HBV at 4 °C for 1 h and (**C**) secreted HBeAg and cccDNA at 7 dpi were measured. (**D**) Cells were fixed and stained for HBc protein at 7 dpi. The percentage of infected cells is denoted at the bottom-right corner of each image.

To analysis NTCP localization at the plasma membrane and interaction affinity with HBV particles, we transfected 333 ng/well of Fhu/hoHA and Fhu/ho157HA IVT mRNA into HepG2

cells. We then performed surface staining with anti-flag antibody, MyrB-atto594, and intracellular staining with anti-HA antibody 24 hpt, following by flow cytometry analysis. Surface expression of NTCP was determined by staining with flag antibody, and total NTCP expression was determined by staining with the HA antibody. Functional HBV binding of these NTCPs was determined by staining with MyrB-atto594. The results revealed approximately two times more FhoHA (18.1%) located on the plasma membrane than FhuHA (8.26%), even though overall expression of both constructs was comparable (39.5% vs. 43.7%) (**Figure 27A**). Replacing residue 157 of huNTCP with the hoNTCP counterpart increased huNTCP localization on the plasma membrane, while replacing residue 157 of hoNTCP with huNTCP counterpart reduced huNTCP localization on the plasma membrane, though with an comparable HA positive cells (**Figure 27A**). We found that hoNTCP accumulated more efficiently at the plasma membrane than did huNTCP; hence, residue 157 of hoNTCP contributed to the increased localization (**Figure 27B**). Similar results regarding MyrB binding with NTCP were observed (**Figure 27C**) and were strongly correlated with NTCP localization (**Figure 27D**). HBV binding affinity was calculated by normalizing the MFI of MyrB-atto594^{+} cells to the flag^{+} cell. Replacement of residue 157 of huNTCP and hoNTCP there did not alter binding affinity with HBV particles (**Figure 27E**), indicating that huNTCP and hoNTCP bind HBV particles with similar binding affinity.

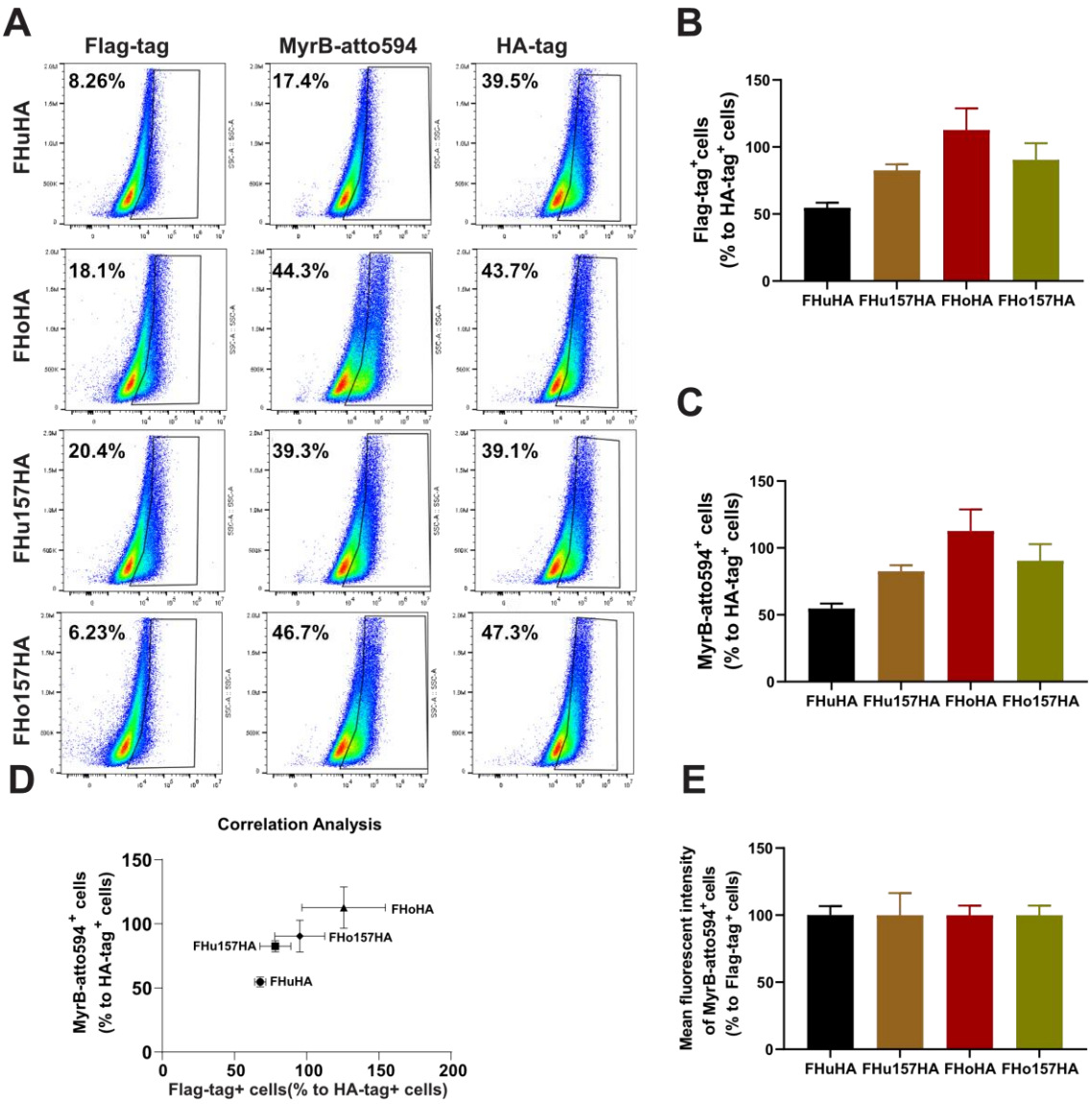

Figure 27: Comparison and characterization flag-tag-NTCP localization and HBV binding affinity. (**A**) Flow cytometry analysis of flag-NTCP-HA surface localization, MyrB-atto 594 binding, and total expression by surface and intracellular staining 24 hpt. (**B, C**) Normalization of flag-tag$^+$ cells and MyrB-atto 594$^+$ cells to HA-tag$^+$ cells. (**D**) Correlation analysis of flag-tag$^+$ cells and MyrB-atto 594$^+$ cells based on normalized to HA-tag$^+$ cells. (**E**) Calculation MFI of flag-tag$^+$ cells based on normalized to MyrB-atto 594$^+$ cells.

To understand whether the higher efficiency of the hoNTCP plasma membrane accumulation is due to its stability, we repeated the transfection of hu/hoHA, Fhu/hoHA, and flag-hu/ho157HA IVT mRNA into HepG2 cells and analyzed protein expression at certain time points (0, 8, 16, 24, 32, 40, and 48 h) by Western blot using the HA antibody (**Figure 28**). Results showed a peak expression at 24 hpt of both variants as well as similar degradation rates 24–48 hpt (**Figure 28A**). Interestingly, replacing residue 157 of huNTCP with the hoNTCP counterpart delayed the degradation of huNTCP, while replacing residue 157 of hoNTCP with huNTCP counterpart accelerated the degradation of hoNTCP (**Figure 28B**). This result indicated that residue 157 of NTCP alters the stability of NTCP, therefore

contributing the variety of HBV infection rates after the replacement of the residues in huNTCP and hoNTCP.

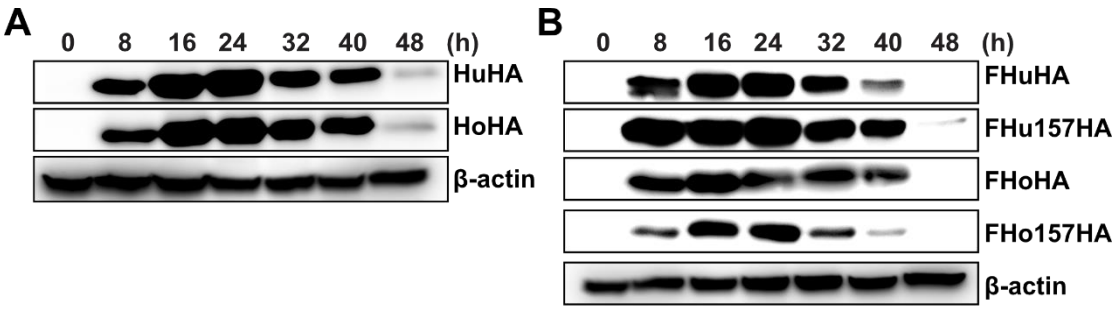

Figure 28: Expression kinetics of huNTCP and hoNTCP variants in HepG2 cells. Western blot analysis the expression kinetics of hu/ho-HA, Fhu/hoHA, and Fhu/ho157HA IVT mRNA in HepG2 cells in 48 hpt.

In summary, we established an IVT mRNA transfection system and selected two stable cell lines to express comparable levels of huNTCP and hoNTCP. Our results indicate that hoNTCP accumulated and was more stably expressed on the plasma membrane than did huNTCP, thus enhancing the binding of HBV particles and improving HBV infection.

2.3 HBV infection in murine hepatocyte cell line-AML12

2.3.1 HoNTCP enhances HBV infection on AML12 cells

Since we can partially explain how hoNTCP enhances HBV infection in human hepatoma cell line HepG2, we were interested in whether hoNTCP can also render murine hepatocyte cell lines susceptible to HBV infection. Several huNTCP-expressing murine liver cell lines were described as showing resistance to HBV infection previously, either due to a lack of essential host factors or the expression of restriction factors interfering with the viral life cycle (Yan et al. 2012; Yan et al. 2013; Li et al. 2014; Lempp et al. 2016a). The identification of murine hepatocytes permissive for *in vitro* HBV infection would be important to inform cell culture models, but also would serve as template for the generation of genetically modified mice supporting *in vivo* infection. Recently, murine hepatocyte cell line AML12 was reported to be susceptible to HBV after the reconstitution of huNTCP. (Lempp et al. 2016b; Qiao et al. 2018). To verify these results, differentiated AML12 cells were transfected with hoNTCP IVT mRNA, following by inoculation with wtHBV (MOI 500 vp/cell) 24 hpt. HepG2-NTCP-K7 cells and another mouse hepatoma cell line Hep56D served as positive and negative controls, respectively. HBeAg were detectable at 7 dpi for HepG2-NTCP-K7 cells and mRNA-transfected AML12 cells but not Hep56D cells (**Figure 29A**). In addition, we transduced Ad-HBV (MOI 5 vp/cell) to show HBV replication from the transfer template in all the cells. These results suggest hoNTCP expressing AML12 cell are susceptible to HBV. The specificity of NTCP-dependent HBV uptake was confirmed by addition of MyrB control. Intracellular HBV DNA and cccDNA were detected in infected HepG2-NTCP-K7 cells and transfected AML12 cells but not in Hep56D cells at 7 dpi (**Figure 29B**). These results indicated that cccDNA was established in AML12 cells, allowing subsequent production of rcDNA and HBeAg.

Next, we further verified that AML12 cells support the full HBV life cycle and evaluated the effects of huNTCP and hoNTCP on HBV infection. Differentiated AML12 cells were transfected with 333 ng/well huNTCP and hoNTCP IVT mRNA, following by HBV infection at MOIs of 500, 1000, and 2000 vp/cell 24 hpt. We implemented MyrB as negative control. At 7 dpi we analyzed various viral parameters (i.e., HBeAg, HBsAg, intracellular cccDNA, pgRNA, rcDNA, and extracellular rcDNA).

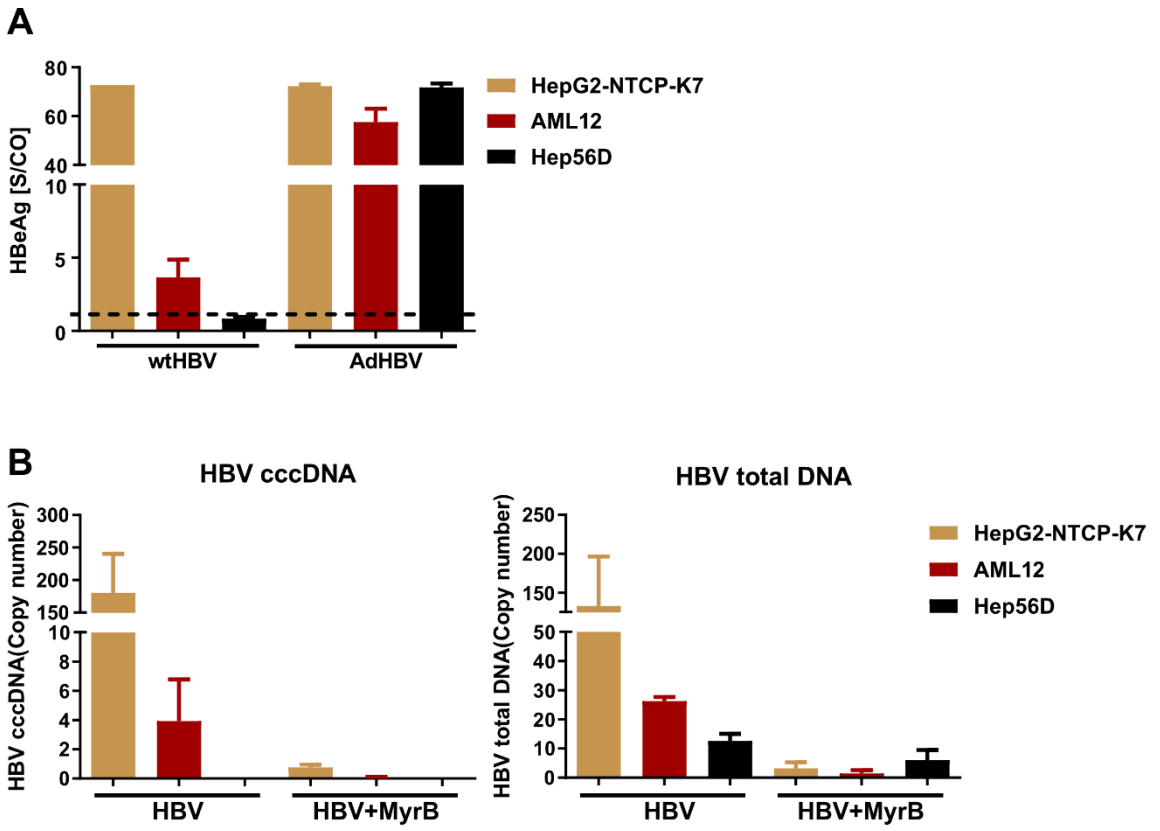

Figure 29: Murine hepatocyte cells AML12 but not Hep56D cells support HBV infection. (**A**) Differentiated AML12 and Hep56D cells were transfected with 333 ng/well hoNTCP IVT mRNA and infected with wt HBV (MOI 500 vp/cell) and Ad-HBV (MOI 5 vp/cell). HBeAg was measured at 7 dpi. HepG2-NTCP-K7 served as a control. (**B**) Intracellular HBV DNA and cccDNA were measured at 7 dpi. 200 nM MyrB added served as controls.

Our results demonstrated that all viral markers were detectable using each MOI and that hoNTCP significantly increased expression of HBeAg, HBsAg, cccDNA, and pgRNA compared to huNTCP (**Figure 30A**). Interestingly, intra- and extracellular HBV DNA in hoNTCP transfected cells were only slightly increased compared to huNTCP (**Figure 30B**), which could suggest a limiting step in the production of progeny rcDNA in AML12 cells. To discriminate HBV DNA identity, we performed a Southern blot to detect the HBV protein-free forms of HBV-DNA including cccDNA, as a Southern blot remains the “gold standard” technique for cccDNA detection. As depicted in the results (**Figure 30C**), rcDNA and cccDNA were detectable in infected AML12 cells upon expression both variants huNTCP and hoNTCP. In addition, DNA was treated either with T5 exonuclease, to degrade non-cccDNA species, or with EcoRI restriction enzymes to linearize cccDNA (**Figure 30C**). These results indicated a robust establishment of HBV infection in AML12 cells upon NTCP expression, in particularly when hoNTCP was expressed.

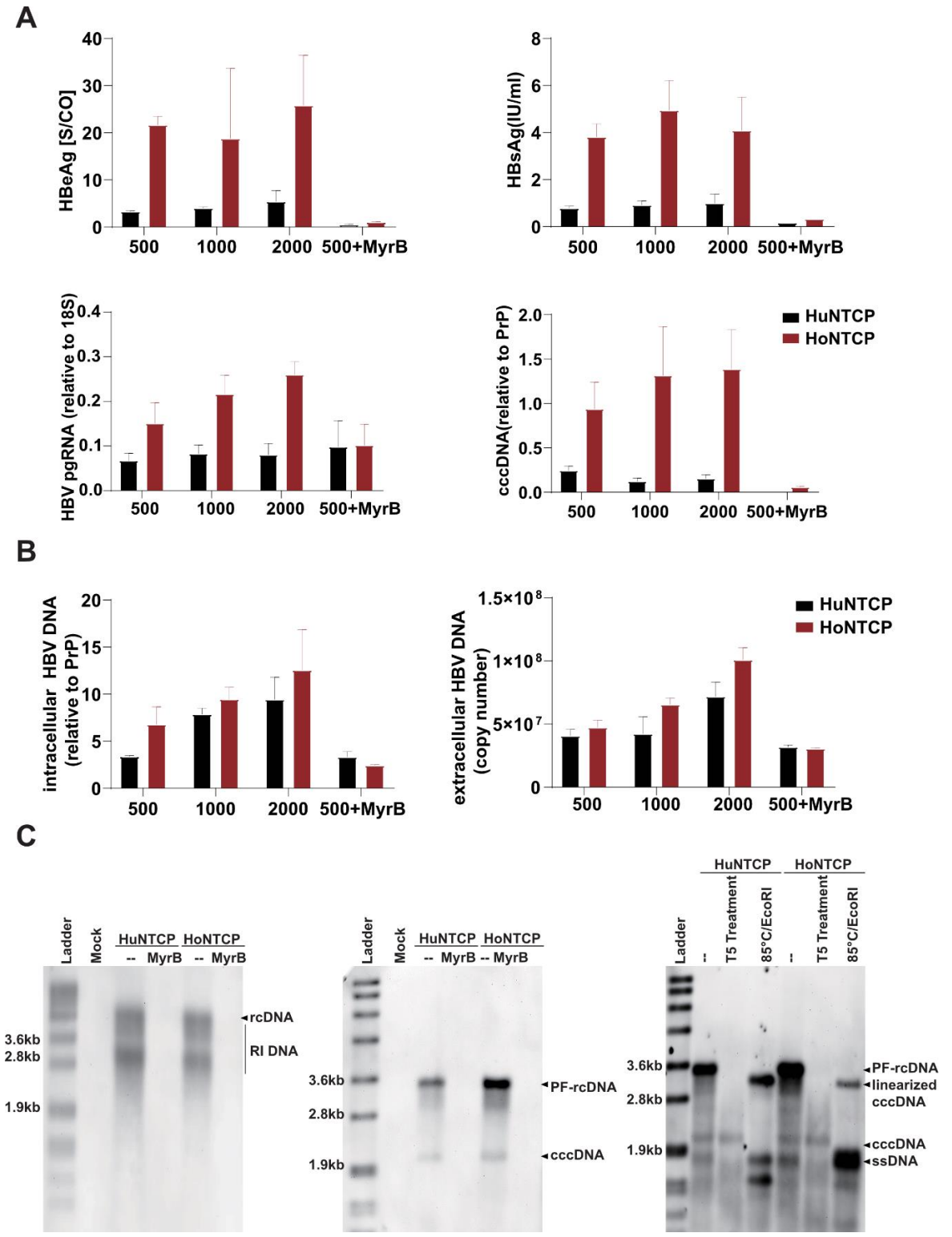

Figure 30: Analysis of AML12 cells permissivity to HBV infection. (**A**) Differentiated AML12 cells were transfected with 333 ng/well huNTCP and hoNTCP IVT mRNA, following by HBV inoculation at MOIs 500, 1000, and 2000 vp/cell 24 hpt. Analysis of different viral parameters was performed at 7 dpi. 200 nM MyrB served as negative control. (**B**) Relative quantification by qPCR of intracellular and extracellular HBV DNA. (**C**) HBV rcDNA (capsid-associated DNA (left)), cccDNA and cccDNA identity by treatment DNA extraction with T5 exonuclease or digestion DNA extraction with EcoRI restriction enzymes (right) were detected by Southern blot with an HBV-DNA probe.

As we were interested in the capability of AML12 to HBV infection expressing huNTCP or hoNTCP, we repeated the transfection as previously described, followed by infection of HBV in a three-fold titration of MOI from 1000 to 3.3 vp/cell 24 hpt. HBV infection was determined by measurement of HBeAg at 7 dpi. Results showed a dose-dependent infection in AML12 cells in the range of MOI 1000 to 33 vp/cell upon hoNTCP expression (**Figure 31**). In contrast, huNTCP expressing AML12 demonstrated HBeAg secretion only in the range of MOI 1000–100 vp/cell (**Figure 31**). The results also indicated that AML12 cells were susceptible to low titer HBV.

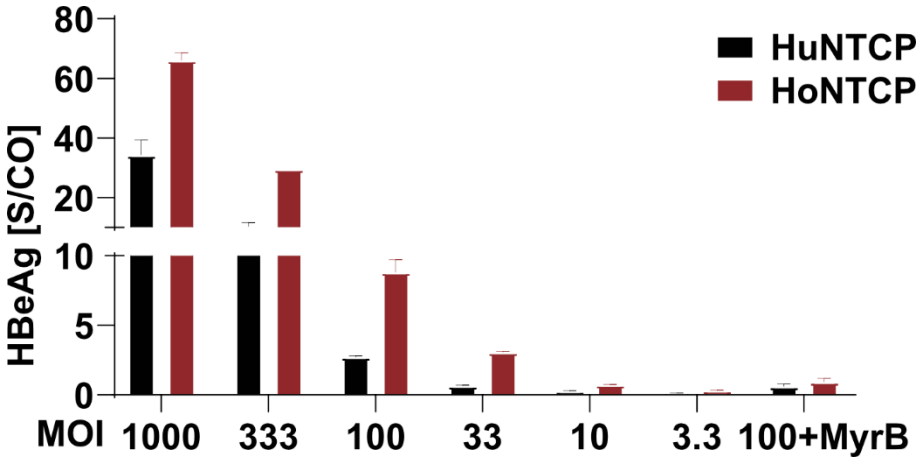

Figure 31: Analysis of HBV dose-dependent infection with NTCP IVT mRNA-derived AML12 cells. Differentiated AML12 cells were transfected with 333 ng/well NTCP IVT mRNA and inoculated with titrated wt HBV staring from MOI 1000 to 3.3 vp/cell for 24 h at 24 hpt. Measurements of secreted HBeAg were performed at 7 dpi. 200 nM MyrB added to inhibit NTCP-HBV interaction served as a control.

In summary, hu/hoNTCP expressing murine hepatocyte cell line AML12 cells are susceptible to HBV infection and support full life cycle of HBV. HBV infection efficiency is improved upon expression hoNTCP compared to huNTCP.

2.3.2 Generation of NTCP expressing AML12 cell lines

In order to understand the characteristics of AML12 cells supporting the full life cycle of HBV upon NTCP expression, we next generated NTCP-expressing AML12 stable cell lines. The mouse-codon-optimized hoNTCP sequence and the huNTCP sequence were inserted into vectors harboring a C-terminal HA-tag sequence, as described in 2.2.1.2. The plasmids encoding huNTCP or hoNTCP were transfected into AML12 cells, and hu/hoNTCP expressing-AML12 cell lines were selected by nine days treatment with kanamycin. For all clones, huNTCP and hoNTCP protein expression, protein folding, and localization on the plasma membrane were confirmed by Western blot or flow cytometry. Western blots results showed that all hoNTCP-transfected AML12 cells demonstrated strong protein expression,

as compared to huNTCP-transfected AML12 that showed only weak levels (**Figure 32A**). FACS analysis demonstrated approximately 70% MyrB-atto594^{+} of AML12-hoNTCP cells, whereas none of the huNTCP expressing cells could be detected (**Figure 32B**). To confirm the functionality of expressed NTCP variants, HBV infection was performed as described elsewhere, using an MOI of 500 vp/cell. HBeAg was measured at 7 dpi showing detectable levels in the supernatant of infected AML12-hoNTCP cells, but not in AML12-huNTCP or parental AML12 cells (**Figure 32C**). This result indicated that, we failed to establish appropriate, AML12-huNTCP cells, while AML12-hoNTCP were successfully established.

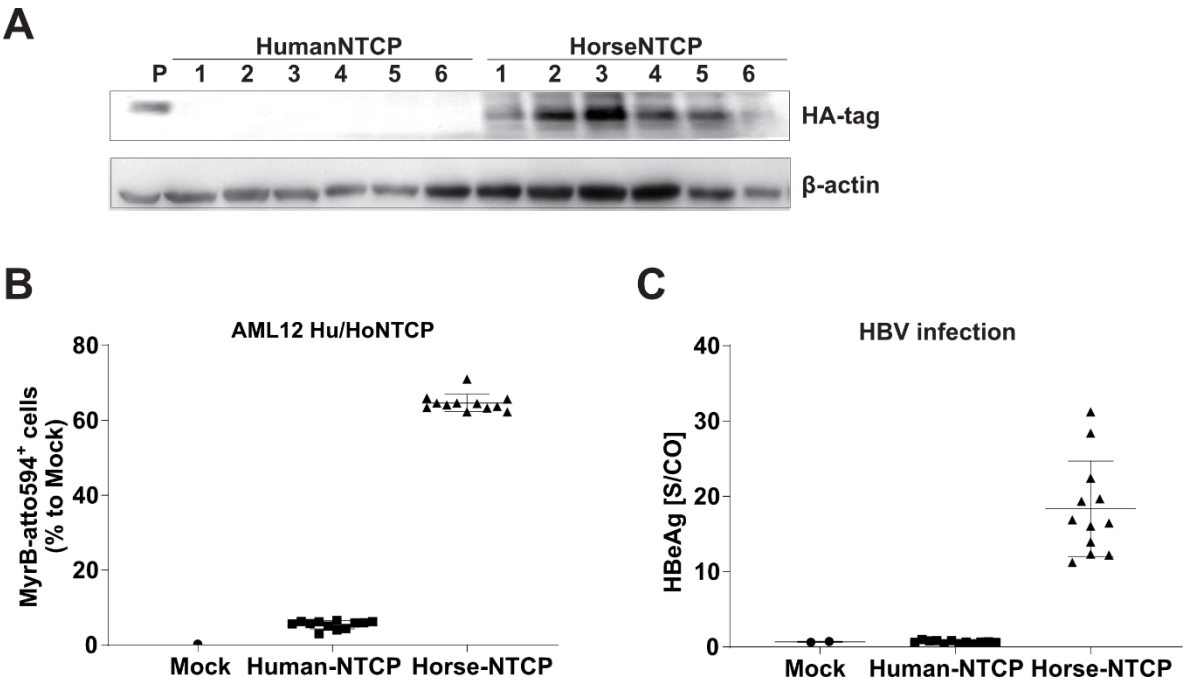

Figure 32: Generation of AML12-Ho/huNTCP cells. (**A**) Western blot analysis of NTCP expression in AML12-huNTCP and AML12-hoNTCP cells after nine days selection with kanamycin treatment. (**B**) AML12-huNTCP and AML12-hoNTCP cells were stained with 50 nM MyrB-atto594 and measured by flow cytometry. (C) Differentiated AML12, AML12-huNTCP, and AML12-hoNTCP were infected with HBV at an MOI of 500 vp/cell, and secreted HBeAg was measured at 7 dpi.

To check HBV infection rates of our AML12-hoNTCP cells, we repeated HBV infection experiments titrating the MOIs from 5000 to100 vp/cell. We implemented HBV infection with an MOI of 1000 vp/cell and MyrB as a control. Intracellular HB core (HBc) protein staining was carried out at 7 dpi to determine the number of HBV-infected cells (**Figure 33A**), and nuclear staining served as cell number control. Secreted HBeAg and extracellular pgRNA and HBV DNA were quantified at 7 dpi to determine HBV replication (**Figure 33B**). The results indicated a dose-dependent HBV infection and replication rate corresponding to the MOI used, peaking at 35.4% HBc positive cells using with an MOI of 5000 vp/cell and no detectable staining at MOI 100 vp/cell. In contrast to HBc staining analysis, more sensitive analysis of HBeAg, pgRNA, and HBV DNA demonstrated detectable levels across the whole

MOI range. To understand the mechanism of hoNTCP rendering AML12 cells susceptible to HBV infection, analysis of the differences of the protein or RNA expression profiles of AML12-hoNTCP and non-susceptible murine hepatoma cell lines should be performed in further studies.

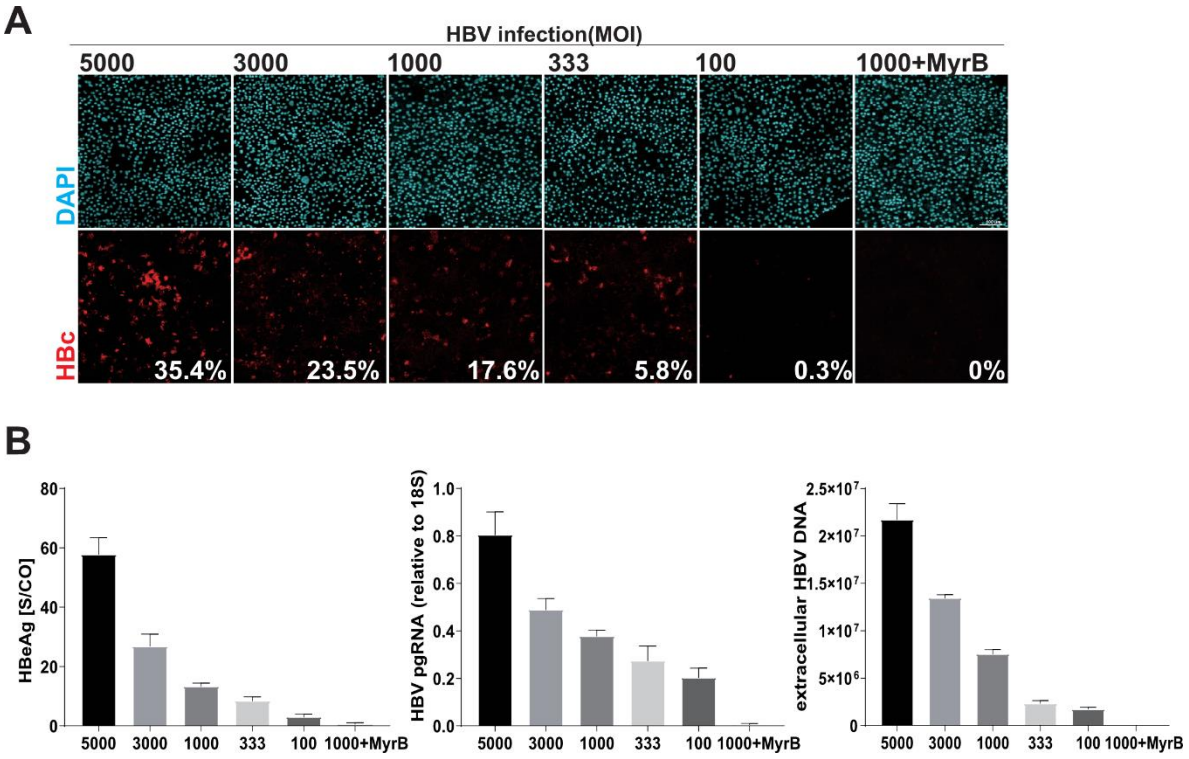

Figure 33: HBV infection rates on AML12-HoNTCP cells. (**A**) Differentiated AML12-hoNTCP cells were infected with titrated MOIs (5000–100 vp/cell) of HBV. 200 nM MyrB added to inhibit NTCP-HBV interaction on AML12-hoNTCP with MOI 1000 vp/cell served as a control. Cells were fixed and stained for HBc protein at 7 dpi, and the percentage of infected cells is denoted at the bottom-right corner of each image. (**B)** HBeAg, intracellular pgRNA, and HBV DNA were measured at 7 dpi.

2.4 Evaluation of HBV entry inhibitors

2.4.1 Two compounds were prescreened for inhibiting HBV infection

Prescreening of novel HBV entry inhibitors were performed by Dr Wettengel and Dr Esser, as described below in this paragraph. HepG2-NTCP-K7 cells were constructed as described in Ko et al. (2018), and HBV-FluoAlexa647 was established, which allowed us to quantify the internalization HBV particles by fluorescence measurement. We screened 2560 candidates from ChemBridge compounds library by adding each compound at 10 µM into the inoculum of HBV-FluoAlexa647 before adding it to differentiated HepG2-NTCP cells, following a fluorescence measurement 24 h post infection. The pilot screen revealed 0.117% hits inhibiting HBV-uptake by ≥40%. Experiments were repeated with 10 candidates for a second round using HBV-FluoAlexa647. Thus, five candidates were validated that were used in a third infection experiment in HepG2-NTCP, as well as HepaRG cells by inoculation with wt HBV, following by HBeAg and cccDNA measurement at 7 dpi (**Figure 34A**)**.** The HBeAg results showed that compounds A and G (henceforth, A0 and G0) inhibited HBV infection up to 50% and 70%, respectively in HepaRG cells (**Figure 34B**). Compound analogues A1–A9 and G1–G13 of A0 and G0 were screened, identifying A2 as inhibiting HBV infection as well. The chemical structure of compounds A0, A2 and G0 were listed in **Fig. 2.41C**.

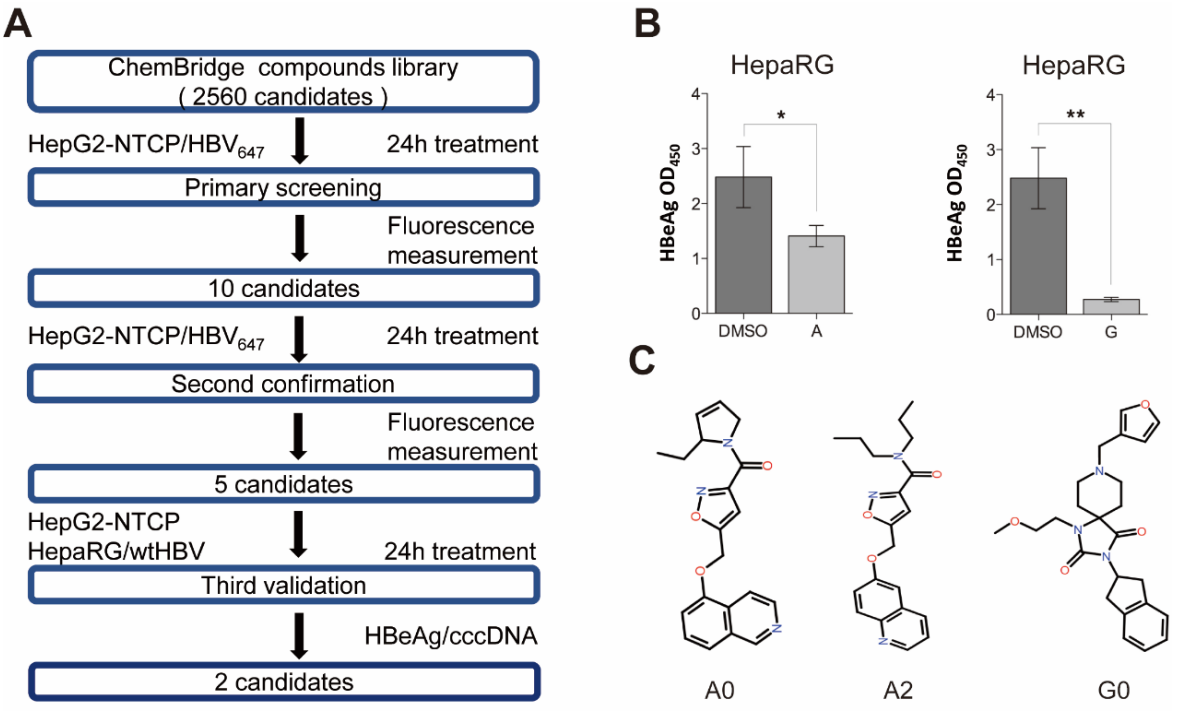

Figure 34: Prescreening compounds to inhibit HBV infection. (**A**) Schematic depiction of the primary screening analysis. HepG2-NTCP cells were predifferentiated, and inoculated with HBV-FluoAlexa647 in combination with one out of 2560 candidates from ChemBridge compounds

library at 10 µM for 24 h. The effects of the compounds on inhibition HBV entry were assessed by fluorescence measurement. The 10 candidates that responded well were tested again in HepG2-NTCP cells for 24 h. 5 candidates out of 10 were assessed for their ability to inhibit wt HBV in HepG2-NTCP and HepaRG cells. (**B**) Secreted HBeAg in supernatant were measured at 7 dpi on HepaRG cells. (**C**) The chemical structure of compounds A0, A2 and G0. The error bars represent the ± SD. **p* < .05; ***p* < .01, as determined by unpaired two-tailed Student's t-tests. [Data were kindly offered by Dr Wettengel and Dr Essner]

The inhibition effects of the compounds A0, A2 and G0 were evaluated on HepG2-NTCP-K7 cells, HepaRG cells and primary human hepatocytes (PHH). PHH cells here represent the 'gold standard' for evaluation of HBV infection. Differentiated HepG2-NTCP-K7 cells, HepaRG cells and PHH cells were inoculated with wt HBV at an MOI of 100 vp/cell in combination with 10 µM of depicted compound. Secreted HBeAg, intracellular HBV DNA and cccDNA were measured at 7 dpi. MyrB treated cells served as a control. Results demonstrated that compounds A0 and A2 reduced extracellular HBeAg, intracellular HBV DNA as well as cccDNA in HepG2-NTCP-K7, HepaRG and PHH cells. In contrast, compound G0 only reduced the HBV infection markers in HepaRG and PHH cells (**Figure 35**). The inhibition effects of A0 and A2 in HepG2-NTCP-K7 cells were comparable (**Figure 35A**) while A0 and G0 showed similar inhibition effects in HepaRG cells (**Figure 35B**). Compound A0 showed better but still comparable inhibition with the other two compounds in PHH cells (**Figure 35B**). The data indicated that we identified three compounds termed A0, A2 and G0, which were capable to inhibit HBV entry into various hepatocytes.

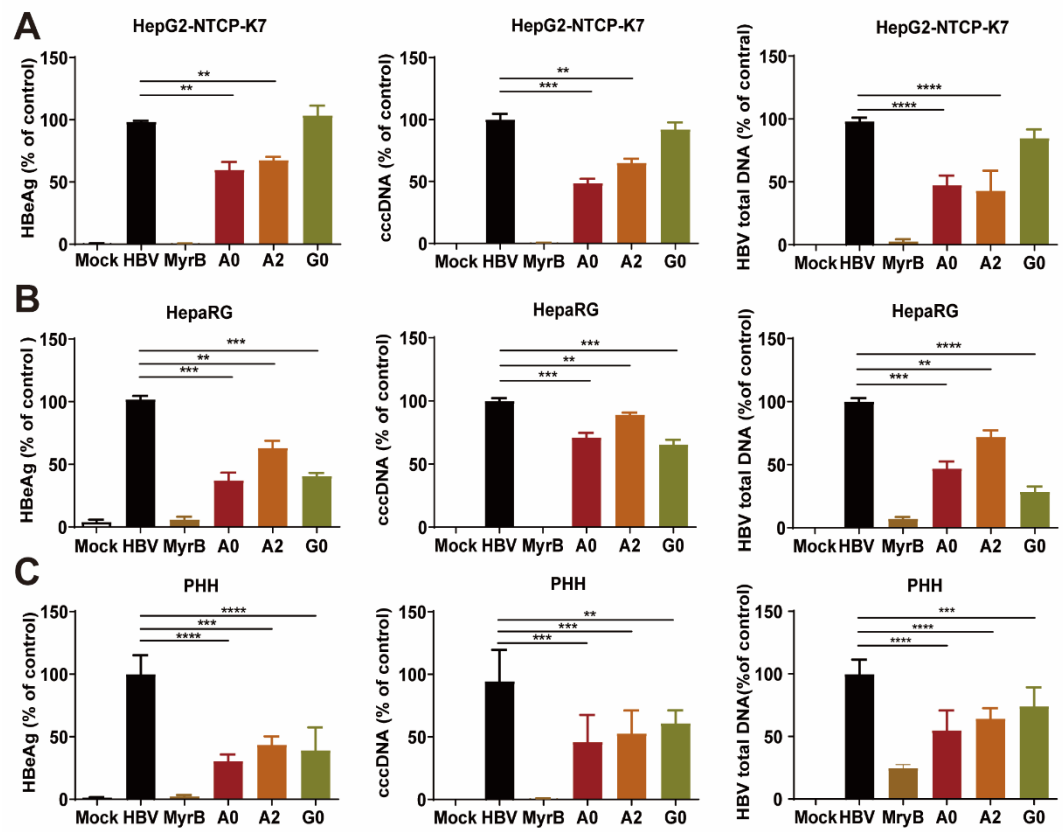

Figure 35: Evaluation of the inhibitory effect of selected compounds on HBV infection on different hepatoma cells. (**A**) Differentiated HepG2-NTCP-K7 cells, (**B**) HepaRG cells and (**C**) PHH cells were inoculated with wt HBV at an MOI of 100 vp/cell and treated with 10 µM of depicted compound. Secreted HBeAg (left), intracellular HBV DNA (right) and cccDNA (middle) were measured at 7 dpi. 200 nM MyrB served as a control. The error bars represent the ± SD. **: $p < .01$; ***: $p < .001$; ****: $p < .0001$), as determined by unpaired two-tailed Student's t-tests.

Next, EC50s of the compounds A2 and G0 (following data missing A0, due to storage issues) were determined. Therefore, differentiated HepG2-NTCP-K7 and HepaRG cells were inoculated with wt HBV at an MOI of 100 vp/cell and treated with effective concentrations of A2 and G0. To determine effects on cell viability, CTB assay was performed 24 hpi. Data were normalized to mock cells (**Figure 36**). Results demonstrated that inoculation of compounds A2 in HepG2-NTCP-K7 and compounds G0 in HepaRG cells had no impact regarding cell viability. In contrast, inoculation of compound A2 in HepaRG cells decreased the cell viability at certain concentrations (**Figure 36A**). Secreted HBeAg in supernatant was measured at 7 dpi to determine EC50 of compounds A2 and G0 in HepG2-NTCP and HepaRG cells. Results showed that compound A2 harboured an EC_{50} of 12.95 µM in HepG2-NTCP and an EC_{50} of 18.27 µM in HepaRG cells. A similar range for compound G0 in HepaRG was observed with an EC_{50} of 13.78µM (**Figure 36B**) and inhibiting effect of G0 in HepG2-NTCP were undetectable in our titration rage (data not shown).

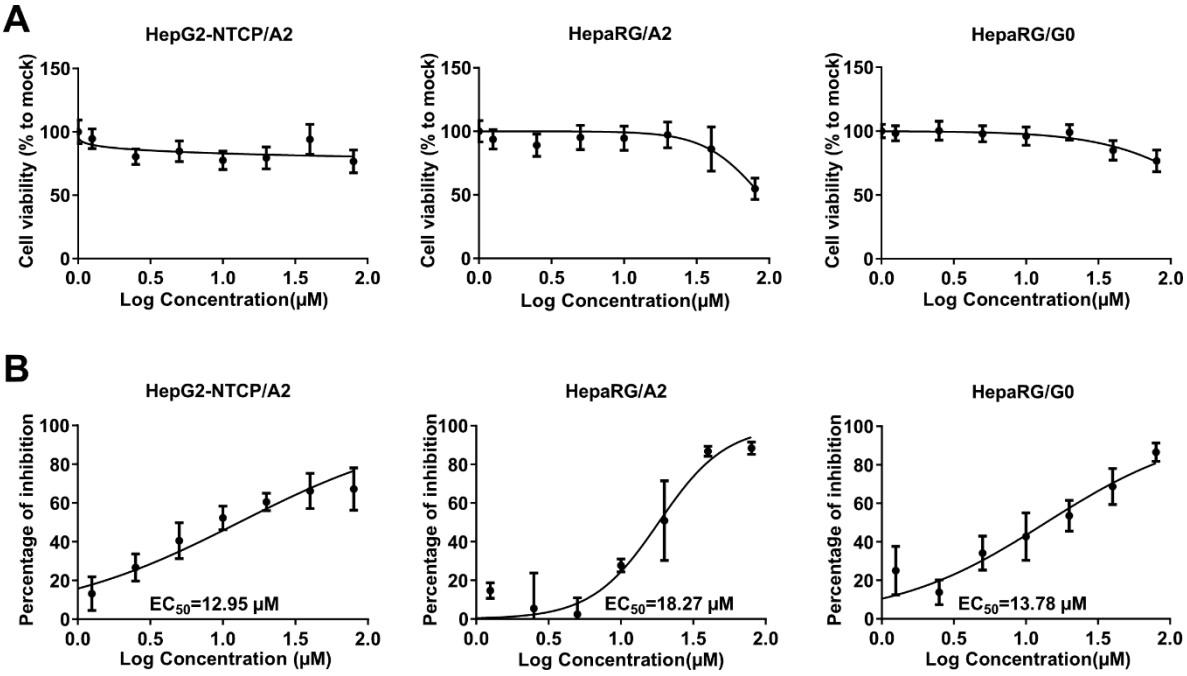

Figure 36: Cell viability and EC50 measurement of compounds A2 and G0 on different hepatoma cells. (**A**) Differentiated HepG2-NTCP-K7 cells and HepaRG cells were inoculated with wtHBV at an MOI of 100 vp/cell and treatment with various concentrations of A2 and G0 in the present PEG for 24 h before the inoculum was removed. Cell viability were determined by CTB assay after removing the inoculum and normalized the measurement of unpresented compounds cells. (**B**) Secreted HBeAg in supernatant was measured at 7 dpi to determine EC50 of compounds A2 and G0 on HepG2-NTCP and HepaRG cells.

In summary, compounds A0, A2 and G0 were screened and demonstrated to be capable of inhibiting HBV entry into hepatoma cells using micromole amounts. Furthermore, the inhibition effects regarding EC50 (except for A0) of the compounds on hepatoma cells were comparable.

2.4.2 Compounds inhibit HBV infection by targeting early steps

Since we were interested in the mechanism of the screened compounds regarding the suppression of HBV infection, we first investigated whether the compounds stimulated innate immune signaling by measurement of secreted IP10 and IL10 in cell culture media. The results indicated that compounds A0, A2 and G0 did not activate innate immunity on different hepatoma cells as extracellular IP10 (**Figure 37A**) and IL10 levels (**Figure 37B**) were comparable or less than untreated controls.

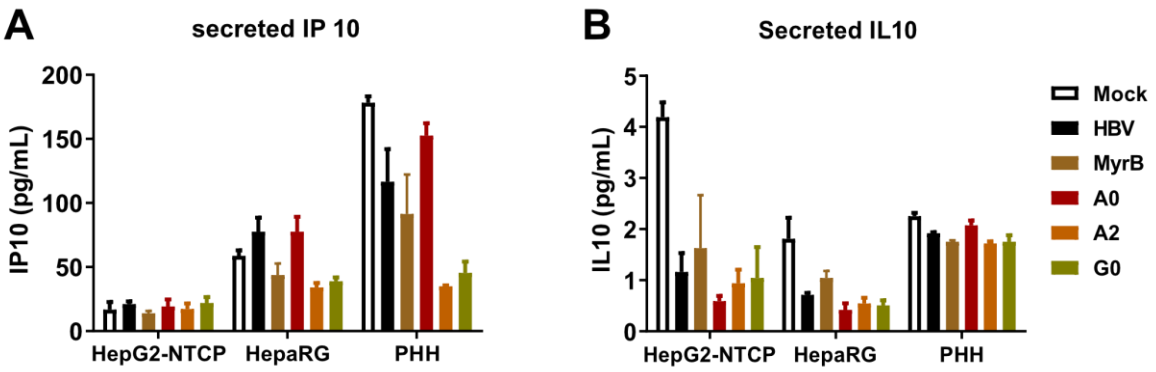

Figure 37: Characterization of the compounds effect on adaptive immunity. Differentiated HepG2-NTCP-K7 cells, HepaRG cells and PHH cells were inoculated with wtHBV at an MOI of 100 vp/cell and treatment with 10 µM compounds in the present PEG for 24 h before the inoculum was removed. Secreted IP10 (**A**) and IL10 (**B**) were measured by ELISA at 7 dpi. 200 nM MyrB added served as a control.

Next, we were interested whether the compounds directly target cells or interfere with replication steps after entry. Differentiated HepG2-NTCP-K7 cells were either pretreated (pre) with compounds A0, A2 and G0, treated during (d0–1) inoculation or after (d1–2) viral infection establishment (**Figure 38A**). Inhibition effects were determined by measuring HBeAg, total HBV DNA and cccDNA levels. Treatment of HepG2-NTCP-K7 cells with compound A0 or A2 during establishment of HBV inoculation significantly reduced HBeAg, total HBV DNA and cccDNA levels (**Figure 38B-D**). However, all markers were not affected when compounds were added either before HBV inoculation or later than 24 h post-infection, suggesting the role of compound A0 and A2 for inhibiting early HBV infection events (**Figure 38B-D**). To investigate whether the compounds affect HBV particle infectivity we preincubated viral particles with depicted compounds prior to infection for 2 h (**Figure 38A**).

The results indicated HBV particle infectivity was not affected as HBeAg, total HBV DNA and cccDNA levels levels did not change compared to DMSO control (**Figure 38B-D**).

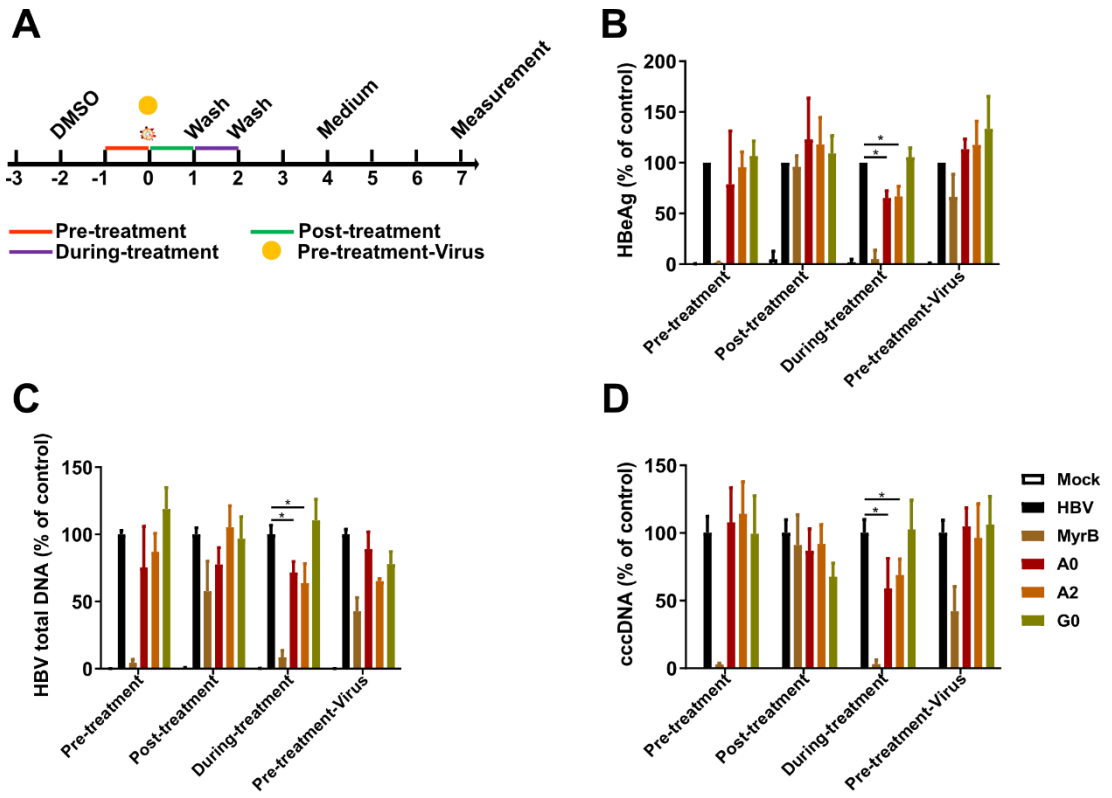

Figure 38: Compounds A0 and A2 inhibiting early HBV infection events. (**A**) HepG2-NTCP-K7 cells were either pretreated (pre) with compounds A0, A2 and G0 or treated during (d0–1) or after (d1–1) viral infection establishment or preincubation with either compound prior to HBV infection for 2 h at an MOI of 100 vp/cell. (**B-D**) HBeAg, HBV total DNA and cccDNA were measured at 7 dpi. The error bars represent the ± SD. **p* < .05, as determined by unpaired two-tailed Student's *t*-tests.

Moreover, additional verification of compounds A2 and G0 on HBV replication was performed by transduced Adeno-HBV1.3X- virus with an MOI of 3 vp/cell on HepG2-NTCP cells, as Adeno-HBV1.3X- virus only expresses HBV proteins but without cccDNA formation. Adeno-GFP was transduced with an MOI of 3 vp/cell on HepG2-NTCP in determining transduction efficiency, adeno-empty virus transduction served as a negative control. Transduction with an MOI of 3 vp/cell AdV was sufficient, since observed GFP expression was as expected (**Figure 39A**). Treatment with compounds A2 and G0 during the inoculation of Adeno-HBV1.3X- did not alter HBeAg secretion 3 days post transduction, indicating that compounds A2 and G0 do not interfere with HBV replication (**Figure 39B**).

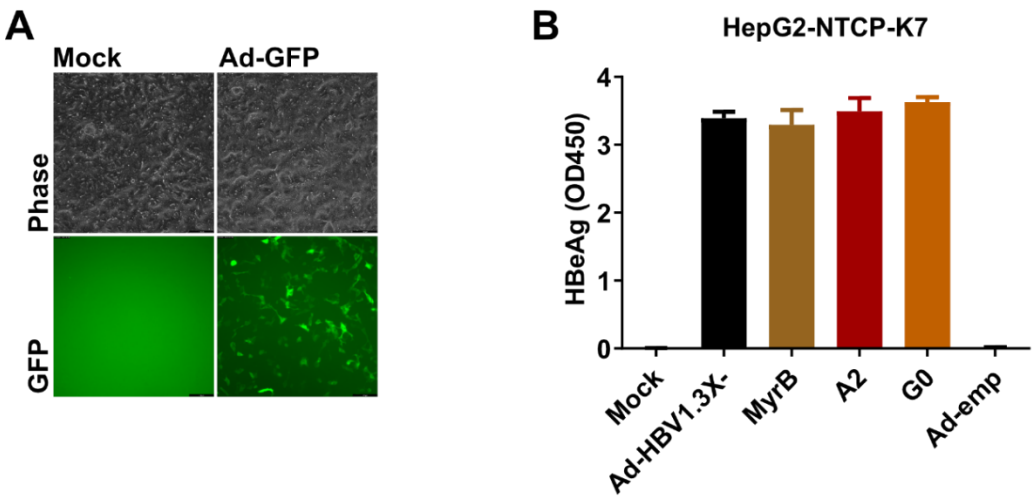

Figure 39: Evaluation inhibition of compounds A2 and G0 on HBV replication. HepG2-NTCP cells was transduced with either Adeno-GFP or Adeno-HBV1.3X- virus at an MOI of 3 vp/cell. Compounds A2 and G0 were added during with inoculation of Adeno-HBV1.3X- virus 24 h before the inoculum was removed. (**A**) Fluorescence images were taken 3 days post transduction to determine transduction efficiency. (**B**) Secreted HBeAg in supernatant was measured at 3 days post transduction. 200 nM MyrB added and Adeno-empty transduction served as controls.

Since it seems that compounds A2 and G0 interfere with early steps of HBV infection, we were interested in whether both compounds target the same stages of HBV infection and whether the compounds inhibit the intracellular capsid reimportation. Differentiated HepG2-NTCP-K7 cells and HepaRG cells were inoculated with wtHBV at an MOI of 100 vp/cell and treated with the depicted compound alone (10 µM) or in combination (5 µM or 10 µM per compound), following by treatment with or without 200 nM MyrB, until the final analysis. The 200 nM MyrB added served as a control during the viral inoculation. Secreted HBeAg and cccDNA were measured at 7 dpi. Treatment with compound combination at 10 µM of each yielded HBeAg and cccDNA levels similar to those of a single compound treatment of A2 at 10 µM but not G0 on HepG2-NTCP cells (**Figure 40A**). Similar results were observed when treatment was performed using a compound combination at 10 µM or with single compound at 10 µM on HepaRG cells (**Figure 40B**). The data indicated that compounds A2 and G0 interfere with different targets, as they did not show synergistic effects towards the restriction of HBV infection. This result was also confirmed by unchanged HBeAg and cccDNA levels when treatment was conducted with compound combination at 5 µM of each on either of cells (**Figure 40**). Prolonged treatment of MyrB on HepG2-NTCP-K7 and HepaRG cells did not change the values of HBeAg, and cccDNA revealed that compounds did not inhibit the intracellular capsid reimportation in infected cells (**Figure 40**).

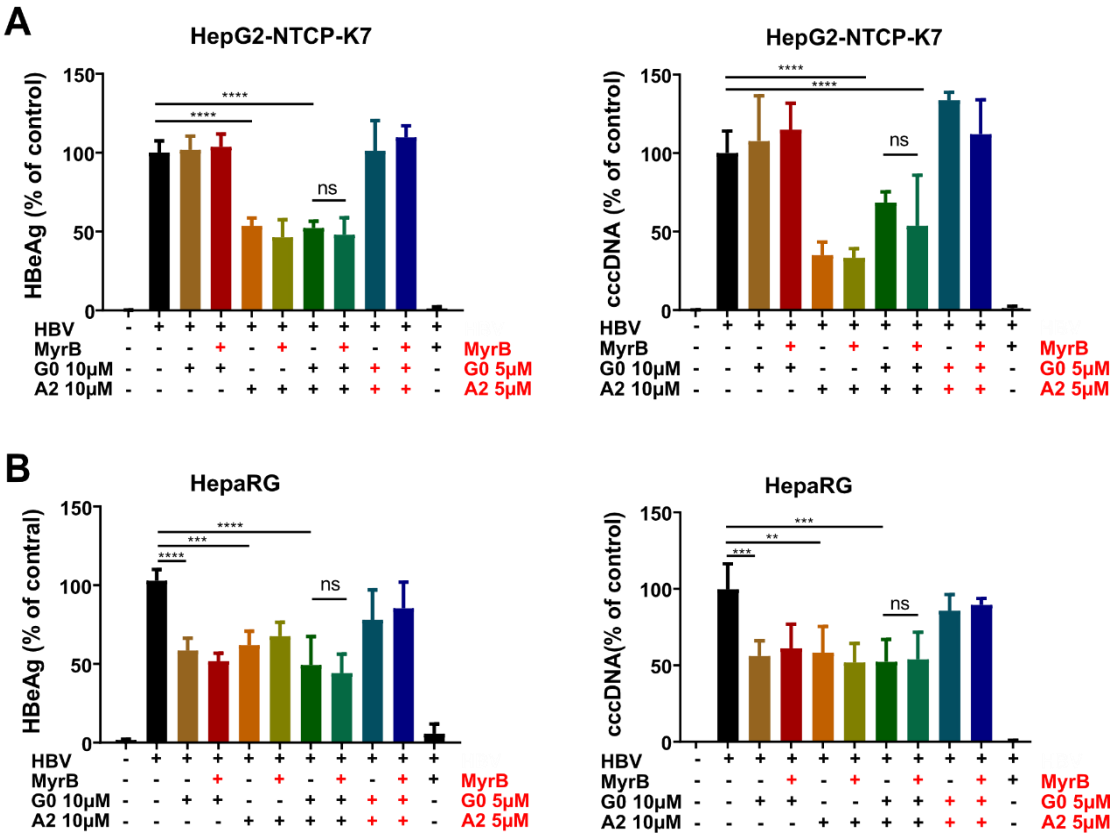

Figure 40: Evaluation of efficacy of either single or combined treatment and with subsequent treatment with entry inhibitors on viral infection. (**A**) Differentiated HepG2-NTCP-K7 cells and (**B**) HepaRG cells were inoculated with wtHBV at an MOI of 100 vp/cell and treatment with either a single compound, at 10 μM, or combined compounds, at 10 μM or 5 μM of each, for 24 h before the inoculum was removed. The cells were treated with or without 200 nM MyrB after the inoculum was removed, until the final analysis. The 200 nM MyrB added served as a control during the viral inoculation. Secreted HBeAg and cccDNA were measured by ELISA and qPCR, respectively, at 7 dpi. The error bars represent the ± SD. **: $p < .01$; ***: $p < .001$; ****: $p < .0001$; ns: no significant), as determined by unpaired two-tailed Student's *t*-tests.

To characterize which stages of the viral life cycle are inhibited by the compounds, we next investigated inhibition effects related to HBV binding and uptake. Differentiated HepG2-NTCP-K7 cells and HepaRG cells were inoculated with wtHBV at an MOI of 100 vp/cell and treated with either compounds at 4 °C for 1 h or shifted to 37 °C for either 6 h or 24 h. At each time point, the cells were either washed or trypsinized prior to harvest for either total bound or intracellular HBV DNA analysis. MyrB and heparin served as controls. Additional, differentiated HepG2-NTCP-K7 cells were incubated with 400 nM MyrB-atto488 and treated with or without unlabeled MyrB (200 nM) or compound A2 or G0 (10 μM) for 30 min before unbound MyrB-atto488 was removed. Compounds A2 and G0 did not interrupt HBV binding with HSPG and NTCP, as total HBV DNA did not change compared with non-treatment group (**Figure 41A**). In addition, bound MyrB-atto488 demonstrated similar levels compared with only MyrB-atto488 inoculation (**Figure 41B**). Compound A2 reduced intracellular HBV total DNA with 24 h treatment on HepG2-NTCP cells (**Figure 41C**) and with 6 h on HepaRG

cells (**Figure 41D**), while compound G0 did not change total intracellular HBV DNA on HepaRG cells after either 6 h or 24 h treatment (**Figure 41D**). These data revealed that compound A2 interrupts HBV entry prior to establishment of HBV infection, but after HBV endocytosis on HepG2-NTCP cells, and inhibits HBV endocytosis on HepaRG cells, while compound G0 interferes with HBV infection prior to the establishment of HBV infection but at later steps of uptake.

In summary, two small molecules, compounds A2 and G0, inhibit HBV infection by targeting the early infection stages of HBV prior to the establishment of HBV infection on hepatoma cells.

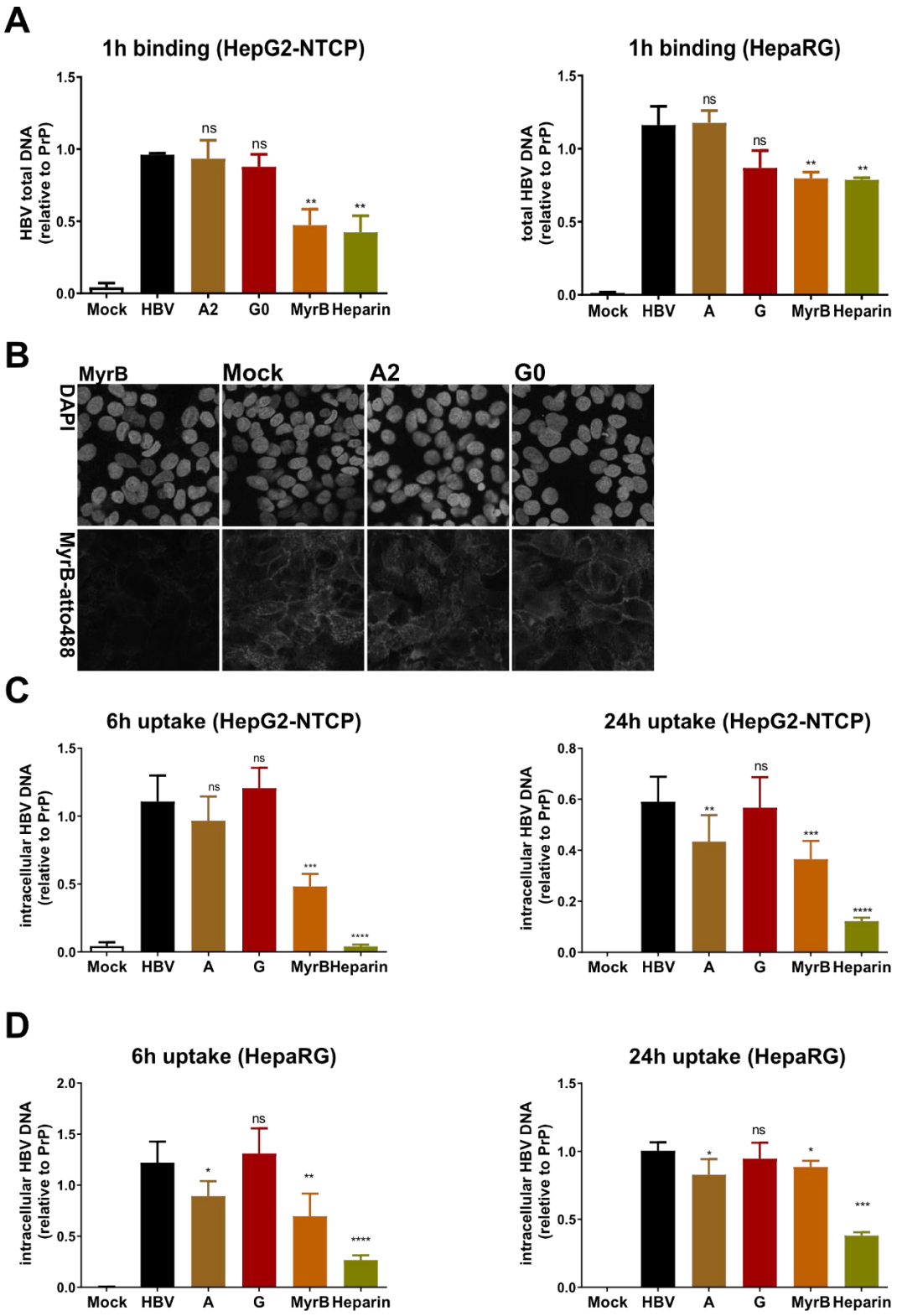

Figure 41: Characterization inhibition effects of compounds A2 and G0 on HBV entry. HBV binding and uptake assay was performed on differentiated HepG2-NTCP-K7 cells and HepaRG cells. Cells were inoculated with wtHBV at an MOI 100 vp/cell and treated with either compounds at 4 °C for 1 hour or shifted to 37 °C for 6 and 24 hours. MyrB and heparin added served as controls. (**A**) HBV binding was analyzed by measuring cell-associated HBV DNA relative to PrP after incubation at 4 °C for 1 hour with subsequent two times PBS wash. (**B**) Differentiated HepG2-NTCP-K7 cells were incubated with 400 nM Atto488-labeled MyrB and treatment with

either with unlabeled MyrB (200 nM) or compound A2 or G0 (10 µM) for 30 mins. Unbound MyrB-atto488 was removed by washing with PBS twice and the cells were fixed with 4% paraformaldehyde and mounted with Flouromount-G containing DAPI. Images were taken by Fluoview FV10i microscope (Olympus). (**C.D**) HBV uptake assay was analyzed by measuring cell-associated HBV DNA relative to PrP after incubation at 37 °C for 6 and 24 hours with subsequent trypsinization. Statistical analysis: Student's unpaired *t*-test (ns: not significant, *p<0.05, **p<0.01, ***p<0.001, ***p<0.0001).

3. Discussion

New therapies to cure chronic hepatitis B virus (HBV) infection have been limited by the lack of suitable animal models. NTCP, a bile acid transporter, has been identified to expand the HBV host range as a species-specific key factor for HBV entry and infection (Burwitz et al. 2017; Lempp et al. 2017; Protzer et al. 2019). In this thesis, species-specific NTCP for HBV binding and infection, the advanced HBV receptor and novel HBV entry inhibitors were studied, as discussed in the following chapters.

3.1 Species specificity of NTCP for HBV infection

To make it easy for screening HBV permissive NTCPs, we have established Cluc-NTCP co-expression constructs that allow to quantify the expression of NTCPs and analyze their function as mediator, activator and trigger of successful HBV infection. Our data demonstrates that co-expression of Cluc-NTCP could solve the shortage of species-specific antibodies and detect NTCP expression sensitively (Figure 7- Figure 13). The NTCP variants detection could also be achieved by either fusion with detection tag or reporter gene. while the quantification of Cluc in supernatant are more convenient and time-saving. To verify the sensitivity of Cluc as a marker to detect NTCP expression and the functionality of co-expressing NTCP for bile acid uptake and HBV infection, we first selected NTCP sequences that have been reported. The NTCPs from macaque (Müller et al. 2018; Wettengel 2019) and pig (Protzer et al. 2019) are not able to bind to MyrB-atto488, thereby preventing viral infection. Mouse NTCP is able to bind to MyrB-atto488 but not support HBV infection unless amino acid replacement at HBV functional domain (Yan et al. 2013). The woodchuck (Fu et al. 2017), ferret (Wettengel 2019), tupaia (Yan et al. 2012; Zhong et al. 2013) NTCPs contain the conserved binding and functional domains, therefore these NTCPs are able to bind to MyrB-atto488 and support viral infection. Those findings were confirmed with our data for the capability of NTCPs mediating HBV infection. However, it has shown that HBV infects gibbon in vivo (Bancroft et al. 1977) and guinea pig primary hepatocytes in vitro (Caroline Gähler 2011). However, opposite results were observed in gibbon and guinea pig NTCPs since gibbon and guinea pig NTCPs are not attachable for MyrB-atto488, though comparable Clucs were detected. The possible reasons for that phenomenon are incorrect sequence information in GenBank database or incorrect protein expression. Capuchin monkey has been found as the host of novel HBV (Carvalho Dominguez Souza et al. 2018) but its NTCP only permits MyrB binding not HBV infection. The only difference at HBV binding domain aa 84-87 is K (Lysine) rather than N (Asparagine) that is conserved in aa position 87 for NTCP permitting HBV infection. Therefore, that will

be interesting whether modification of K87 to 87N can endow activity of capuchin monkey NTCP for HBV infection.

To discover other possible hosts of HBV, we analyzed the capability of NTCPs from *Mammals, Amphibia, Actinopteri and Aves* mediating HBV infection. Human HBV belongs to *orthohepadnaviridae* family and mainly infects mammals (Summers et al. 1978; Mason et al. 1980; Schaefer 2007). Our data demonstrates that the NTCPs that mediate human HBV entry into hepatoma cells mainly adapt from mammals that include woodchuck, ferret, tupaia, horse, rabbit, whale, big brown bat, cat, rhinoceros, aardvark and hedgehog (Figure 8, Figure 9 and Figure 14). Horse NTCP was found to enable HepG2 cells more efficiently for HBV infection than human NTCP either after normalization to secreted Cluc or before normalization. This observation offers the possibility that horse might be a host susceptible for HBV infection or horse HBV is in presence in the horse world. This hypothesis has been confirmed by a recent publication that HBV related Equid HBV (Eq HBV) occurs globally in donkeys and zebras by screening of 2917 specimens from equid (Rasche et al. 2021). In addition, alternative entry mechanism of EqHBV is suggested because deltavirus pseudotypes carrying human HBV and EqHBV infect primary horse hepatocytes while EqHBV deltavirus pseudotypes are unable to infect human cells upon human NTCP expression (Rasche et al. 2021). Furthermore, Equine hepacivirus (EHcV), which is related homologues of hepatitis C virus (HCV) was identified in Western and Eastern countries (Tanaka et al. 2014; Walter et al. 2017). Those discoveries demonstrate that the Equid family as another host of Hepatitis virus could serve as an animal model for preclinical testing of novel therapies for CHB as well as HCV infection. Duck HBV (DHBV) genome contains high variability preS (Sprengel et al. 1985; Urban and Gripon 2002) and human myr-preS-peptide are not able to block DHBV in duck primary hepatocytes (Urban and Gripon 2002). The duck HBV and probably duck NTCP reveal the different preS-NTCP interaction pattern in the bird world than mammal world.

3.2 Overcoming the entry-barriers of hepatocytes for HBV infection

Overcoming entry-level barriers of hepatocyte cell lines or hepatocytes are considered to develop new cell culture and animal models that allow HBV infection. We further demonstrate that human and murine hepatocyte cell lines complemented with HBV permissive NTCP allow HBV infection establishment (chapter2.1-2.3). Direct overexpression of human NTCP in hepatocytes is one way to allow HBV entry. In this study, HepG2 and AML12 cells expressing hu/hoNTCP allowed HBV entry and cccDNA formation, thereby supporting complete life cycle of HBV. Expression of human NTCP in macaque and pig hepatocytes overcome the entry-barrier for HBV infection *in vitro* and enables HBV

infection *in vivo* of macaques (Burwitz et al. 2017; Lempp et al. 2017). However, complement of murine hepatocytes either *in vitro* or *in vivo* with human NTCP only render mice susceptible for HDV infection rather than HBV (He et al. 2015; Lempp et al. 2017). This evidence suggests that there are host factors limiting HBV infection.

The second method to overcome entry-barrier of hepatocytes is to modify species-specific NTCP that enables NTCP permissive for HBV. The motifs aa 157-165 and 84-87 of NTCP are determined as crucial domains for mediating HBV binding and infection (Yan et al. 2012; Yan et al. 2013). Swapping HBV binding domains aa157-167 of pig NTCP and aa157-165 of macaque NTCP with its counterparts of human NTCP make it possible to mediate HBV entry into HepG2 cell (Wettengel 2019; Protzer et al. 2019). Moreover, complement of humanized-pig NTCP in pig hepatocytes enables HBV infection in vitro and in vivo (Protzer et al. 2019). Additionally, replacement of the residues aa 84-87 of mouse NTCP with its counterparts of human NTCP only renders mouse susceptible for HDV rather than HBV (He et al. 2016) while HepG2 cells permit HBV and HDV infection upon the modified mouse NTCP expression (Yan et al. 2013). Similar with mouse NTCP modification at the region aa 84-87, mutation hamster NTCP residues at 84-87 to 84R and 87N made it possible to mediate HBV infection (Figure 11). The modification of hamster NTCP should break the entry-barrier for HBV in hamster hepatocytes.

3.3 The impacts of other domains or amino acids for HBV infection

Except of the two important motifs for HBV infection, the other domains or amino acids are also crucial for viral infection. For instance, the S267F variants abolish bile-acid uptake and HBV infection, but without altering its expression or localization (Yan et al. 2014; Hu et al. 2016). This thesis demonstrates that NTCP only holding the two conserved motifs at aa position 84-87 and 157-165 are insufficient for HBV infection (Figure 12 and Figure 13). Goat and cow NTCPs are able to bind to MyrB-atto488 but permit low or no HBV infection, though they harbor the same aa at the position 84-87 with cat NTCP. However, modification the F82 to 82V of goat and cow NTCPs only significantly improved the efficiency of HBV infection. The NTCPs from seal, dog and little brown bat are able to bind to MyrB-atto488 and consist the conserved residues at aa 84-87 but without establishment of HBV infection. Alignment of the NTCP sequence of horse, seal and dog show that single mutation dog/seal NTCPs T78A did not change the capability of dog and seal NTCPs on mediating HBV infection. Chimeric horse-dog and seal-horse NTCPs mediating HBV infection on HepG2 cells reveal that functional domains are missing at the N-terminus of dog NTCP and C-terminus of seal NTCP. Similar with seal and dog NTCP, little brown bat NTCP is insufficient to support HBV infection, though little brown bat NTCP binds to MyrB-atto488 and contains

the conserved residues at aa 84-87. The shortage capability for permitting HBV infection of seal, dog and little brown bat NTCPs shows that there are still other functional domains unidentified.

The other domains could also impair NTCP function for HBV infection. The localization of NTCP on the plasma membrane is relative with the C-terminal domains as shown by mutation of the C-terminal tyrosine-based sorting motifs (Y307-EK-I and Y321-K-A-A) or truncation of the C-terminal reducing NTCP localization on the cellular membrane (Appelman et al. 2021). The N-terminal glycosylation status at aa position 5 and 11 also influence the NTCP function since the absence of both glycosylations reduce the NTCP abundancy at the plasma membrane (Appelman et al. 2021; Le et al. 2021). Whereas the opposite conclusion has been obtained for the nonglycosylated forms that is still capable to mediate HBV infection (Lee et al. 2018). These findings indicate that the complete functional NTCP requires mature and robust domains or forms of NTCP protein.

3.4 The comparison of huNTCP and hoNTCP for mediating HBV infection

3.4.1 The platforms for comparison of huNTCP and hoNTCP for HBV infection

As we were interested in the underlying mechanism that hoNTCP enhancement of HBV infection in human and murine hepatoma cells compared to huNTCP, therefore the comparison platforms for expression comparable total NTCP proteins were needed. We obtained similar levels of huNTCP and hoNTCP expressing hepatoma cells by either transfection of the same amount of huNTCP and hoNTCP IVT mRNA or generation of HepG2-huNTCP and HepG2-hoNTCP stable cells (Figure 16- Figure 20). However, our experiments demonstrate that the approach of IVT mRNA transfection is much faster and convenient compared to stable cells generation. Synthetic mRNA is introduced as it provides viral-free, non-integration, zero-footprint method for protein expression (Oh and Kessler 2018). In contrast, selection of specific characteristics cell lines often shows highly different cellular homeostasis compared to the original cell population (Sommeregger et al. 2016). IVT mRNA production is fast using pDNA templates for T7 based synthesis and could be boosted when using PCR based templates harboring a T7 promotor (Stadler et al. 2021). In addition, cytotoxicity, protein expression and functionality of introduced IVT mRNA in differentiated hepatoma cells could be optimized by different cap structures (standard cap vs. ARCA) and nucleotide modifications (UTP and CTP analogs) (Oswald et al. 2021).

Transfection of same amount of IVT mRNA resulted in similar levels of huNTCP and hoNTCP expression in differentiated hepatoma cells. However, similar levels of huNTCP

and hoNTCP protein led to distinguishable ratios for MyrB-atto488 binding and MFI, suggesting unequal capability of plasma membrane localization or viral binding affinity. The high binding efficiency of hoNTCP with MyrB-atto 488 was confirmed using additional stable cells that expressed comparable huNTCP and hoNTCP. Staining HepG2-huNTCP and HeG2-hoNTCP by MyrB-atto488 showed comparable MyrB-atto488 positive cells but with a high MFI of HepG2-hoNTCP. Those findings indicate that hoNTCP binding to MyrB-atto488 occurs by very high binding efficiency compared to huNTCP. Altogether, our data suggests that IVT mRNA is a feasible tool to express exogenous proteins at least in cell culture levels.

3.4.2 HoNTCP enhances HBV infection via high surface localization efficiency

Infection studies with different MOIs in huNTCP and hoNTCP expressing cells demonstrate a dose-dependent infected cell numbers and single cell viral load (Figure 21). Similar results were shown in HepG2-NTCP-K7 cells that were infected with an increasing MOI (Ko et al. 2018). In addition, our results also demonstrate that hoNTCP improves infected cell numbers and cccDNA copy number of single cell compared to huNTCP expressing in HepG2 cells (Figure 21). The enhancement of HBV infection mediated by hoNTCP is initiated by facilitating more HBV particles bound to target cell membrane (Tab.1). The inefficient conversion of incoming rcDNA to cccDNA was reported as a rate-limited step in establishing productive infection (Chakraborty et al. 2020). However, HBV internalization and infection kinetic studies in this thesis reveal high intracellular encapsidated rcDNA trafficking efficiency and conversion efficiency of rcDNA to cccDNA in HepG2 cells upon hoNTCP expression compared to cells expressing comparable huNTCP. These findings indicate that hoNTCP plays a significant intracellular role for HBV establishment.

A certain threshold of NTCP surface localization levels regulates HBV infection (Oswald et al. 2021). In this thesis, we demonstrate that hoNTCP locates on plasma membrane much more efficiently than huNTCP that resulting in high amount HBV binding and infection (Figure 26 and Figure 27). In addition, hoNTCP localization are influenced by swapping of aa157 of huNTCP and hoNTCP. Swapping either of the two motifs or both indicate that aa 157-165-175 of hoNTCP promoting HBV infection. Single replacement of those three amino acids between huNTCP and hoNTCP demonstrate that G157 of hoNTCP enhances HBV particles bound on cell surface and viral infection (Figure 22- Figure 24). Importantly, the single aa at 157 of hoNTCP is involved in the delayed degradation of the NTCP proteins, thereby retaining more NTCP molecules on the plasma membrane. Moreover, flow cytometry analysis demonstrates that hoNTCP contains comparable binding affinity with huNTCP (Figure 27). There are several possibilities that cause high plasma membrane localization levels of hoNTCP. Solute transportation requirement of liver cells is reported to

regulates NTCP surface localization levels (Anwer and Stieger 2014). This might offer the possibility that horse liver cells need to take up high amount of bile acid to keep the balance of microenvironment. Abolishment both glycated residues of N-terminal glycosylation site of NTCP dropped the NTCP abundancy at plasma membrane, thereby reducing HBV infection efficiency, demonstrating that modification status also influence plasma membrane localization (Appelman et al. 2017; Le et al. 2021). The other post-translational regulations by cAMP and modifications (e.g., protein kinase C isoforms, S-nitrosylation, phosphorylation and dephosphorylation) were reported to affect the plasma membrane localization levels (Anwer and Stieger 2014). However, whether those modifications and regulations are involving in high levels localization on plasma membrane of hoNTCP still remain to be further investigated.

3.5 NTCP expression levels regulate HBV infection efficiency

HBV infection efficiency is relative to inoculated MOI and the presence of PEG and DMSO (Gripon et al. 1993; Ni et al. 2014; Ko et al; 2018). Our data shows that HBV infection efficiency is strongly correlated to NTCP expression levels. Dose-dependent NTCP expression derived from increased transient mRNA influences HBV binding and infection (Figure 16 and Figure 17). Transient of increasing NTCP mRNA resulted in a maximum NTCP expression at 1000ng/well, along with a clearly increasing curve of MyrB-atto488 binding cells and MFI of MyrB-atto488 positive cell, demonstrating a dose-dependent localization level of NTCP on plasma membrane. Similar result was reported that transfection different concentrations of NTCP IVT mRNA shows a dose-dependency of MyrB binding susceptibility of hepatoma cells (Oswald et al. 2021). However, high amounts of NTCP mRNA (1000 ng and 2000 ng) and low amounts of NTCP mRNA (<100 ng) transient in HepG2 cells reduced HBV infection efficiency compared to 333 ng and 100 ng NTCP mRNA transient cells (Figure 17). In contrast, highest HBV infection efficiency was observed at 1000ng/well of human NTCP mRNA transfection in HepG2 cells (Oswald et al. 2021). This phenomenon might be explained by overexpression of exogenous NTCP influencing the cellular metabolism homeostasis compared to the native cell population (Wang et al. 2020), especially when excessive physiological amounts of IVT mRNA are used for translation. HepaRG cells express lower levels of NTCP upon differentiation in a non-transformed and physiological system that support efficient HBV infection as it shares similar characteristics with PHH (Marion et al. 2010). Therefore, a certain threshold of NTCP expression is required to promote HBV entry and infection, and that infection efficiency at least in cell culture depends on the surface NTCP.

3.6 Potential intracellular roles for NTCP in HBV entry

Along with the discovery of NTCP as entry receptor for HBV, its functions as mediator for HBV specific binding and internalization were depicted (Yan et al. 2012; Ni et al. 2014; Chakraborty et al. 2020). However, besides the function of NTCP as a receptor, our results also show an intracellular, unknown role of NTCP for HBV infection. Similar levels of HBV particles bound to HepG2-NTCP-K7 cells and HepG2-hoNTCP cells, while two to three times of intracellular HBV DNA 24hpi and cccDNA 7dpi were observed in HepG2-NTCP-K7 cells compared to HepG2-hoNTCP cells (Tab 1). In addition, HepG2-NTCP-K7 cells express high amount of NTCP compared to HepG2-hoNTCP cells (data not shown). This study suggests that high amount of NTCP expression may enhance either HBV particles or capsids transportation. Since cellular entry of HBV mimicking particles (bio-nanocapsules coupled with myristoylated L-protein of HBsAg) is mainly driven by HSPG-mediated endocytosis regardless of NTCP expression, cell-surface NTCP may not be involved in HBV attachment to cell surface as well as its uptake, but an intracellular roles of NTCP (Somiya et al. 2016). Similar results were observed as add-in heparin blocked most of HBV binding as well as uptake while MyrB only reduced low amount of viral binding and uptake (Figure 41). The low block efficiency may be explained by the insufficient concentration of MyrB but same amount MyrB resulted in rarely cccDNA formation (Figure 35, Figure 38, Figure 40 and Figure 41).

HBV entry and trafficking are supposed to be mediated by endocytosis in either clathrin or caveolin-dependent manner in hepatoma cells (Macovei et al. 2010; Herrscher et al. 2020). NTCP has been described that co-localization with Rab4 in the early endosome and with Rab11 in the recycling endosome, but undetectable in the late endosome (Sarkar et al. 2006). These studies were confirmed as HBV escapes from early endosomes in the presence of NTCP (Chakraborty 2020). Altogether, those data suggest that NTCP interact with HBV particles at plasma membrane and subsequently may play intracellular roles for HBV entry by endocytosis.

3.7 AML12 cells are susceptible for HBV infection upon NTCP expression

The discovery of NTCP overcomes the entry-levels barrier for HBV infection but host factors of mouse restrict HBV infection *in vitro* and *in vivo* in mice (Li et al. 2014; He et al. 2015; Lempp et al. 2017). However, the murine hepatocyte cell line AML12 cells was found susceptive for HBV infection upon overexpression of human NTCP (Lempp et al. 2016b; Qiao et al. 2018). Our data demonstrate that AML12 cells complemented with NTCP, especially hoNTCP, allows efficient establishment of HBV infection and formation cccDNA

(Figure 29- Figure 30). Moreover, overexpression of hoNTCP in AML12 cells allowed for the establishment of low MOI HBV infection (Figure 31). Infection assay with different MOIs of HBV on huNTCP- and hoNTCP IVT mRNA transfected AML12 cells indicates that AML12 cells overexpression of hoNTCP support much lower amounts of HBV for establishment of viral infection compared to huNTCP. The cccDNA as the robust HBV infection marker was detected by a specific southern blot (Guo et al. 2007; Ko et al. 2018). Our data, rcDNA and cccDNA southern blot analysis, indicate cccDNA establishment in the AML12 cells (Figure 30). Moreover, T5 exonuclease treatment where non-cccDNA species are digested (Xia et al. 2016) and restriction enzyme digestion that linearizes cccDNA (Ko et al. 2018) further confirmed the cccDNA identity.

AML12 cells were immortalized from isolated primary hepatocytes of TGFα transgenic CD1 mice. Our results show that CD1 mice is not the main reason for susceptibility of AML12 cells. To confirm the purity of AML12 cells, multiplex cell contamination test was performed. The results exclude other species cells contamination and indicate the cells are original from mice. CD1 mice background, TGFα and immortalization process may lead to missing factors expression in AML12 cells that are responsible for either trafficking viral particles, capsids or establishment cccDNA. That overexpression of TGFα on murine hepatoma cells did not alter the capability for HBV infection (Lempp et al. 2016b) excludes the possibility of TGFα as the missing factor. For CD1 mice, the intrahepatic expression of NTCP failing to form cccDNA indicate that CD1 mice are not able to support establishment of HBV infection (data not shown). However, CD1 mice contains entire immune system, therefore challenge with HBV in CD1 mice may result in immune response against HBV, following with HBV clearance. The other possibility is that immortalization process from CD1 primary hepatocytes to AML12 cells may change protein expression profile and concludes the susceptibility of AML12 cell for HBV infection. The huge different of mRNA profile for CD1 primary hepatocytes and AML12 cells (data not shown, RNA seq was performed by Andreas Oswald) have demonstrated the hypothesis that AML12 cell line is a new cell line compared with its original primary hepatocytes. Therefore, specific factors-related susceptibility of AML12 cells for HBV infection remains to be further investigated.

Mice serum derived HBV from transgenic mice infects chimpanzees, revealing the mice hepatocytes producing infectious virions (Guidotti et al. 1999). However, our data demonstrate that progeny virus produced by AML12 cells are not infectious, even though high level of the HBV DNA genome was detected in the supernatant (data not shown). Either co-culture of infected and naïve AML12-hoNTCP cells or transfer supernatant of infected AML12-hoNTCP to naïve AML12-hoNTCP cells did not result in new infection in naïve

AML12-hoNTCP cells (data not shown). Detection of cccDNA in AML12HBV10 cells indicate that uncoated viral capsid reimport into the nucleus for cccDNA establishment (Xu et al. 2010; Cui et al. 2015). However, without NTCP expression in AML12HBV10 cells, the experiment excludes cccDNA formation derived from infectious particles. In addition, high amount of Dane particles is required to achieve sufficient HBV infection (Ko et al. 2018; Wettengel et al. 2021). With those findings, the shortage of viral spreading between AML12-hoNTCP cells could be explained by either low titer progeny virus production or nonfunctional HBsAg induced by AML12 cells.

3.8 The impacts of new compounds on HBV establishment

Currently, PEG-IFNα and NA such as ETV and TDF are the first line drugs for treatment CHB patients that eliminate cccDNA and suppress viral replication, respectively. However, neither single nor combined treatment of CHB leads to a loss of HBsAg. Thus, more effective therapies that target multiple steps during life cycle, thereby strongly blocking cccDNA formation and reducing viral replication are needed to be developed. The HBV entry inhibitor MyrB, which is under evaluation in a phase IIa clinical trial, is able to prevent viral spreading between hepatocytes but therefore must be delivered by intravenous injection, thus is not suitable for general HBV infected patients (Blank et al. 2018) .

In our study, we reported and demonstrated three novel compounds as anti-HBV agents by inhibiting early stages of viral infection without stimulating immune response (chapter 2.4). Treatment with compounds A0, A2 and G0 during establishment of infection significantly reduced cccDNA levels in HepG2-NTCP-K7 cells, PHH and HepaRG cells (Figure 35); however, at concentrations around 10-20 µM were needed to inhibit HBV entry (Figure 36). Neither pretreatment of cells before HBV infection for 24 h nor treatment after cccDNA establishment affected cccDNA levels, indicating a targeting of early stages of HBV infection (Figure 38). HAP_R01 was shown targeting extracellular HBV particles by preincubation of HBV particles with the antiviral compounds and reduces particle infectivity (Ko et al. 2019). In our study, pretreatment of viral particles with either compound did not alter the levels of cccDNA establishment (Figure 38). IFNα triggers innate and adaptive immune responses, resulting in the elimination of the cccDNA (Bloom et al. 2018). Similar IP10 and IL10 levels were measured of the compound treatment and non-treatment group, indicating that compounds interfere unknown HBV-host interactions rather than stimulating innate immune responses (Figure 37).

To investigate whether those two compounds target same stages or HBV-host interaction, combined treatment of the two compounds on HepG2-NTCP-K7 cells and HepaRG cells

were performed. Our results indicate A2 and G0 target different stages of viral infection as similar HBeAg and cccDNA were measured compared to single treatment group (Figure 40). Heparin and MyrB add-in assay reduce HBV preS1 binding to cellular membrane that is mediated by either HSPG and NTCP (Yan et al. 2012; Ni et al. 2014; Somiya et al. 2016; Chakraborty et al. 2020). That HBV particles bound on HepG2-NTCP-K7 cells and HepaRG cells after treatment by A2 and G0 were not significantly reduced demonstrate that A2 and G0 did not interrupt HBV binding with HSPG and NTCP (Figure 41). Prolonged treatment up to 24 hours when the cccDNA is first detected (Ko et al. 2018; Chakraborty et al. 2020), indicate that compound A2 inhibits HBV endocytosis on HepaRG cells and interrupts HBV entry prior to establishment of HBV infection but after HBV endocytosis into HepG2-NTCP cells(Figure 41). Recently, five components, e.g., PCNA, the replication factor C complex, DNA polymerase δ, FEN-1 and DNA ligase 1, that lagging strand synthesis forming cccDNA were reported (Wei and Ploss 2020). The G0 interferes with the establishment of the HBV infection may undergo impairment rcDNA to form cccDNA as 24 hours treatment didn't alter HBV total DNA levels but converted cccDNA formation was reduced. However, the mechanism of how A2 and G0 inhibiting HBV endocytosis and cccDNA, respectively, still need further investigation.

3.9 Summary

In this study, we have established Cluc-NTCP co-expression constructs that allows quantifying the expression of NTCPs and analyzing their function as mediator, activator and trigger of successful HBV infection. Co-expression of Cluc-NTCP could solve the shortage of species-specific antibodies and detect NTCP expression sensitively. We also have proved that only NTCP from *Mammals*, including aardvark, rabbit, whale, big brown bat, cat, rhinoceros and horse, in contrast to *Amphibia, Actinopteri and Aves* allows HBV binding and uptake. The evaluation of selected NTCP variants highlights the importance of two functional domains at aa 82-87 and aa 157-165 of NTCP to support HBV infection. Besides the two functional domains, additional unknown motifs may also play a role to complete NTCP function in mediating HBV infection. Notably, we described horseNTCP as an advanced HBV receptor to enhance HBV infection in human and murine hepatocytes cell lines compared to humanNTCP. Thus, horse NTCP is a promising candidate to create new *in vitro* and *in vivo* models and help to clarify NTCPs mode of action during HBV entry. Moreover, murine hepatocytes cell line AML12 permitting HBV infection upon NTCP expression have paved new ways to develop animal models for HBV infection.

Last but not least, we also identified two HBV inhibitors that target different steps before HBV infection establishment. The two novel HBV inhibitors might be able to be used for combined drugs to treat CHB.

4. Materials and Methods

4.1 Materials

4.1.1 Cell lines

Name	Description
HepG2-NTCP-K7	HepG2 derived clone transduced with lentiviral based expression cassette for NTCP (Ko et al. 2018).
HepG2	Hepatocellular carcinoma cell line (Knowles et al. 1980).
HepaRG	Human hepatoma cells, can be differentiated into hepatocyte- and biliary-like cells, susceptible to HBV infection (Gripon et al. 2002).
AML12	Murine hepatocyte cell lines overexpressing human TGF α (Wu et al. 1994).
HepG2-huNTCP	HepG2 derived clone stably overexpressing human NTCP.
HepG2-hoNTCP	HepG2 derived clone stably overexpressing horse NTCP.
AML12-hoNTCP	AML12 derived clone stably overexpressing horse NTCP.
E. coli TOP10	Chemically competent E. coli (Thermo Scientific)
Ecoli 10-BETA	Chemically competent E. coli (NEB)
E. coli Dam-/Dcm-	Chemically competent E. coli (NEB)

4.1.2 Cell culture media

Cells	Components	Standard	Differentiation
HepaRG/ AML12	William's E medium	500 ml	500 ml
	FBS (fetal bovine serum) Fetal clone II	10 %	10 %
	Penicillin/streptomycin	100 U/ml	100 U/ml
	Glutamine	2 mM	2 mM
	Human insulin	0.023 U/ml	0.023 U/ml
	Hydrocortisone	4.7 µg/ml	4.7 µg/ml
	Gentamicin	80 µg/ml	80 µg/ml
	DMSO		1.8%
PHH	William's E medium	500 ml	500 ml
	FBS (fetal bovine serum) Fetal clone II	2 %	2 %
	Penicillin/streptomycin	100 U/ml	100 U/ml
	Glutamine	2 mM	2 mM
	Human insulin	0.023 U/ml	0.023 U/ml
	Hydrocortisone	4.7 µg/ml	4.7 µg/ml
	Gentamicin	80 µg/ml	80 µg/ml
	DMSO		1.8 %
HepG2/ HepG2-NTCP-K7	Dulbecco's Modified Eagle's Medium	500 ml	500 ml
	Heat-inactivated fetal calf serum (FCS)	10 %	10 %
	Penicillin/streptomycin	100 U/ml	100 U/ml
	Glutamine	2 mM	2 mM

	Non-essential amino acids	1 x	1 x
	Sodium pyruvate	1 mM	1 mM
	DMSO		2.5%

4.1.3 Oligonucleotides for PCR

Oligonucleotides were purchased from Microsynth AG, Balgach, Switzerland.

Name	**Sequence (5'-3')**
cccDNA 2251+	agctgaggcggtatcta
cccDNA 92-	gcctattgattggaaagtatgt
HBV DNA 1745	ggagggatacatagaggttccttga
HBV DNA 1844	gttgcccgtttgtcctctaattc
PRNP F	tgctgggaagtgccatgag
PRNP R	cggtgcatgttttcacgatagta
18s F	aaacggctaccacatccaag
18s R	cctccaatggatcctcgtta
pgRNA F	ctcctccagcttatagacc
pgRNA R	gtgagtgggcctacaaa
SheepNTCP F	gatccgggcccagaggccttcaatgagtcttccccg
CowNTCP F	gatccgggcccagaggccttcaacgaatcttccccg
HorseNTCP F	gatccgggcccagaggcccacaatgcgtccac
RabbitNTCP F	gatccgggcccagaggcgcacaacgagtccg
Big brown batNTCP F	gatccgggcccagaggccctcaatg
LittlebrownbatNTCP F	gatccgggcccagagcctaccagagtagac
Cat NTCP FF	gatccgggcccagagccccacaatgt
DanRerNTCP F	gatccgggcccagtggtcacaattaatccaactac
DogNTCP F	gatccgggcccagacgcccccaacatc
DolphinNTCP F	gatccgggcccagaggccctcaatgag
RhinoceNTCP F	gatccgggcccagaggcccacaatgcatc
SealNTCP F	gatccgggcccagaggcccacaatgtga
AardvarkNTCP F	gatccgggcccagagaccctgaacacgtc
XenopusNTCP F	gatccgggcccaaatgacagcagggaacaaga
DuckNTCP F	gatccgggcccaaacaagtccaggggagcctct
AllNTCP R	cagcgggtttaa actcaaggggcttc
Mouse NTCP F	gat ccg ggc cca gag gcg cac aac gta tcagcc
Mouse NTCP R	cag cgg gtttaaactcaa ggggct tc atg ctaatttgccatct
HamsterNTCP8487 F	gtcctgggcaaggtcttccgtttgaaaaatattgaggcactggccatcc
HamsterNTCP8487 R	ggatggccagtgcctcaatatttttcaaacggaagaccttgcccaggac
Goat NTCP F82V F	ctgggcaaggtcttccagctgaacaacgtc
Goat NTCP F82V R	gacgttgttcagctggaagaccttgcccag
CowNTCPF82V F	cctttggactgggcaaggtcttccagctgaataac
CowNTCPF82V R	gttattcagctggaagaccttgcccagtccaaagg
HorseDoSe NTCP F	ctggttctcattccttgcaccatagggatc
HorseDoSe NTCP R	gatccctatggtgcaaggaatgagaaccag
DogT78A F	caccttgcccagcgcgaaggcagtgagag
DogT78A R	ctctcactgccttcgcgctgggcaaggtg
SealT78A F	accttgcccagcgcgaaggcagtgagg
SealT78A R	cctcactgccttcgcgctgggcaaggt
Horse ntcp 157164 R	aaggaatgagaaccaggaccagt**gatatgacaatgcc**tttatagggtacc ttgtc
Horse ntcp 164175 F	cactggtcctggttctcattccttgcaccatagggatcgtcctcaatgcc

Humanntcp 157164 R	aggaatgagaaccaggatcagtga**tatcacgatgc**ctccatagggcacctt g
Humanntcp157164 F	cactgatcctggttctcattccttgcaccatagggatcttcctcaaatcc
HuNTCPR84QK86N R	gtgcctcaatgttattcagctggaagaccttgcc
HuNTCPR84QK86N F	ggcaaggtcttccagctgaataacattgaggca
HoNTCPQ84RN86K F	caaggtcttccggctgaagaacgtggag
HoNTCPQ84RN86KR	cctccacgttcttcagccggaagaccttg
HuNTCP K157G F	acaaggtgccctatggaggcatcgtgata-
HuNTCP K157G R	tatcacgatgcctccatagggcaccttgtcc
HuNTCP V164I F	cgtgatatcactgatcctggttctcattc
HuNTCP V164I R	gagaaccaggatcagtgatatcacga
HuNTCP V175F F	caccatagggatcttcctcaaatccaaa
HuNTCP V175F R	tttggatttgaggaagatccctatggtgc
HoNTCP G157K F	acaaggtaccctataaaggcattgtcatatc
HoNTCP G157K R	atgacaatgcctttatagggtaccttgtct
HoNTCP I164V F	attgtcatatcactggtcctggttctcattc
HoNTCP I164V R	aatgagaaccaggaccagtgatatgacaa
HoNTCP F175V F	caccatagggatcgtcctcaatgccaaa
HoNTCP F175V R	ttggcattgaggacgatccctatggtgc
mRNAallntcpHA R	gtggtgggatccctaagcgtaatctggaacatcgtatgggtaggctgtgcaa ggggagca
mRNA HuNTCP F	agctggctagcgccaccatggaggcccacaacgcgtc
mRNA HoNTCP F	agctggctagcgccaccatggaggcccacaatgcgtc
mRNA HuNTCP Flag F	agctggctagcgccaccatggactacaaagacgatgacgacaaggaggc ccacaacgcgtc
mRNA HoNTCP Flag F	agctggctagcgccaccatggactacaaagacgatgacgacaaggaggc ccacaatgcgtc
pcDNA-HuNTCP F	gacaggctcgagtgccaccatggaggcccacaacgcgtc
pcDNA-HoNTCP F	gacaggctcgagtgccaccatggaggcccacaatgcgtc
pcDNA-allntcpHA RFC	agcgggcggccgcctaagcgtaatctggaacatcgtatgggtaggctgtgc aaggggagca
pcDNA-Hontcp4mice F	gacaggctcgagtgccaccatggaagcccacaacgccagc
pcDNA-Hontcp4miHA R	agcgggcggccgcctaagcgtaatctggaacatcgtatgggtaggcggta caagggctgcac

4.1.4 Kits

Product	**Supplier**
GeneJET Gel Extraction Kit	Fermentas, St. Leon-Rot, Germany
GeneJET Plasmid Miniprep Kit	Thermo Scientific Scientific Scientific, Schwerte, Germany
Lightcycler 480 SYBR Green I Master mix	Roche, Mannheim, Germany
NucleoSpin RNA isolation Kit	Machery-Nagel, Düren, Germany
NucleoSpin Tissue Kit	Machery-Nagel, Düren, Germany
SuperScript III First-Strand Synthesis SuperMix for qRT-PCR	Invitrogen, Carlsbad, CA, USA
DIG Luminescent Detection Kit	Roche, Mannheim, Germany
hiscribe t7 arca mrna kit (with tailing)	New England Biolabs, Ipswich, USA
Phusion HotStart II High-Fidelity PCR Kit	Thermo Fisher Scientific, Waltham, USA

Human IP 10 ELISA kit	Biolegend, San Diego, CA, USA
Human IL 10 ELISA kit	Biolegend, San Diego, CA, USA

4.1.5 Antibodies

Name	Supplier	Catalogue number
NTCP	abcam	ab131084
HA	abcam	ab9110
flag	abcam	Ab205606
HBV core	Cell marque	Ruo21611030
b-actin	sigma	AC-15
HRP-Anti-mouse	Sigma-Aldrich	A0168
HRP-Anti-rabbit	Sigma-Aldrich	A0545

4.1.6 Plasmids

Name	Encoding features
pDNA-T7-huNTCPHA	Production template human NTCP fused with HA tag
pDNA-T7-hoNTCPHA	Production template horse NTCP fused with HA tag
pDNA-T7-FLAGhoNTCPHA	Production template horse NTCP fused with FLAGtag and HA tag
pDNA-T7-FLAGhuNTCPHA	Production template human NTCP fused with FLAGtag and HA tag
pDNA-T7-FLAGhoNTCP157HA	Production template horse NTCPG157K fused with FLAGtag and HA tag
pDNA-T7-FLAGhuNTCP157HA	Production template human NTCPK157G fused with FLAGtag and HA tag
pcDNA3.1_CMV_CLuc_LS_NTCPs	Encodes the gene cassette from Cypridiana luciferase, the linker sequence (LS) and the corresponding NTCP sequence, the NTCP sequences were then cloned from the respective synthesized sequences (via the primers NTCP-Synth-fw and NTCP-Synth-rv) or the corresponding pcDNA3.1 plasmid into this vector with Bsp120I and MssI)
pcDNA3.1_CMV_CLuc_LS_huNTCP-TDtomato	Encodes Cluc and huNTCP-TDtomato fusion proteins
pRR_TTR_huNTCP	Encodes huNTCP proteins
pRR_TTR_hoNTCP	Encodes hoNTCP proteins
pRR_TTR_hoNTCP op2mice	Encodes mice-condon optimized hoNTCP proteins
pcDNA6.2_hyPB	Encodes the hyperactive Piggy-Bac transposase (kindly made available by Prof. Roland Rad, Klinikum rechts der Isar of the Technical University of Munich

4.1.7 Chemicals and reagents

Chemical or reagent	Supplier
Agar-agar	Roth, Karlsruhe, Germany
Agarose	Peqlab, Erlangen, Germany
Amersham ECL Prime Western Blotting Detection Reagent	GE Healthcare Life Sciences, Freiburg, Germany
Ampicillin	Roth, Karlsruhe, Germany
APS	Roth, Karlsruhe, Germany
Blasticidin S HCl	Invitrogen, Carlsbad, USA
Collagen R	Serva Electrophoresis, Heidelberg, Germany
DMSO	Sigma-Adlrich, Steinheim, Germany
Ethanol	Roth, Karlsruhe, Germany
FCS (heat-inactivated)	Gibco/Invitrogen, Carlsbad, USA
FBS Fetalclone II, Hyclone	GE Healthcare Life Sciences, Freiburg, Germany
Dulbecco's Modified Eagle's Medium	Gibco/Invitrogen, Carlsbad, USA
Fish (herring) sperm DNA	Invitrogen, Carlsbad, USA
Formaldehyde	Roth, Karlsruhe, Germany
Geneticin (G418)	Thermo Scientific, Rockford, USA
Gentamicin	Ratiopharm, Ulm, Germany
Glutamine	Sigma-Aldrich, Steinheim, Germany
Hydrocortisone	Pfizer, New York, USA
Insulin (Insuman Rapid)	Sanofi Aventis, Frankfurt, Germany
CellTiter-Blue (CTB)	Promega, Madison,USA
Isopropanol	Roth, Karlsruhe, Germany
LDS Sample Buffer, Non-Reducing (4X)	Thermo Scientific, Rockford, USA
Lipofectamine 3000	Life Technologies, Carlsbad, USA
Lipofectamine MessengerMax	Life Technologies, Carlsbad, USA
Methanol	Roth, Karlsruhe, Germany
Milk powder	Roth, Karlsruhe, Germany
NaCl	Roth, Karlsruhe, Germany
OptiMEM	Gibco/Invitrogen, Carlsbad, USA
Non-essential amino acids 100x	Gibco/Invitrogen, Carlsbad, USA
Page Ruler Plus Prestained protein ladder	Thermo Scientific, Rockford, USA
PBS	Gibco/Invitrogen, Carlsbad, USA
PEG6000	Merck, Hohenbrunn, Germany
Penicillin/streptomycin	Gibco/Invitrogen, Carlsbad, USA
Pierce RIPA buffer	Thermo Scientific, Rockford, USA
Polyacrylamide	Roth, Karlsruhe, Germany
Protease Inhibitor (complete)	Roche, Mannheim, Germany
RotiSafe	Roth, Karlsruhe, Germany
Sodium pyruvate	Gibco/Invitrogen, Carlsbad, USA
SDS	Roth, Karlsruhe, Germany
SmartLadder DNA (10kb)	Eurogentec, Seraing, Belgium
ssRNA Ladder	New England Biolabs, Ipswich, USA
Low Range ssRNA Ladder	New England Biolabs, Ipswich, USA
T5 Exonuclease	New England Biolabs, Ipswich, USA

TEMED	Roth, Karlsruhe, Germany
Tris base	Roth, Karlsruhe, Germany
Tris HCl	Roth, Karlsruhe, Germany
Trypan blue	Gibco/Invitrogen, Carlsbad, USA
Trypsin	Gibco/Invitrogen, Carlsbad, USA
Tween 20	Roth, Karlsruhe, Germany
Yeast extract	Roth, Karlsruhe, Germany
Loading Dye 2x RNA	New England Biolabs, Ipswich, USA
EDTA	Roth, Karlsruhe, Germany
Pseudo-UTP (Ψ-UTP)	Jena Bioscience, Jena, Germany
5-Methyl-CTP (m5CTP)	Jena Bioscience, Jena, Germany
William's medium E	Gibco/Invitrogen, Carlsbad, USA
3-(2,3-dihydro-1H-inden-2-yl)-8-(3-furylmethyl)-1-(2-methoxyethyl)-1,3,8-triazaspiro [4.5] decane-2,4-dione (G0)	ChemBridge, San Diego, USA
5-({3-[(2-ethyl-2,5-dihydro-1H-pyrrol-1-yl) carbonyl] isoxazol-5yl} methoxy) isoquinoline (A0)	ChemBridge, San Diego, USA
N,N-dipropyl-5-[(quinolin-6-yloxy) methyl] isoxazole-3carboxamide(A2)	ChemBridge, San Diego, USA
Heparin	Ratiopharm, Ulm, Deutschland
Cypridina Luciferin	PJK, Kleinblittersdorf, Deutschland

4.1.8 Laboratory equipment and consumables

Product	**Supplier**
Amersham Hybond PVDF membrane	GE Healthcare Life Sciences, Freiburg, Germany
Amersham nylon membrane Hybond N+	GE Healthcare Life Sciences, Freiburg, Germany
BEP (HBeAg measurement)	Siemens Molecular Diagnostics, Marburg, Germany
Cell culture flasks and plates	TPP, Trasadingen, Switzerland
Cell culture incubator HERAcell 150i	Thermo Scientific, Rockford, USA
Centricon Plus-70	Merck Millipore, Billerica, USA
Centrifuge 5417C / 5417R	Eppendorf, Hamburg, Germany
ELISA 96well plates Nunc	Thermo Scientific, Rockford, USA
Falcon tubes 15ml, 50ml	Greiner Bio One, Kremsmünster, Austria
Fluorescence microscope CKX41	Olympus, Hamburg, Germany
Freezing container	Thermo Fisher Scientific, Waltham, USA
Fusion Fx7 (chemiluminescence detection; UV light system)	Peqlab, Erlangen, Germany
Gel chambers (agarose gel electrophoresis)	Peqlab, Erlangen, Germany
Gel chambers (SDS-PAGE)	Bio-Rad, Hercules, USA
Heating block	Eppendorf, Hamburg, Germany
Hemocytometer	Brand, Wertheim, Germany
Light Cycler 480 II	Roche, Mannheim, Germany
Nanodrop Photometer	Implen, Munich, Germany
Pipette "Accu-jet pro"	Brand, Wertheim, Germany

Pipette filter tips	Starlab, Ahrensburg, Germany
Pipette tips 2 - 50ml	Greiner Bio One, Kremsmünster, Austria
Pipettes	Eppendorf, Hamburg, Germany
PVDF membrane	Bio-Rad, Hercules, USA
qPCR 96-well plates	4titude, Berlin, Germany
Reaction tubes	Eppendorf, Hamburg, Germany
Sterile filters 0.45µm	Merck, Millipore, Billerica, USA
Sterile hood	Heraeus, Hanau, Germany
Tecan plate reader Infinite F200	Tecan, Männedorf, Switzerland
Transwells 0.4 µm	Corning, Amsterdam, The Netherlands
Ultracentrifuge Beckman SW40 rotor	Beckman Coulter, Brea, USA
Western Blotting Chamber (Transblot SD Semi-Dry)	Bio-Rad, Hercules, USA
Western Blotting Chamber (Wet Blot)	Bio-Rad, Hercules, USA
Whatman paper	Bio-Rad, Hercules, USA
Architect	Abbott Laboratories, Chicago, IL, USA
Cryo vials	Greiner Bio One, Kremsmünster, Austria
Cytoflex	Beckman Coulter, Brea, CA, USA
Fuorescence microscope LEICA DM8i	Leica Biosystems, Wetzlar, Germany
Confocal microscope, FV10i	Olympus, Hamberg, Germany

4.1.9 Software

Software name	**Supplier**
Graph Pad Prism 8.4.1.	Graph Pad, La Jolla, USA
Image J	NIH, Bethesda, USA
LightCycler 480 Software	Roche, Mannheim, Germany
Windows 10	Microsoft, Redmond, USA
FlowJo, LLC	BD, Franklin Lakes, USA
Windows 7/8/10, MS Office	Microsoft, Redmond, USA
Affinity designer 1.9	Serif (Europe) Ltd, Nottingham, UK
Serial Cloner 2.6.1	Serial Basics, Paris, France

4.2 Methods

4.2.1 Cell culture

All used cells were cultured under standard cell culture conditions (37 °C, 5 % CO2, 95 % humidity) and cell culture experiments were carried out with mycoplasma-negative cells under sterile conditions. HepG2 cells and derived cell lines were cultured in complete DMEM medium and passaged twice a week with a maximum dilution of 1:10. The seed HepG2 cells and derived cell lines were differentiated for two days for HBV infection (Ko et al. 2018). AML12 cells and derived cell lines were cultured in complete William's E medium and passaged twice a week with a maximum dilution of 1:10. AML12 cells and derived cell lines were differentiated for two days for HBV infection. HepaRG cells were seeded and grown for two weeks in William's E complete medium and then differentiated for another two weeks in William's E differentiation medium (Gripon et al. 2002). Only fully differentiated HepaRG (dHepaRG) cells were used for HBV infection (Gripon et al. 2002). Isolated fresh PHH cells were maintained in PHH standard medium for one day and then maintained in PHH differentiation medium for HBV infection.

4.2.2 Cloning

To obtain different NTCPs' expression plasmids, the primers consist appropriate restriction enzyme sites were designed and PCR processes were performed by using 2x Phusion Mastermix (NEB). For PCR reaction, 1 µL template (synthesis sequence stock solution 10 ng/µL; plasmids: 100 ng/µL) was mixed with 2 µL forward primer (10 µM), 2 µL reverse primer (10 µM), 20 µL H2O and 25 µL 2x Phusion Mastermix. Samples were transferred to PCR machine using following program: 94°C 5 min (1 Cycle); 94°C 10s, 60°C 15 s, 72°C 40 s (40 Cycles); 72°C 10 min (1 Cycle), 4°C (cooling). PCR products were checked in 1% agarose gels (0.5 g agarose solved in 50 mL 1x TAE buffer with 5 µL RotiSafe) and visualized on UV-table of Fusion Fx7 machine (Peqlab). Then PCR products were extracted from gels using gel extraction kit (Thermo Scientific). The extracted PCR products as well as target plasmids were digested by appropriate restriction enzymes. Therefore, 7 µL of PCR products or 7 µL of prediluted plasmids (~ 10 µg) were mixed with 1 µL of each restriction enzymes, 1 µL of FastDigest Buffer (10x) and incubated 30 mins at 37°C. The digested PCR products or plasmids were analyzed by gel and extracted from gel using gel extraction kit (Thermo Scientific) according to the manufacturer's protocols. For the DNA fragments ligation, the inserts and target plasmids were mixed with moler ratio at 1:3 plus with 1 µL T4 Ligase and 1 µL ligation Buffer (10x) (Invitrogen) for 20mins at room temperature. The ligation products were then transformed into E.coli TOP10 using heat-

shock for 90 s at 42°C, following with recovery for 1 h at 37°C (after addition of 200 µL SOC medium) and incubation overnight on selective antibiotics containing LB plates. Clones were transferred to 3 mL LB medium containing selective antibiotics and incubated overnight at 37°C. Isolation of plasmids was performed using GeneJet Miniprep Kit (Thermo Scientific) according to manufacturer's instructions. To analysis correct clones, PCR was performed mentioned above. The correct clones were analyzed using Sanger sequencing (GATC) for correct sequences.

For sequence mutation, additional PCR was performed to get two separated DNA sequences that contain 15-20bp overlap sequence and target mutation(s). Then the standard cloning procedures mentioned above (two separated DNA sequences mixed as templates) were carried out to get mutated NTCPs expression plasmids.

4.2.3 Production of in vitro transcribed (IVT) mRNA

IVT mRNAs were produced according the protocol mentioned in Oswald et al. 2021.

4.2.4 Transfection

Plasmids transfection was performed using Lipofectamine 3000 (Invitrogen) according to manufacturer's protocol. For mRNA transfection, lipofectamine Messenger Max (Invitrogen) was used with 1:3 ratio of plasmid(µg) and transfection regent(µL) according to manufacturer's instructions at cell confluence 90-100% or during differentiation.

4.2.5 Fluorescence microscopy and Confocal Microscopy

For fluorescence microscopy, cells were stained with either MyrB-atto488 or MyrB-atto594 at 50mM for 15mins and washed with PBS to removed unbound MyrB-atto488 or MyrB-atto594. Fluorescence images were obtained with 20x objectives in phase contrast using Leica DMi8 fluorescence microscope.

For confocal microscopy, cells on coverslips were fixed with 4 % PFA for 10 minutes at room temperature after washing with PBS. Then cells were washed once with PBS, permeabilized with 0.5 % saponin in PBS for 10 minutes and blocked with 0.1 % saponin and 10 % goat serum for 2 hours. Primary antibody was added into blocking solution and kept on cells overnight at 4 °C. After three times washing with PBS, cells were incubated in secondary antibody with 0.1 % saponin and 2 % goat serum for two hours at room temperature. Subsequently cells were washed three times with PBS and mounted on slides using Fluoromount G. Fluorescence images were obtained using Olypus fluorescence microscope.

4.2.6 Flow cytometry

For flow cytometry analysis of MyrB staining, cells were stained with either MyrB-atto488 or MyrB-atto594 at 50mM for 15mins, washed with PBS, detached with trypsin for 10 min at 37°C, resuspended in FACS Buffer (PBS with 1% FBS) and transferred to 96 V well plates. Cells were washed once and resuspended in FACS Buffer.

For flow cytometry analysis flag-NTCP-HA expressing cells, the cells were washed once with PBS, detached with trypsin and transferred to V-bottom 96 wells plate. Cell pellets were suspended with 50ul FACS buffer/well containing flag-antibody (abcam 1:700) and NIR (Thermo 1: 2000). The plates were incubated on ice for 30 mins and subsequently added 150 ul FACS buffer/well. Cell pellets were suspended again with 50ul FACS buffer/well containing 2nd antibody (Thermo 1:1000) and MyrB-atto594 (1: 1000). After incubation in dark, 4°C on ice for 30 mins, cells were subsequent added 150 ul FACS buffer/well to dilute and wash the unbound antibody. Then the cells were added 70-75ul /well Cytofix (BD Cytofix/Cytoperm™) for fixation & permeabilization in dark, 4°C on ice for 17min, following with adding 150ul/well Perm/wash buffer to dilute and wash cytofix. The cells were then incubated with HA-antibody (abcam 1:700) and 2nd antibody in Perm/wash buffer in subsequently. Finally, the cell pellets were suspended with 200 FACS buffer/well.

All flow cytometry analyses were performed with Cytoflex machine and data processing was performed using FlowJo software.

4.2.7 HBV uptake and infection assay

HBV uptake (Chakraborty et al. 2020) and infection (Ko et al. 2018) were performed as described. Briefly, HBV stock was mixed with appropriated differentiation medium, 4% polyethylengylcol 6000 (PEG 6000) solution, vortexed and added to cells. For the uptake assay, the plates were incubated on ice for 1 hour and then shifted to normal cell culture condition for certain time points (1, 3, 6 and 24 hours). For HBV infection, the cells were incubated under normal cell culture condition for 24 hours, following twice PBS wash and complemented with fresh differentiation medium. 200 nM MyrB added to infection mixture services as infection controls.

4.2.8 Taurocholate Uptake assay

[^{3}H] taurocholate uptake assay for all cell lines were performed as previously described (Kubitz et al. 2004). Briefly, Hot Mix stock ((1940 µL basal medium, 66 µL 15 mM cold TC (Sigma-Aldrich) and 1 µL hot TC (Hartmann Analytic, Braunschweig, Germany)) was prepared and diluted at 1:10 in basal medium. 250 µL/well of hot mix was added to the

samples and incubated for 15 min at 37 °C. Cells were placed on iced after incubation and washed three times with ice-cold PBS after hot mix removed. Next, cells were lysed with 500 µL lysis buffer (0.05 % SDS, 0.25 mM NaOH) and lysed cells were transferred to scintillation vials. Finally, 4 mL scintillation liquid was added, vials were closed and vortexed for 30 s. Measurement of ^{3}H taurocholate was performed with a scintillation analyzer.

4.2.9 DNA isolation

Total cellular DNA or extracellular DNA were extracted using Genomic DNA tissue kit (Machery&Nagel).

4.2.10 DNA T5 digestion

DNA T5 digestion was performed according to protocol (Xia et al. 2016). 8.5 µL cellular DNA, 1 µL NEBuffer 4 (10x) and 0.5 µL of T5 Exonuclease (10 U) (NEB) were mixed and incubated for 30 min at 37°C with subsequent heating inactivation for 5 min at 99°C. Samples were 4-fold diluted with 30 µL ddH2O to exclude interferon of remaining buffer components for qPCR reaction.

4.2.11 Isolation of total RNA and cDNA synthesis

Total cellular RNA was extracted using RNA isolation Kit (Machery&Nagel). cDNA synthesis was performed using SuperScript III First-Strand Synthesis SuperMix for qRT-PCR (Invitrogen).

4.2.12 Quantification of viral HBV markers using qPCR

Total HBV DNA, cccDNA, HBV pgRNA were determined by qPCR using LightCycler480 Real-time PCR system (Roche) and normalized to reference genes PRNP or 18S. Each of qPCR reaction consisted 5 µL LightCycler 480 SYBR Green I Master mix (Roche, 2×), 0.5 µL of each primer (20 µM) and 4 µL of DNA or cDNA template. HBeAg quantification was performed using automated BEP III system (Siemens, Healthcare).

qPCR program for HBV DNA and PRP:

	T [°C]	t [sec]	Ramp [°C/sec]	Acquisition mode	Cycles
Denaturation	95	300	4.4		1
Amplification	95	25	4.4	Single	40
	60	10	2.2		
	72	30	4.4		

Melting	95	1	4.4	continuous: 5/°C	1
	65	60	2.2		
	95		0.11		
Cooling	40	30	2.2		1

qPCR program for HBV cccDNA:

	T [°C]	**t [sec]**	**Ramp [°C/sec]**	**Acquisition mode**	**Cycles**
Denaturation	95	600	4.4		1
Amplification	95	15	4.4	Single	50
	60	5	2.2		
	72	45	4.4		
	88	2	4.4		
Melting	95	1	4.4	continuous: 5/°C	1
	65	15	2.2		
	95		0.11		
Cooling	40	30	2.2		1

qPCR program for pgRNA and 18S:

	T [°C]	**t [sec]**	**Ramp [°C/sec]**	**Acquisition mode**	**Cycles**
Denaturation	95	300	4.4		1
Amplification	95	15	4.4	Single	45
	60	10	2.2		
	72	25	4.4		
Melting	95	10	4.4	continuous: 5/°C	1
	65	60	2.2		
	95		0.11		
Cooling	40	1	2.2		1

4.2.13 Statistical analysis

Numeric values are presented as means with standard deviation. Calculation of p-values was performed with Student's unpaired two-tailed *t*-test with Welch's correction or one-way *ANOVA* using Prism 8.4.1 software.

5. References

Addison, William R.; Walters, Kathie-Anne; Wong, Winnie W. S.; Wilson, John S.; Madej, Danuta; Jewell, Lawrence D.; Tyrrell, D. Lorne J. (2002): Half-life of the duck hepatitis B virus covalently closed circular DNA pool in vivo following inhibition of viral replication. In *Journal of virology* 76 (12), pp. 6356–6363. DOI: 10.1128/jvi.76.12.6356-6363.2002.

Allweiss, Lena; Dandri, Maura (2016): Experimental in vitro and in vivo models for the study of human hepatitis B virus infection. In *Journal of hepatology* 64 (1 Suppl), S17-S31. DOI: 10.1016/j.jhep.2016.02.012.

Anindita Chakraborty (2020): Characterization of Early Events in Hepatitis B Virus Infection. PhD. Technischen Universität München, München. Virologie.

Anwer, M. Sawkat; Stieger, Bruno (2014): Sodium-dependent bile salt transporters of the SLC10A transporter family: more than solute transporters. In *Pflügers Archiv - European Journal of Physiology* 466 (1), pp. 77–89. DOI: 10.1007/s00424-013-1367-0.

Appelman, Monique D.; Chakraborty, Anindita; Protzer, Ulrike; McKeating, Jane A.; van de Graaf, Stan F. J. (2017): N-Glycosylation of the Na+-Taurocholate Cotransporting Polypeptide (NTCP) Determines Its Trafficking and Stability and Is Required for Hepatitis B Virus Infection. In *PloS one* 12 (1), e0170419. DOI: 10.1371/journal.pone.0170419.

Appelman, Monique D.; Wettengel, Jochen M.; Protzer, Ulrike; Oude Elferink, Ronald P. J.; van de Graaf, Stan F. J. (2021): Molecular regulation of the hepatic bile acid uptake transporter and HBV entry receptor NTCP. In *Biochimica et biophysica acta. Molecular and cell biology of lipids* 1866 (8), p. 158960. DOI: 10.1016/j.bbalip.2021.158960.

Bancroft, W. H.; Snitbhan, R.; Scott, R. M.; Tingpalapong, M.; Watson, W. T.; Tanticharoenyos, P. et al. (1977): Transmission of hepatitis B virus to gibbons by exposure to human saliva containing hepatitis B surface antigen. In *The Journal of infectious diseases* 135 (1), pp. 79–85. DOI: 10.1093/infdis/135.1.79.

Blank, A.; Eidam, A.; Haag, M.; Hohmann, N.; Burhenne, J.; Schwab, M. et al. (2018): The NTCP-inhibitor Myrcludex B: Effects on Bile Acid Disposition and Tenofovir Pharmacokinetics. In *Clinical pharmacology and therapeutics* 103 (2), pp. 341–348. DOI: 10.1002/cpt.744.

Bloom, Kristie; Maepa, Mohube Betty; Ely, Abdullah; Arbuthnot, Patrick (2018): Gene Therapy for Chronic HBV-Can We Eliminate cccDNA? In *Genes* 9 (4). DOI: 10.3390/genes9040207.

Bock, C. T.; Schwinn, S.; Locarnini, S.; Fyfe, J.; Manns, M. P.; Trautwein, C.; Zentgraf, H. (2001): Structural organization of the hepatitis B virus minichromosome. In *Journal of molecular biology* 307 (1), pp. 183–196. DOI: 10.1006/jmbi.2000.4481.

Bruns, M.; Miska, S.; Chassot, S.; Will, H. (1998): Enhancement of hepatitis B virus infection by noninfectious subviral particles. In *Journal of virology* 72 (2), pp. 1462–1468. DOI: 10.1128/JVI.72.2.1462-1468.1998.

Burwitz, Benjamin J.; Wettengel, Jochen M.; Mück-Häusl, Martin A.; Ringelhan, Marc; Ko, Chunkyu; Festag, Marvin M. et al. (2017): Hepatocytic expression of human sodium-taurocholate cotransporting polypeptide enables hepatitis B virus infection of macaques. In *Nature communications* 8 (1), p. 2146. DOI: 10.1038/s41467-017-01953-y.

Caroline Gähler (2011): Association of Hepatitis B Virus derived lipopeptides to serum factors and model membranes. PhD. Ruprecht-Karls-Universität Heidelberg, Heidelberg. Naturwissenschaftlich-Mathematischen Gesamtfakultät.

Carvalho Dominguez Souza, Breno Frederico de; König, Alexander; Rasche, Andrea; Oliveira Carneiro, Ianei de; Stephan, Nora; Corman, Victor Max et al. (2018): A novel hepatitis B virus species discovered in capuchin monkeys sheds new light on the evolution of primate hepadnaviruses. In *Journal of hepatology* 68 (6), pp. 1114–1122. DOI: 10.1016/j.jhep.2018.01.029.

Chakraborty, Anindita; Ko, Chunkyu; Henning, Christin; Lucko, Aaron; Harris, James M.; Chen, Fuwang et al. (2020): Synchronised infection identifies early rate-limiting steps in the hepatitis B virus life cycle. In *Cellular microbiology* 22 (12), e13250. DOI: 10.1111/cmi.13250.

Chen, Margaret; Sällberg, Matti; Hughes, Janice; Jones, Joyce; Guidotti, Luca G.; Chisari, Francis V. et al. (2005): Immune tolerance split between hepatitis B virus precore and core proteins. In *Journal of virology* 79 (5), pp. 3016–3027. DOI: 10.1128/JVI.79.5.3016-3027.2005.

Cheng, Dongliang; Han, Bing; Zhang, Wei; Wu, Wei (2021): Clinical effects of NTCP-inhibitor myrcludex B. In *Journal of viral hepatitis*. DOI: 10.1111/jvh.13490.

Chisari, F. V.; Filippi, P.; McLachlan, A.; Milich, D. R.; Riggs, M.; Lee, S. et al. (1986): Expression of hepatitis B virus large envelope polypeptide inhibits hepatitis B surface antigen secretion in transgenic mice. In *Journal of virology* 60 (3), pp. 880–887. DOI: 10.1128/JVI.60.3.880-887.1986.

Chisari, F. V.; Pinkert, C. A.; Milich, D. R.; Filippi, P.; McLachlan, A.; Palmiter, R. D.; Brinster, R. L. (1985): A transgenic mouse model of the chronic hepatitis B surface antigen carrier state. In *Science (New York, N.Y.)* 230 (4730), pp. 1157–1160. DOI: 10.1126/science.3865369.

Corti, Davide; Benigni, Fabio; Shouval, Daniel (2018): Viral envelope-specific antibodies in chronic hepatitis B virus infection. In *Current opinion in virology* 30, pp. 48–57. DOI: 10.1016/j.coviro.2018.04.002.

Crowther, R. A.; Kiselev, N. A.; Böttcher, B.; Berriman, J. A.; Borisova, G. P.; Ose, V.; Pumpens, P. (1994): Three-dimensional structure of hepatitis B virus core particles determined by electron cryomicroscopy. In *Cell* 77 (6), pp. 943–950. DOI: 10.1016/0092-8674(94)90142-2.

Cui, Xiuji; Guo, Ju-Tao; Hu, Jianming (2015): Hepatitis B Virus Covalently Closed Circular DNA Formation in Immortalized Mouse Hepatocytes Associated with Nucleocapsid Destabilization. In *Journal of virology* 89 (17), pp. 9021–9028. DOI: 10.1128/JVI.01261-15.

Dane, D. S.; Cameron, C. H.; Briggs, M. (1970): Virus-like particles in serum of patients with Australia-antigen-associated hepatitis. In *The Lancet* 1 (7649), pp. 695–698. DOI: 10.1016/s0140-6736(70)90926-8.

Datta, Sibnarayan; Chatterjee, Soumya; Veer, Vijay; Chakravarty, Runu (2012): Molecular biology of the hepatitis B virus for clinicians. In *Journal of clinical and experimental hepatology* 2 (4), pp. 353–365. DOI: 10.1016/j.jceh.2012.10.003.

Döring, Barbara; Lütteke, Thomas; Geyer, Joachim; Petzinger, Ernst (2012): The SLC10 carrier family: transport functions and molecular structure: Elsevier (Co-Transport Systems, 70). In *Current topics in membranes*, pp. 105–168.

Fanning, Gregory C.; Zoulim, Fabien; Hou, Jinlin; Bertoletti, Antonio (2019): Therapeutic strategies for hepatitis B virus infection: towards a cure. In *Nature reviews. Drug discovery* 18 (11), pp. 827–844. DOI: 10.1038/s41573-019-0037-0.

Freyend, M. John von; Untergasser, A.; Arzberger, S.; Oberwinkler, H.; Drebber, U.; Schirmacher, P.; Protzer, U. (2011): Sequential control of hepatitis B virus in a mouse model of acute, self-resolving hepatitis B. In *Journal of viral hepatitis* 18 (3), pp. 216–226. DOI: 10.1111/j.1365-2893.2010.01302.x.

Fu, Liran; Hu, Hongjie; Liu, Yang; Jing, Zhiyi; Li, Wenhui (2017): Woodchuck sodium taurocholate cotransporting polypeptide supports low-level hepatitis B and D virus entry. In *Virology* 505, pp. 1–11. DOI: 10.1016/j.virol.2017.02.006.

Gerlich, W. H.; Robinson, W. S. (1980): Hepatitis B virus contains protein attached to the 5' terminus of its complete DNA strand. In *Cell* 21 (3), pp. 801–809. DOI: 10.1016/0092-8674(80)90443-2.

Gilead (2020). Available online at https://www.gilead.com/news-and-press/press-room/press-releases/2020/12/gilead-sciences-to-acquire-myr-gmbh, updated on 12/10/2020, checked on 8/5/2021.

Glebe, Dieter; Aliakbari, Mehriar; Krass, Peter; Knoop, Eva V.; Valerius, Klaus P.; Gerlich, Wolfram H. (2003): Pre-s1 antigen-dependent infection of Tupaia hepatocyte cultures with human hepatitis B virus. In *Journal of virology* 77 (17), pp. 9511–9521. DOI: 10.1128/jvi.77.17.9511-9521.2003.

Glebe, Dieter; Urban, Stephan (2007): Viral and cellular determinants involved in hepadnaviral entry. In *World journal of gastroenterology* 13 (1), pp. 22–38. DOI: 10.3748/wjg.v13.i1.22.

Gripon, P.; Diot, C.; Guguen-Guillouzo, C. (1993): Reproducible high level infection of cultured adult human hepatocytes by hepatitis B virus: effect of polyethylene glycol on adsorption and penetration. In *Virology* 192 (2), pp. 534–540. DOI: 10.1006/viro.1993.1069.

Gripon, P.; Diot, C.; Thézé, N.; Fourel, I.; Loreal, O.; Brechot, C.; Guguen-Guillouzo, C. (1988): Hepatitis B virus infection of adult human hepatocytes cultured in the presence of dimethyl sulfoxide. In *Journal of virology* 62 (11), pp. 4136–4143. DOI: 10.1128/JVI.62.11.4136-4143.1988.

Gripon, Philippe; Cannie, Isabelle; Urban, Stephan (2005): Efficient inhibition of hepatitis B virus infection by acylated peptides derived from the large viral surface protein. In *Journal of virology* 79 (3), pp. 1613–1622. DOI: 10.1128/JVI.79.3.1613-1622.2005.

Gripon, Philippe; Rumin, Sylvie; Urban, Stephan; Le Seyec, Jacques; Glaise, Denise; Cannie, Isabelle et al. (2002): Infection of a human hepatoma cell line by hepatitis B virus. In *Proceedings of the National Academy of Sciences of the United States of America* 99 (24), pp. 15655–15660. DOI: 10.1073/pnas.232137699.

Guidotti, L. G.; Matzke, B.; Schaller, H.; Chisari, F. V. (1995): High-level hepatitis B virus replication in transgenic mice. In *Journal of virology* 69 (10), pp. 6158–6169. DOI: 10.1128/JVI.69.10.6158-6169.1995.

Guidotti, L. G.; Rochford, R.; Chung, J.; Shapiro, M.; Purcell, R.; Chisari, F. V. (1999): Viral clearance without destruction of infected cells during acute HBV infection. In *Science (New York, N.Y.)* 284 (5415), pp. 825–829. DOI: 10.1126/science.284.5415.825.

Guo, Haitao; Jiang, Dong; Zhou, Tianlun; Cuconati, Andrea; Block, Timothy M.; Guo, Ju-Tao (2007): Characterization of the intracellular deproteinized relaxed circular DNA of hepatitis B virus: an intermediate of covalently closed circular DNA formation. In *Journal of virology* 81 (22), pp. 12472–12484. DOI: 10.1128/JVI.01123-07.

Guo, Yan-Hai; Li, Yong-Nian; Zhao, Jin-Rong; Zhang, Ju; Yan, Zhen (2011): HBc binds to the CpG islands of HBV cccDNA and promotes an epigenetic permissive state. In *Epigenetics* 6 (6), pp. 720–726. DOI: 10.4161/epi.6.6.15815.

Hagenbuch, B.; Meier, P. J. (1994): Molecular cloning, chromosomal localization, and functional characterization of a human liver Na+/bile acid cotransporter. In *Journal of Clinical Investigation* 93 (3), pp. 1326–1331. DOI: 10.1172/JCI117091.

Hallén, S.; Mareninova, O.; Brändén, M.; Sachs, G. (2002): Organization of the membrane domain of the human liver sodium/bile acid cotransporter. In *Biochemistry* 41 (23), pp. 7253–7266. DOI: 10.1021/bi012152s.

Hartman, Zachary C.; Kiang, Anne; Everett, Ruth S.; Serra, Delila; Yang, Xiao Y.; Clay, Timothy M.; Amalfitano, Andrea (2007): Adenovirus infection triggers a rapid, MyD88-regulated transcriptome response critical to acute-phase and adaptive immune responses in vivo. In *Journal of virology* 81 (4), pp. 1796–1812. DOI: 10.1128/JVI.01936-06.

He, Wenhui; Cao, Zhiliang; Mao, Fengfeng; Ren, Bijie; Li, Yunfei; Li, Dan et al. (2016): Modification of Three Amino Acids in Sodium Taurocholate Cotransporting Polypeptide Renders Mice Susceptible to Infection with Hepatitis D Virus In Vivo. In *Journal of virology* 90 (19), pp. 8866–8874. DOI: 10.1128/JVI.00901-16.

He, Wenhui; Ren, Bijie; Mao, Fengfeng; Jing, Zhiyi; Li, Yunfei; Liu, Yang et al. (2015): Hepatitis D Virus Infection of Mice Expressing Human Sodium Taurocholate Co-transporting Polypeptide. In *PLoS pathogens* 11 (4), e1004840. DOI: 10.1371/journal.ppat.1004840.

Hehle, Verena; Beretta, Maxime; Bourgine, Maryline; Ait-Goughoulte, Malika; Planchais, Cyril; Morisse, Solen et al. (2020): Potent human broadly neutralizing antibodies to hepatitis B virus from natural controllers. In *The Journal of experimental medicine* 217 (10). DOI: 10.1084/jem.20200840.

Herrscher, Charline; Pastor, Florentin; Burlaud-Gaillard, Julien; Dumans, Amélie; Seigneuret, Florian; Moreau, Alain et al. (2020): Hepatitis B virus entry into HepG2-NTCP cells requires clathrin-mediated endocytosis. In *Cellular microbiology*, e13205. DOI: 10.1111/cmi.13205.

Ho, Richard H.; Leake, Brenda F.; Roberts, Richard L.; Lee, Wooin; Kim, Richard B. (2004): Ethnicity-dependent polymorphism in Na+-taurocholate cotransporting polypeptide (SLC10A1) reveals a domain critical for bile acid substrate recognition. In *The Journal of biological chemistry* 279 (8), pp. 7213–7222. DOI: 10.1074/jbc.M305782200.

Hu, Hui-Han; Liu, Jessica; Lin, Yu-Ling; Luo, Wun-Sheng; Chu, Yu-Ju; Chang, Chia-Lin et al. (2016): The rs2296651 (S267F) variant on NTCP (SLC10A1) is inversely associated with chronic hepatitis B and progression to cirrhosis and hepatocellular carcinoma in patients with chronic hepatitis B. In *Gut* 65 (9), pp. 1514–1521. DOI: 10.1136/gutjnl-2015-310686.

Hu, Jianming; Lin, You-Yu; Chen, Pei-Jer; Watashi, Koichi; Wakita, Takaji (2019): Cell and Animal Models for Studying Hepatitis B Virus Infection and Drug Development. In *Gastroenterology* 156 (2), pp. 338–354. DOI: 10.1053/j.gastro.2018.06.093.

Hu, Nien-Jen; Iwata, So; Cameron, Alexander D.; Drew, David (2011): Crystal structure of a bacterial homologue of the bile acid sodium symporter ASBT. In *Nature* 478 (7369), pp. 408–411. DOI: 10.1038/nature10450.

Huang, Hsiu-Chen; Chen, Chun-Chi; Chang, Wen-Cheng; Tao, Mi-Hua; Huang, Cheng (2012a): Entry of hepatitis B virus into immortalized human primary hepatocytes by clathrin-dependent endocytosis. In *Journal of virology* 86 (17), pp. 9443–9453. DOI: 10.1128/JVI.00873-12.

Huang, Li-Rung; Gäbel, Yvonne A.; Graf, Steffi; Arzberger, Silke; Kurts, Christian; Heikenwalder, Mathias et al. (2012b): Transfer of HBV genomes using low doses of adenovirus vectors leads to persistent infection in immune competent mice. In *Gastroenterology* 142 (7), 1447-50.e3. DOI: 10.1053/j.gastro.2012.03.006.

Hwang, Jeong-Ryul; Park, Sung-Gyoo (2018): Mouse models for hepatitis B virus research. In *Laboratory animal research* 34 (3), pp. 85–91. DOI: 10.5625/lar.2018.34.3.85.

Jacquet, Stéphanie; Pons, Jean-Baptiste; Bernardo, Ariel de; Ngoubangoye, Barthélémy; Cosset, François-Loic; Régis, Corinne et al. (2019): Evolution of Hepatitis B Virus Receptor

NTCP Reveals Differential Pathogenicities and Species Specificities of Hepadnaviruses in Primates, Rodents, and Bats. In *Journal of virology* 93 (5). DOI: 10.1128/JVI.01738-18.

Jung, Diana; Hagenbuch, Bruno; Fried, Michael; Meier, Peter J.; Kullak-Ublick, Gerd A. (2004): Role of liver-enriched transcription factors and nuclear receptors in regulating the human, mouse, and rat NTCP gene. In *American journal of physiology. Gastrointestinal and liver physiology* 286 (5), G752-61. DOI: 10.1152/ajpgi.00456.2003.

Kang, Connie; Syed, Yahiya Y. (2020): Bulevirtide: First Approval. In *Drugs* 80 (15), pp. 1601–1605. DOI: 10.1007/s40265-020-01400-1.

Kim, C. M.; Koike, K.; Saito, I.; Miyamura, T.; Jay, G. (1991): HBx gene of hepatitis B virus induces liver cancer in transgenic mice. In *Nature* 351 (6324), pp. 317–320. DOI: 10.1038/351317a0.

Knowles, B. B.; Howe, C. C.; Aden, D. P. (1980): Human hepatocellular carcinoma cell lines secrete the major plasma proteins and hepatitis B surface antigen. In *Science (New York, N.Y.)* 209 (4455), pp. 497–499. DOI: 10.1126/science.6248960.

Ko, Chunkyu; Bester, Romina; Zhou, Xue; Xu, Zhiheng; Blossey, Christoph; Sacherl, Julia et al. (2019): A New Role for Capsid Assembly Modulators To Target Mature Hepatitis B Virus Capsids and Prevent Virus Infection. In *Antimicrobial agents and chemotherapy* 64 (1). DOI: 10.1128/AAC.01440-19.

Ko, Chunkyu; Chakraborty, Anindita; Chou, Wen-Min; Hasreiter, Julia; Wettengel, Jochen M.; Stadler, Daniela et al. (2018): Hepatitis B virus genome recycling and de novo secondary infection events maintain stable cccDNA levels. In *Journal of hepatology* 69 (6), pp. 1231–1241. DOI: 10.1016/j.jhep.2018.08.012.

Ko, Chunkyu; Michler, Thomas; Protzer, Ulrike (2017): Novel viral and host targets to cure hepatitis B. In *Current opinion in virology* 24, pp. 38–45. DOI: 10.1016/j.coviro.2017.03.019.

Ko, Chunkyu; Su, Jinpeng; Festag, Julia; Bester, Romina; Kosinska, Anna D.; Protzer, Ulrike (2021): Intramolecular recombination enables the formation of hepatitis B virus (HBV) cccDNA in mice after HBV genome transfer using recombinant AAV vectors. In *Antiviral research* 194, p. 105140. DOI: 10.1016/j.antiviral.2021.105140.

Kobayashi, Naoki; Nishikawa, Makiya; Hirata, Kazuhiro; Takakura, Yoshinobu (2004): Hydrodynamics-based procedure involves transient hyperpermeability in the hepatic cellular membrane: implication of a nonspecific process in efficient intracellular gene delivery. In *The journal of gene medicine* 6 (5), pp. 584–592. DOI: 10.1002/jgm.541.

König, Alexander; Döring, Barbara; Mohr, Christina; Geipel, Andreas; Geyer, Joachim; Glebe, Dieter (2014): Kinetics of the bile acid transporter and hepatitis B virus receptor Na+/taurocholate cotransporting polypeptide (NTCP) in hepatocytes. In *Journal of hepatology* 61 (4), pp. 867–875. DOI: 10.1016/j.jhep.2014.05.018.

Kramvis, Anna (2014): Genotypes and genetic variability of hepatitis B virus. In *Intervirology* 57 (3-4), pp. 141–150. DOI: 10.1159/000360947.

Kubitz, Ralf; Sütfels, Gerrit; Kühlkamp, Thomas; Kölling, Ralf; Häussinger, Dieter (2004): Trafficking of the bile salt export pump from the Golgi to the canalicular membrane is regulated by the p38 MAP kinase. In *Gastroenterology* 126 (2), pp. 541–553. DOI: 10.1053/j.gastro.2003.11.003.

Ladner, S. K.; Otto, M. J.; Barker, C. S.; Zaifert, K.; Wang, G. H.; Guo, J. T. et al. (1997): Inducible expression of human hepatitis B virus (HBV) in stably transfected hepatoblastoma cells: a novel system for screening potential inhibitors of HBV replication. In *Antimicrobial agents and chemotherapy* 41 (8), pp. 1715–1720. DOI: 10.1128/AAC.41.8.1715.

Landmann, L.; Angermuller, S.; Rahner, C.; Stieger, B. (1998): Expression, distribution, and activity of Na+,K+-ATPase in normal and cholestatic rat liver. In *The journal of*

histochemistry and cytochemistry : official journal of the Histochemistry Society 46 (3), pp. 405–410. DOI: 10.1177/002215549804600315.

Langley, David R.; Walsh, Ann W.; Baldick, Carl J.; Eggers, Betsy J.; Rose, Ronald E.; Levine, Steven M. et al. (2007): Inhibition of hepatitis B virus polymerase by entecavir. In *Journal of virology* 81 (8), pp. 3992–4001. DOI: 10.1128/JVI.02395-06.

Le, Connie; Sirajee, Reshma; Steenbergen, Rineke; Joyce, Michael A.; Addison, William R.; Tyrrell, D. Lorne (2021): In Vitro Infection with Hepatitis B Virus Using Differentiated Human Serum Culture of Huh7.5-NTCP Cells without Requiring Dimethyl Sulfoxide. In *Viruses* 13 (1). DOI: 10.3390/v13010097.

Lee, Jiwon; Zong, Li; Krotow, Alexander; Qin, Yanli; Jia, Lucy; Zhang, Jiming et al. (2018): N-Linked Glycosylation Is Not Essential for Sodium Taurocholate Cotransporting Polypeptide To Mediate Hepatitis B Virus Infection In Vitro. In *Journal of virology* 92 (15). DOI: 10.1128/JVI.00732-18.

Lempp, Florian A.; Mutz, Pascal; Lipps, Christoph; Wirth, Dagmar; Bartenschlager, Ralf; Urban, Stephan (2016a): Evidence that hepatitis B virus replication in mouse cells is limited by the lack of a host cell dependency factor. In *Journal of hepatology* 64 (3), pp. 556–564. DOI: 10.1016/j.jhep.2015.10.030.

Lempp, Florian A.; Qu, Bingqian; Wang, Yong-Xiang; Urban, Stephan (2016b): Hepatitis B Virus Infection of a Mouse Hepatic Cell Line Reconstituted with Human Sodium Taurocholate Cotransporting Polypeptide. In *Journal of virology* 90 (9), pp. 4827–4831. DOI: 10.1128/JVI.02832-15.

Lempp, Florian A.; Urban, Stephan (2014): Inhibitors of hepatitis B virus attachment and entry. In *Intervirology* 57 (3-4), pp. 151–157. DOI: 10.1159/000360948.

Lempp, Florian A.; Wiedtke, Ellen; Qu, Bingqian; Roques, Pierre; Chemin, Isabelle; Vondran, Florian W. R. et al. (2017): Sodium taurocholate cotransporting polypeptide is the limiting host factor of hepatitis B virus infection in macaque and pig hepatocytes. In *Hepatology (Baltimore, Md.)* 66 (3), pp. 703–716. DOI: 10.1002/hep.29112.

Li, Hanjie; Zhuang, Qiuyu; Wang, Yuze; Zhang, Tianying; Zhao, Jinghua; Zhang, Yali et al. (2014): HBV life cycle is restricted in mouse hepatocytes expressing human NTCP. In *Cellular & molecular immunology* 11 (2), pp. 175–183. DOI: 10.1038/cmi.2013.66.

Li, Wenhui (2015): The hepatitis B virus receptor. In *Annual review of cell and developmental biology* 31, pp. 125–147. DOI: 10.1146/annurev-cellbio-100814-125241.

Long, Quanxin; Yan, Ran; Hu, Jieli; Cai, Dawei; Mitra, Bidisha; Kim, Elena S. et al. (2017): The role of host DNA ligases in hepadnavirus covalently closed circular DNA formation. In *PLoS pathogens* 13 (12), e1006784. DOI: 10.1371/journal.ppat.1006784.

Lucifora, Julie; Arzberger, Silke; Durantel, David; Belloni, Laura; Strubin, Michel; Levrero, Massimo et al. (2011): Hepatitis B virus X protein is essential to initiate and maintain virus replication after infection. In *Journal of hepatology* 55 (5), pp. 996–1003. DOI: 10.1016/j.jhep.2011.02.015.

Lucifora, Julie; Protzer, Ulrike (2016): Attacking hepatitis B virus cccDNA--The holy grail to hepatitis B cure. In *Journal of hepatology* 64 (1 Suppl), S41-S48. DOI: 10.1016/j.jhep.2016.02.009.

Lucifora, Julie; Salvetti, Anna; Marniquet, Xavier; Mailly, Laurent; Testoni, Barbara; Fusil, Floriane et al. (2017): Detection of the hepatitis B virus (HBV) covalently-closed-circular DNA (cccDNA) in mice transduced with a recombinant AAV-HBV vector. In *Antiviral research* 145, pp. 14–19. DOI: 10.1016/j.antiviral.2017.07.006.

Lucifora, Julie; Xia, Yuchen; Reisinger, Florian; Zhang, Ke; Stadler, Daniela; Cheng, Xiaoming et al. (2014): Specific and nonhepatotoxic degradation of nuclear hepatitis B virus

cccDNA. In *Science (New York, N.Y.)* 343 (6176), pp. 1221–1228. DOI: 10.1126/science.1243462.

Luo, Jun; Cui, Xiuji; Gao, Lu; Hu, Jianming (2017): Identification of an Intermediate in Hepatitis B Virus Covalently Closed Circular (CCC) DNA Formation and Sensitive and Selective CCC DNA Detection. In *Journal of virology* 91 (17). DOI: 10.1128/JVI.00539-17.

Macovei, Alina; Radulescu, Cristina; Lazar, Catalin; Petrescu, Stefana; Durantel, David; Dwek, Raymond A. et al. (2010): Hepatitis B virus requires intact caveolin-1 function for productive infection in HepaRG cells. In *Journal of virology* 84 (1), pp. 243–253. DOI: 10.1128/JVI.01207-09.

Marcellin, Patrick; Heathcote, E. Jenny; Buti, Maria; Gane, Ed; Man, Robert A. de; Krastev, Zahary et al. (2008): Tenofovir disoproxil fumarate versus adefovir dipivoxil for chronic hepatitis B. In *The New England journal of medicine* 359 (23), pp. 2442–2455. DOI: 10.1056/NEJMoa0802878.

Marion, Marie-Jeanne; Hantz, Olivier; Durantel, David (2010): The HepaRG cell line: biological properties and relevance as a tool for cell biology, drug metabolism, and virology studies. In *Methods in molecular biology (Clifton, N.J.)* 640, pp. 261–272. DOI: 10.1007/978-1-60761-688-7_13.

Mason, W. S.; Seal, G.; Summers, J. (1980): Virus of Pekin ducks with structural and biological relatedness to human hepatitis B virus. In *Journal of virology* 36 (3), pp. 829–836. DOI: 10.1128/JVI.36.3.829-836.1980.

Meier, Anja; Mehrle, Stefan; Weiss, Thomas S.; Mier, Walter; Urban, Stephan (2013): Myristoylated PreS1-domain of the hepatitis B virus L-protein mediates specific binding to differentiated hepatocytes. In *Hepatology (Baltimore, Md.)* 58 (1), pp. 31–42. DOI: 10.1002/hep.26181.

Mercer, D. F.; Schiller, D. E.; Elliott, J. F.; Douglas, D. N.; Hao, C.; Rinfret, A. et al. (2001): Hepatitis C virus replication in mice with chimeric human livers. In *Nature medicine* 7 (8), pp. 927–933. DOI: 10.1038/90968.

Meyer, S. de; Gong, Z. J.; Suwandhi, W.; van Pelt, J.; Soumillion, A.; Yap, S. H. (1997): Organ and species specificity of hepatitis B virus (HBV) infection: a review of literature with a special reference to preferential attachment of HBV to human hepatocytes. In *Journal of viral hepatitis* 4 (3), pp. 145–153. DOI: 10.1046/j.1365-2893.1997.00126.x.

Milich, D. R.; Jones, J. E.; Hughes, J. L.; Maruyama, T.; Price, J.; Melhado, I.; Jirik, F. (1994): Extrathymic expression of the intracellular hepatitis B core antigen results in T cell tolerance in transgenic mice. In *Journal of immunology (Baltimore, Md. : 1950)* 152 (2), pp. 455–466.

Milich, D. R.; Jones, J. E.; Hughes, J. L.; Price, J.; Raney, A. K.; McLachlan, A. (1990): Is a function of the secreted hepatitis B e antigen to induce immunologic tolerance in utero? In *Proceedings of the National Academy of Sciences of the United States of America* 87 (17), pp. 6599–6603. DOI: 10.1073/pnas.87.17.6599.

Müller, Simon F.; König, Alexander; Döring, Barbara; Glebe, Dieter; Geyer, Joachim (2018): Characterisation of the hepatitis B virus cross-species transmission pattern via Na+/taurocholate co-transporting polypeptides from 11 New World and Old World primate species. In *PloS one* 13 (6), e0199200. DOI: 10.1371/journal.pone.0199200.

Nassal, Michael (2015): HBV cccDNA: viral persistence reservoir and key obstacle for a cure of chronic hepatitis B. In *Gut* 64 (12), pp. 1972–1984. DOI: 10.1136/gutjnl-2015-309809.

Ni, Yi; Lempp, Florian A.; Mehrle, Stefan; Nkongolo, Shirin; Kaufman, Christina; Fälth, Maria et al. (2014): Hepatitis B and D viruses exploit sodium taurocholate co-transporting polypeptide for species-specific entry into hepatocytes. In *Gastroenterology* 146 (4), pp. 1070–1083. DOI: 10.1053/j.gastro.2013.12.024.

Nkongolo, Shirin; Ni, Yi; Lempp, Florian A.; Kaufman, Christina; Lindner, Thomas; Esser-Nobis, Katharina et al. (2014): Cyclosporin A inhibits hepatitis B and hepatitis D virus entry by cyclophilin-independent interference with the NTCP receptor. In *Journal of hepatology* 60 (4), pp. 723–731. DOI: 10.1016/j.jhep.2013.11.022.

Oh, Sanders; Kessler, John A. (2018): Design, Assembly, Production, and Transfection of Synthetic Modified mRNA. In *Methods (San Diego, Calif.)* 133, pp. 29–43. DOI: 10.1016/j.ymeth.2017.10.008.

Oswald, Andreas; Chakraborty, Anindita; Ni, Yi; Wettengel, Jochen M.; Urban, Stephan; Protzer, Ulrike (2021): Concentration of Na+-taurocholate-cotransporting polypeptide expressed after in vitro-transcribed mRNA transfection determines susceptibility of hepatoma cells for hepatitis B virus. In *Scientific reports* 11 (1), p. 19799. DOI: 10.1038/s41598-021-99263-3.

Petersen, Joerg; Dandri, Maura; Mier, Walter; Lütgehetmann, Marc; Volz, Tassilo; Weizsäcker, Fritz von et al. (2008): Prevention of hepatitis B virus infection in vivo by entry inhibitors derived from the large envelope protein. In *Nature biotechnology* 26 (3), pp. 335–341. DOI: 10.1038/nbt1389.

Pollicino, Teresa; Belloni, Laura; Raffa, Giuseppina; Pediconi, Natalia; Squadrito, Giovanni; Raimondo, Giovanni; Levrero, Massimo (2006): Hepatitis B virus replication is regulated by the acetylation status of hepatitis B virus cccDNA-bound H3 and H4 histones. In *Gastroenterology* 130 (3), pp. 823–837. DOI: 10.1053/j.gastro.2006.01.001.

Protzer, Ulrike; Wettengel, Jochen; JESKE, Samuel; FISCHER, Konrad; SCHNIEKE, Angelika (2019): HEPATITIS B AND/OR HEPATITIS D-PERMISSIVE CELLS AND ANIMALS. Applied for by TECHNISCHE UNIVERSITAET MUENCHEN. App. no. PCT/EP2019/066449. Patent no. WO 2019/243564 A1.

Qi, Yonghe; Gao, Zhenchao; Xu, Guangwei; Peng, Bo; Liu, Chenxuan; Yan, Huan et al. (2016): DNA Polymerase κ Is a Key Cellular Factor for the Formation of Covalently Closed Circular DNA of Hepatitis B Virus. In *PLoS pathogens* 12 (10), e1005893. DOI: 10.1371/journal.ppat.1005893.

Qiao, Luhua; Sui, Jianhua; Luo, Guangxiang (2018): Robust Human and Murine Hepatocyte Culture Models of Hepatitis B Virus Infection and Replication. In *Journal of virology* 92 (23). DOI: 10.1128/JVI.01255-18.

Rajbhandari, Ruma; Chung, Raymond T. (2016): Treatment of Hepatitis B: A Concise Review. In *Clinical and translational gastroenterology* 7 (9), e190. DOI: 10.1038/ctg.2016.46.

Rasche, Andrea; Lehmann, Felix; Goldmann, Nora; Nagel, Michael; Moreira-Soto, Andres; Nobach, Daniel et al. (2021): A hepatitis B virus causes chronic infections in equids worldwide. In *Proceedings of the National Academy of Sciences of the United States of America* 118 (13). DOI: 10.1073/pnas.2013982118.

Rijckborst, V.; Sonneveld, M. J.; Janssen, H. L. A. (2011): Review article: chronic hepatitis B - anti-viral or immunomodulatory therapy? In *Alimentary pharmacology & therapeutics* 33 (5), pp. 501–513. DOI: 10.1111/j.1365-2036.2010.04555.x.

Rippin, S. J.; Hagenbuch, B.; Meier, P. J.; Stieger, B. (2001): Cholestatic expression pattern of sinusoidal and canalicular organic anion transport systems in primary cultured rat hepatocytes. In *Hepatology (Baltimore, Md.)* 33 (4), pp. 776–782. DOI: 10.1053/jhep.2001.23433.

Rivière, Lise; Gerossier, Laetitia; Ducroux, Aurélie; Dion, Sarah; Deng, Qiang; Michel, Marie-Louise et al. (2015): HBx relieves chromatin-mediated transcriptional repression of hepatitis B viral cccDNA involving SETDB1 histone methyltransferase. In *Journal of hepatology* 63 (5), pp. 1093–1102. DOI: 10.1016/j.jhep.2015.06.023.

Rivkin, Anastasia (2005): A review of entecavir in the treatment of chronic hepatitis B infection. In *Current medical research and opinion* 21 (11), pp. 1845–1856. DOI: 10.1185/030079905X65268.

Samuel, D.; Muller, R.; Alexander, G.; Fassati, L.; Ducot, B.; Benhamou, J. P.; Bismuth, H. (1993): Liver transplantation in European patients with the hepatitis B surface antigen. In *The New England journal of medicine* 329 (25), pp. 1842–1847. DOI: 10.1056/NEJM199312163292503.

Sarkar, Souvik; Bananis, Eustratios; Nath, Sangeeta; Anwer, M. Sawkat; Wolkoff, Allan W.; Murray, John W. (2006): PKCzeta is required for microtubule-based motility of vesicles containing the ntcp transporter. In *Traffic (Copenhagen, Denmark)* 7 (8), pp. 1078–1091. DOI: 10.1111/j.1600-0854.2006.00447.x.

Schaefer, Stephan (2007): Hepatitis B virus taxonomy and hepatitis B virus genotypes. In *World journal of gastroenterology* 13 (1), pp. 14–21. DOI: 10.3748/wjg.v13.i1.14.

Schmitz, André; Schwarz, Alexandra; Foss, Michael; Zhou, Lixin; Rabe, Birgit; Hoellenriegel, Julia et al. (2010): Nucleoporin 153 arrests the nuclear import of hepatitis B virus capsids in the nuclear basket. In *PLoS pathogens* 6 (1), e1000741. DOI: 10.1371/journal.ppat.1000741.

Schreiner, Sabrina; Nassal, Michael (2017): A Role for the Host DNA Damage Response in Hepatitis B Virus cccDNA Formation-and Beyond? In *Viruses* 9 (5). DOI: 10.3390/v9050125.

Schulze, Andreas; Gripon, Philippe; Urban, Stephan (2007): Hepatitis B virus infection initiates with a large surface protein-dependent binding to heparan sulfate proteoglycans. In *Hepatology (Baltimore, Md.)* 46 (6), pp. 1759–1768. DOI: 10.1002/hep.21896.

Schulze-Bergkamen, Henning; Untergasser, Andreas; Dax, Andreas; Vogel, Heiko; Büchler, Peter; Klar, Ernst et al. (2003): Primary human hepatocytes – a valuable tool for investigation of apoptosis and hepatitis B virus infection. In *Journal of hepatology* 38 (6), pp. 736–744. DOI: 10.1016/S0168-8278(03)00120-X.

Seeger, Christoph; Mason, William S. (2015): Molecular biology of hepatitis B virus infection. In *Virology* 479-480, pp. 672–686. DOI: 10.1016/j.virol.2015.02.031.

Seeger, Christoph; Sohn, Ji A. (2014): Targeting Hepatitis B Virus With CRISPR/Cas9. In *Molecular therapy. Nucleic acids* 3, e216. DOI: 10.1038/mtna.2014.68.

Sells, M. A.; Chen, M. L.; Acs, G. (1987): Production of hepatitis B virus particles in Hep G2 cells transfected with cloned hepatitis B virus DNA. In *Proceedings of the National Academy of Sciences of the United States of America* 84 (4), pp. 1005–1009. DOI: 10.1073/pnas.84.4.1005.

Shimura, Satomi; Watashi, Koichi; Fukano, Kento; Peel, Michael; Sluder, Ann; Kawai, Fumihiro et al. (2017): Cyclosporin derivatives inhibit hepatitis B virus entry without interfering with NTCP transporter activity. In *Journal of hepatology* 66 (4), pp. 685–692. DOI: 10.1016/j.jhep.2016.11.009.

Somiya, Masaharu; Liu, Qiushi; Yoshimoto, Nobuo; Iijima, Masumi; Tatematsu, Kenji; Nakai, Tadashi et al. (2016): Cellular uptake of hepatitis B virus envelope L particles is independent of sodium taurocholate cotransporting polypeptide, but dependent on heparan sulfate proteoglycan. In *Virology* 497, pp. 23–32. DOI: 10.1016/j.virol.2016.06.024.

Sommeregger, Wolfgang; Mayrhofer, Patrick; Steinfellner, Willibald; Reinhart, David; Henry, Michael; Clynes, Martin et al. (2016): Proteomic differences in recombinant CHO cells producing two similar antibody fragments. In *Biotechnology and bioengineering* 113 (9), pp. 1902–1912. DOI: 10.1002/bit.25957.

Sprengel, R.; Kuhn, C.; Will, H.; Schaller, H. (1985): Comparative sequence analysis of duck and human hepatitis B virus genomes. In *Journal of medical virology* 15 (4), pp. 323–333. DOI: 10.1002/jmv.1890150402.

Sprinzl, M. F.; Oberwinkler, H.; Schaller, H.; Protzer, U. (2001): Transfer of hepatitis B virus genome by adenovirus vectors into cultured cells and mice: crossing the species barrier. In *Journal of virology* 75 (11), pp. 5108–5118. DOI: 10.1128/JVI.75.11.5108-5118.2001.

Stadler, Daniela; Kächele, Martin; Jones, Alisha N.; Hess, Julia; Urban, Christian; Schneider, Jessica et al. (2021): Interferon-induced degradation of the persistent hepatitis B virus cccDNA form depends on ISG20. In *EMBO reports* 22 (6), e49568. DOI: 10.15252/embr.201949568.

Summers, J.; Smolec, J. M.; Snyder, R. (1978): A virus similar to human hepatitis B virus associated with hepatitis and hepatoma in woodchucks. In *Proceedings of the National Academy of Sciences of the United States of America* 75 (9), pp. 4533–4537. DOI: 10.1073/pnas.75.9.4533.

Takeuchi, Junko S.; Fukano, Kento; Iwamoto, Masashi; Tsukuda, Senko; Suzuki, Ryosuke; Aizaki, Hideki et al. (2019): A Single Adaptive Mutation in Sodium Taurocholate Cotransporting Polypeptide Induced by Hepadnaviruses Determines Virus Species Specificity. In *Journal of virology* 93 (5). DOI: 10.1128/JVI.01432-18.

Tanaka, Tomohisa; Kasai, Hirotake; Yamashita, Atsuya; Okuyama-Dobashi, Kaori; Yasumoto, Jun; Maekawa, Shinya et al. (2014): Hallmarks of hepatitis C virus in equine hepacivirus. In *Journal of virology* 88 (22), pp. 13352–13366. DOI: 10.1128/JVI.02280-14.

Tatematsu, Kanako; Tanaka, Yasuhito; Kurbanov, Fuat; Sugauchi, Fuminaka; Mano, Shuhei; Maeshiro, Tatsuji et al. (2009): A genetic variant of hepatitis B virus divergent from known human and ape genotypes isolated from a Japanese patient and provisionally assigned to new genotype J. In *Journal of virology* 83 (20), pp. 10538–10547. DOI: 10.1128/JVI.00462-09.

Tropberger, Philipp; Mercier, Alexandre; Robinson, Margaret; Zhong, Weidong; Ganem, Don E.; Holdorf, Meghan (2015): Mapping of histone modifications in episomal HBV cccDNA uncovers an unusual chromatin organization amenable to epigenetic manipulation. In *Proceedings of the National Academy of Sciences of the United States of America* 112 (42), E5715-24. DOI: 10.1073/pnas.1518090112.

Urban, Stephan; Bartenschlager, Ralf; Kubitz, Ralf; Zoulim, Fabien (2014a): Strategies to inhibit entry of HBV and HDV into hepatocytes. In *Gastroenterology* 147 (1), pp. 48–64. DOI: 10.1053/j.gastro.2014.04.030.

Urban, Stephan; Bartenschlager, Ralf; Kubitz, Ralf; Zoulim, Fabien (2014b): Strategies to inhibit entry of HBV and HDV into hepatocytes. In *Gastroenterology* 147 (1), pp. 48–64. DOI: 10.1053/j.gastro.2014.04.030.

Urban, Stephan; Gripon, Philippe (2002): Inhibition of duck hepatitis B virus infection by a myristoylated pre-S peptide of the large viral surface protein. In *Journal of virology* 76 (4), pp. 1986–1990. DOI: 10.1128/jvi.76.4.1986-1990.2002.

Velkov, Stoyan; Ott, Jördis J.; Protzer, Ulrike; Michler, Thomas (2018): The Global Hepatitis B Virus Genotype Distribution Approximated from Available Genotyping Data. In *Genes* 9 (10). DOI: 10.3390/genes9100495.

Walter, Stephanie; Rasche, Andrea; Moreira-Soto, Andrés; Pfaender, Stephanie; Bletsa, Magda; Corman, Victor Max et al. (2017): Differential Infection Patterns and Recent Evolutionary Origins of Equine Hepaciviruses in Donkeys. In *Journal of virology* 91 (1). DOI: 10.1128/JVI.01711-16.

Wang, Gang; Guan, Jun; Khan, Nazif U.; Li, Guojun; Shao, Junwei; Zhou, Qihui et al. (2021): Potential capacity of interferon-α to eliminate covalently closed circular DNA (cccDNA) in hepatocytes infected with hepatitis B virus. In *Gut pathogens* 13 (1), p. 22. DOI: 10.1186/s13099-021-00421-9.

Wang, Jing; Tian, Ruicheng; Shan, Yuhua; Li, Jingjing; Gao, Hongxiang; Xie, Chenjie et al. (2020): Metabolomics study of the metabolic changes in hepatoblastoma cells in response to NTCP/SLC10A1 overexpression. In *The international journal of biochemistry & cell biology* 125, p. 105773. DOI: 10.1016/j.biocel.2020.105773.

Watashi, Koichi; Sluder, Ann; Daito, Takuji; Matsunaga, Satoko; Ryo, Akihide; Nagamori, Shushi et al. (2014): Cyclosporin A and its analogs inhibit hepatitis B virus entry into cultured hepatocytes through targeting a membrane transporter, sodium taurocholate cotransporting polypeptide (NTCP). In *Hepatology (Baltimore, Md.)* 59 (5), pp. 1726–1737. DOI: 10.1002/hep.26982.

Watashi, Koichi; Wakita, Takaji (2015): Hepatitis B Virus and Hepatitis D Virus Entry, Species Specificity, and Tissue Tropism. In *Cold Spring Harbor Perspectives in Medicine* 5 (8), a021378. DOI: 10.1101/cshperspect.a021378.

Wei, Lei; Ploss, Alexander (2020): Core components of DNA lagging strand synthesis machinery are essential for hepatitis B virus cccDNA formation. In *Nature microbiology* 5 (5), pp. 715–726. DOI: 10.1038/s41564-020-0678-0.

Wettengel (2019): Tropismus- und Spezies-determinierende Faktoren des Hepatitis-B-Virus. PhD. Technischen Universität München, München. Virologie.

Wettengel, Jochen M.; Linden, Bianca; Esser, Knud; Laue, Michael; Burwitz, Benjamin J.; Protzer, Ulrike (2021): Rapid and Robust Continuous Purification of High-Titer Hepatitis B Virus for In Vitro and In Vivo Applications. In *Viruses* 13 (8). DOI: 10.3390/v13081503.

WHO (2021). Available online at https://www.who.int/news-room/fact-sheets/detail/hepatitis-b, updated on Hepatitis B, Fact sheet, Updated July 2021, checked on 8/4/2021.

Wu, J. C.; Merlino, G.; Fausto, N. (1994): Establishment and characterization of differentiated, nontransformed hepatocyte cell lines derived from mice transgenic for transforming growth factor alpha. In *Proceedings of the National Academy of Sciences of the United States of America* 91 (2), pp. 674–678. DOI: 10.1073/pnas.91.2.674.

Xia, Yuchen; Stadler, Daniela; Ko, Chunkyu; Protzer, Ulrike (2016): Analyses of HBV cccDNA Quantification and Modification. In: Guo H., Cuconati A. (eds). Hepatitis B Virus. Methods in Molecular Biology: Humana Press, New York, NY (1540). Available online at https://doi.org/10.1007/978-1-4939-6700-1_6.

Xu, Chunxiao; Guo, Haitao; Pan, Xiao-Ben; Mao, Richeng; Yu, Wenquan; Xu, Xiaodong et al. (2010): Interferons accelerate decay of replication-competent nucleocapsids of hepatitis B virus. In *Journal of virology* 84 (18), pp. 9332–9340. DOI: 10.1128/JVI.00918-10.

Xu, Zaichao; Zhao, Li; Zhong, Youquan; Zhu, Chengliang; Zhao, Kaitao; Teng, Yan et al. (2021): A Novel Mouse Model Harboring Hepatitis B Virus Covalently Closed Circular DNA. In *Cellular and molecular gastroenterology and hepatology*. DOI: 10.1016/j.jcmgh.2021.11.011.

Yan, Huan; Li, Wenhui (2015): Sodium taurocholate cotransporting polypeptide acts as a receptor for hepatitis B and D virus. In *Digestive diseases (Basel, Switzerland)* 33 (3), pp. 388–396. DOI: 10.1159/000371692.

Yan, Huan; Peng, Bo; He, Wenhui; Zhong, Guocai; Qi, Yonghe; Ren, Bijie et al. (2013): Molecular determinants of hepatitis B and D virus entry restriction in mouse sodium taurocholate cotransporting polypeptide. In *Journal of virology* 87 (14), pp. 7977–7991. DOI: 10.1128/JVI.03540-12.

Yan, Huan; Peng, Bo; Liu, Yang; Xu, Guangwei; He, Wenhui; Ren, Bijie et al. (2014): Viral entry of hepatitis B and D viruses and bile salts transportation share common molecular determinants on sodium taurocholate cotransporting polypeptide. In *Journal of virology* 88 (6), pp. 3273–3284. DOI: 10.1128/JVI.03478-13.

Yan, Huan; Zhong, Guocai; Xu, Guangwei; He, Wenhui; Jing, Zhiyi; Gao, Zhenchao et al. (2012): Sodium taurocholate cotransporting polypeptide is a functional receptor for human hepatitis B and D virus. In *eLife* 3. DOI: 10.7554/eLife.00049.

Yang, Priscilla L.; Althage, Alana; Chung, Josan; Chisari, Francis V. (2002): Hydrodynamic injection of viral DNA: a mouse model of acute hepatitis B virus infection. In *Proceedings of the National Academy of Sciences of the United States of America* 99 (21), pp. 13825–13830. DOI: 10.1073/pnas.202398599.

Zhang, Yong-Yuan; Zhang, Bai-Hua; Theele, Daniel; Litwin, Samuel; Toll, Eugene; Summers, Jesse (2003): Single-cell analysis of covalently closed circular DNA copy numbers in a hepadnavirus-infected liver. In *Proceedings of the National Academy of Sciences of the United States of America* 100 (21), pp. 12372–12377. DOI: 10.1073/pnas.2033898100.

Zhang, Zhenfeng; Zehnder, Benno; Damrau, Christine; Urban, Stephan (2016): Visualization of hepatitis B virus entry - novel tools and approaches to directly follow virus entry into hepatocytes. In *FEBS letters* 590 (13), pp. 1915–1926. DOI: 10.1002/1873-3468.12202.

Zhong, Guocai; Yan, Huan; Wang, Haimin; He, Wenhui; Jing, Zhiyi; Qi, Yonghe et al. (2013): Sodium taurocholate cotransporting polypeptide mediates woolly monkey hepatitis B virus infection of Tupaia hepatocytes. In *Journal of virology* 87 (12), pp. 7176–7184. DOI: 10.1128/JVI.03533-12.

Zhou, Xiaoming; Levin, Elena J.; Pan, Yaping; McCoy, Jason G.; Sharma, Ruchika; Kloss, Brian et al. (2014): Structural basis of the alternating-access mechanism in a bile acid transporter. In *Nature* 505 (7484), pp. 569–573. DOI: 10.1038/nature12811.

Zoulim, Fabien; Lebossé, Fanny; Levrero, Massimo (2016): Current treatments for chronic hepatitis B virus infections. In *Current opinion in virology* 18, pp. 109–116. DOI: 10.1016/j.coviro.2016.06.004.

Acknowledgement

First, I thank Prof. Ulrike Protzer for giving me the opportunity to do my PhD thesis in this lab and her guidance throughout whole study. I am especially grateful for your valuable scientific advice, the fruitful discussions and room for my own ideas.

Moreover, I thank my second supervisor Prof. Percy Knolle for his time and the valuable input during my thesis committee meetings.

I would like to thank Dr. Jochen Wettengel and Dr. Britta Möhl-Meinke. Many thanks for intensively discussing my project, giving me very useful scientific advice and reviewing my thesis. Meeting with you was always very helpful.

I also like to thank Dr. Andreas Oswald, Dr. Jinpeng Su, Zhe Xie thoroughly reviewing my thesis. It significantly improved with your suggestions, and I have learned much from you regarding scientific writing.

I would like to thank Dr. Lili Zhao, Dr. Chunkyu Ko, Dr. Wen-Min Chou and Cho-Chin Cheng as my colleagues and as my good friends. You not only have helped me through the tough times but also have motivated me to become a better person.

Special thanks go to Romina Bester, Philipp Hagen and Theresa Asen, you are among the most important people in this lab, without your organizational help, no orders, replacements and repairs would take place.

I would like to thank my colleagues, Dr. Julia Sacherl, Dr. Martin Kächele, Laura Walheim, Dr. Anindita Chakraborty, Dr. Daniela Stadler, Dr. Anna Kosinska, Dr. Oliver Quitt and all other members of the Institute of Virology for creating such a pleasant work environment and for warmly supporting me there.

Additionally, I am thankful for the financial support of the “China Scholarship Council”.

I also thank my family and friends outside the lab for their continuous support, good thoughts and positive energy, which was always a great motivation for me.

Appendix

Optimized hoNTCP sequence based on mice codon:

ATGGAAGCCCACAACGCCAGCACCCCTCTGAACTTCACCCTGCCTCCAAACTTCGGC
AAGAGGCCTACAGATCTGGCCCTGAGCGTGATCCTGGTGCTGATGCTGTTCATCGTGA
TGTTCAGCCTGGGCTGCACCATGGAATTTGGCAAGATCAAGGCCCACTTCTGGAAGC
CTAAAGGCCTGGCTATCGCCCTGGTGGCTCAGTACGGAATCATGCCCCTGACAGCTTT
CGCCCTGGGCAAAGTGTTCCAGCTGAACAACGTGGAAGCCCTGGCCATCCTCGTGTG
TGGATGTTCTCCTGGCGGCAACCTGAGCAACATCTTTAGCCTGGCCATGAAGGGCGA
CATGAACCTGTCTATCGTGATGACAACCTGCAGCACCTTCTTCGCTCTGGGCATGATG
CCCCTGCTGCTGTACGTGTACTCCAGAGGCATCTACGAGGGCGACCTGAAGGACAAG
GTCCCATACGGCGGAATCGTGATCAGCCTGATTCTGGTGCTCATCCCCTGCACAATCG
GCATCTTCCTGAACGCCAAGAGGCCCCAGTACGCCCGGTACATGGTCAAGAGCGGCA
TGATCATTATGCTGCTGTTCTCCGTGGCCGTGGCCGCTCTGTCTGCTATCAACGTGGG
CAAGAGCATCATGTTTGTGATGACCCCTCATCTGCTGGCCACCAGCAGCCTGATGCCT
TTCATCGGTTTTCTGCTGGGCTACATGCTGAGCGCCCTGTTCAGACTGAACGGCAGAT
GTAGAAGAACCGTGTCCATGGAAACCGGCTGCCAGAATGTACAGCTGTGCAGCACAAT
CCTGAACGTGACATTCCCTCTGGAGGTGATCGGCCCTCTGTTCTTCTTCCCACTGCTG
TATATGATCTTCCAGCTCGGCGAGGGACTGCTGCTGATCGCTCTGTTTAGATGCTACGA
GAAGATGAAGCCCAGCAAGGACAAGACCAAGATGATCTACACCGCCGCCACCACCGA
GGAAACAATCCCTGGCGCTCTCGGCAACGGCACCCACAAGGGAAAAGAGTGCAGCC
CTTGTACCGCC